MAX-PLANCK-INSTITUT
FÜR METEOROLOGIE

Human-induced threats to the stability of the Amazon Rainforest

Arim Yoon

Hamburg 2026

Berichte zur Erdsystemforschung
Reports on Earth System Science

296
2026

Hinweis

Die Berichte zur Erdsystemforschung werden vom Max-Planck-Institut für Meteorologie in Hamburg in unregelmäßiger Abfolge herausgegeben.

Sie enthalten wissenschaftliche und technische Beiträge, inklusive Dissertationen.

Die Beiträge geben nicht notwendigerweise die Auffassung des Instituts wieder.

Die "Berichte zur Erdsystemforschung" führen die vorherigen Reihen "Reports" und "Examensarbeiten" weiter.

Anschrift / Address

Max-Planck-Institut für Meteorologie
Bundesstrasse 53
20146 Hamburg
Deutschland

Tel./Phone: +49 (0)40 4 11 73 - 0
Fax: +49 (0)40 4 11 73 - 298

name.surname@mpimet.mpg.de
www.mpimet.mpg.de

Notice

The Reports on Earth System Science are published by the Max Planck Institute for Meteorology in Hamburg. They appear in irregular intervals.

They contain scientific and technical contributions, including PhD theses.

The Reports do not necessarily reflect the opinion of the Institute.

The "Reports on Earth System Science" continue the former "Reports" and "Examensarbeiten" of the Max Planck Institute.

Layout

Bettina Diallo and Norbert P. Noreiks
Communication

Copyright

Human-induced threats to the stability of the Amazon Rainforest

Arim Yoon

Hamburg 2026

Arim Yoon
aus Daegu, South Korea

Max-Planck-Institut für Meteorologie
The International Max Planck Research School on Earth System Modelling
(IMPRS-ESM)
Bundesstrasse 53
20146 Hamburg

Tag der Disputation: 11. November 2025

Folgende Gutachter empfehlen die Annahme der Dissertation:
Dr. Cathy Hohenegger
Prof. Dr. Victor Brovkin

Vorsitzender des Promotionsausschusses:
Prof. Dr. Hermann Held

Dekan der MIN-Fakultät:
Prof. Dr.-Ing. Norbert Ritter

Titelgrafik: *photo by Arim Yoon,*
Amazon rainforest taken from the top of the ATTO tower on 02/10/2023

Berichte zur Erdsystemforschung / Max-Planck-Institut für Meteorologie 296
Reports on Earth System Science / Max Planck Institute for Meteorology 2026

ISSN 1614-1199 - doi: 0.17617/2.3691249

Arim Yoon

Human-induced threats to the stability of the Amazon Rainforest

ABSTRACT

The Amazon Rainforest needs sufficient rainfall to sustain its forest. Under ongoing human-induced disturbances such as deforestation and warming, concerns about reduced rainfall and the potential for forest collapse have been a long-standing question. Climate models have been used to answer the question. However, those models rely on parameterized convection and/or prescribed boundary conditions. Empirical-based parameterization has been known to introduce biases in projecting precipitation, and boundary conditions fail to capture large-scale feedbacks, limiting the ability to represent physical processes. To overcome these limitations, this thesis investigates the impact of these disturbances using a global storm-resolving climate model with 5 km horizontal resolution, resolving convection explicitly.

The thesis addresses two main questions: (1) How does annual mean precipitation, including extreme events, respond to complete Amazon deforestation? and (2) How do different aspects of CO_2-induced warming—namely direct radiative effects and ocean warming—together with a coupled simulation, affect Amazon rainfall? Results from the first question show that basin-averaged mean precipitation remains largely unchanged after complete deforestation, challenging the widespread expectation that Amazonian deforestation leads to a substantial decline in rainfall. This resilience in rain is due to enhanced moisture convergence that compensates for the decrease. However, increased convergence leads to more frequent and intense violent, short-duration rainfall events. Accompanied by warmer and windier environments, such changes in extreme events could hinder forest regrowth after deforestation.

To answer the second question, both ocean-atmosphere coupled and atmosphere-only (AMIP) simulations were analyzed. Under the SSP3-7.0 scenario, the coupled simulation shows a decrease in annual precipitation averaged over the Amazon. This reduction is driven by weakened moisture convergence, which enables a positive feedback within the moisture balance equation: reduced convergence lowers precipitation, which depletes soil moisture, suppresses evapotranspiration, and further reduces rainfall. In contrast, AMIP simulations show an increase in precipitation, though driven by different mechanisms depending on the aspect of CO_2-induced warming-direct radiative or ocean warming effects. In the simulation with the radiative effect, enhanced moisture convergence triggers a positive feedback. On the other hand, in the simulation with the ocean warming, increased evapotranspiration sustains precipitation despite reduced convergence. It is due to ample soil moisture, which keeps high evapotranspiration.

Overall, my results present the first assessment of the Amazon's hydrological response to deforestation and CO_2-induced warming using a global storm-resolving model. This marks a meaningful step forward, as it overcomes key limitations of cli-

mate models previously used. The deforestation results offer a new interpretation of a more resilient Amazonian mean precipitation, while underscoring the need to account for extreme events. Beyond the advantages of using a storm-resolving model, the separation of different effects of CO_2-induced warming provides a way to think about how precipitation may evolve in a warming world through a moisture feedback loop.

ZUSAMMENFASSUNG

Der Amazonas-Regenwald ist auf ausreichende Niederschläge angewiesen, um sein Ökosystem zu erhalten. Angesichts anhaltender, vom Menschen verursachter Störungen wie Entwaldung und Erwärmung bestehen seit Langem Bedenken hinsichtlich abnehmender Niederschläge und eines möglichen Zusammenbruchs des Waldes. Zur Beantwortung dieser Frage wurden Klimamodelle eingesetzt. Diese Modelle basieren jedoch auf parametrisierten Konvektionsprozessen und/oder vorgegebenen Randbedingungen. Es ist bekannt, dass empirisch basierte Parametrisierungen zu Verzerrungen in der Niederschlagsprojektion führen, während feste Randbedingungen großskalige Rückkopplungen nicht erfassen können, was die realitätsnahe Abbildung physikalischer Prozesse einschränkt. Um diese Einschränkungen zu überwinden, untersucht diese Arbeit die Auswirkungen solcher Störungen mithilfe eines globalen sturmauflösenden Klimamodells mit einer horizontalen Auflösung von 5 km, das Konvektion explizit auflöst. Die Arbeit behandelt zwei zentrale Fragestellungen: (1) Wie reagiert der mittlere Jahresniederschlag – einschließlich extremer Ereignisse – auf eine vollständige Entwaldung des Amazonas? und (2) Wie beeinflussen verschiedene Aspekte der CO_2-induzierten Erwärmung – insbesondere direkte Strahlungseffekte und die Erwärmung der Meeresoberfläche – zusammen mit einer gekoppelten Simulation den Niederschlag über dem Amazonasgebiet? Die Ergebnisse zur ersten Fragestellung zeigen, dass der beckenweit gemittelte Jahresniederschlag nach vollständiger Entwaldung weitgehend unverändert bleibt, was die weit verbreitete Erwartung infrage stellt, dass eine Entwaldung des Amazonas zu einem deutlichen Rückgang der Niederschläge führt. Diese Resilienz des Niederschlags lässt sich durch eine verstärkte Feuchtekonvergenz erklären, die den Rückgang kompensiert. Allerdings führt die erhöhte Konvergenz zu häufigeren und intensiveren, kurzzeitigen Starkniederschlägen. In Kombination mit wärmeren und windigeren Bedingungen könnten solche Extremereignisse die Wiederbewaldung nach der Entwaldung erschweren.

Zur Beantwortung der zweiten Fragestellung wurden sowohl gekoppelten Ozean-Atmosphäre-Simulationen als auch Atmosphären-Only-Simulationen (AMIP) analysiert. Im SSP3-7.0-Szenario zeigt die gekoppelte Simulation einen Rückgang des jahreszeitlich gemittelten Niederschlags über dem Amazonas. Dieser Rückgang wird durch eine abgeschwächte Feuchtekonvergenz verursacht, die eine positive Rückkopplung innerhalb der Feuchtigkeitsbilanz in Gang setzt: Weniger Konvergenz führt zu weniger Niederschlag, was die Bodenfeuchte reduziert, die Evapotranspiration unterdrückt und den Niederschlag weiter verringert. Im Gegensatz dazu zeigen die AMIP-Simulationen einen Anstieg des Niederschlags, allerdings durch unterschiedliche Mechanismen – je nachdem, ob die CO_2-induzierte Erwärmung durch direkte Strahlungseffekte oder durch ozeanische Erwärmung verursacht wird. In der Simulation mit dem Strahlungseffekt löst eine verstärkte Feuchtekonvergenz eine positive Rückkopplung aus. In der Simulation mit ozeanischer Erwärmung hingegen bleibt der Niederschlag trotz reduzierter Konvergenz

durch erhöhte Evapotranspiration stabil. Dies ist auf ausreichend vorhandene Bodenfeuchte zurückzuführen, die eine hohe Evapotranspiration ermöglicht.

Insgesamt liefert diese Arbeit die erste Bewertung der hydrologischen Reaktion des Amazonas auf Entwaldung und CO_2-induzierte Erwärmung unter Verwendung eines globalen sturmauflösenden Modells. Dies stellt einen bedeutenden Fortschritt dar, da zentrale Einschränkungen herkömmlicher Klimamodelle überwunden werden. Die Ergebnisse zur Entwaldung bieten eine neue Interpretation eines widerstandsfähigeren mittleren Niederschlags im Amazonasgebiet, verdeutlichen jedoch gleichzeitig die Notwendigkeit, Extremereignisse stärker zu berücksichtigen. Über die Vorteile des sturmauflösenden Modells hinaus bietet die getrennte Betrachtung verschiedener Aspekte der CO_2-induzierten Erwärmung eine neue Perspektive darauf, wie sich Niederschläge in einer sich erwärmenden Welt über feuchtigkeitsgesteuerte Rückkopplungsmechanismen entwickeln könnten.

PUBLICATIONS RELATED TO THIS DISSERTATION

The following three publications are part of this dissertation and are included in the appendix:

Appendix A
Yoon, A., Hohenegger, C., (2025a): " Muted Amazon rainfall response to deforestation in a global storm-resolving model.", In: *Geophysical Research Letters, 52(4), e2024GL110503.*

Appendix B
Yoon, A. et al., (2025b): "Extreme events in the Amazon after deforestation", In *review in Earth System Dynamics*.

Appendix C
Yoon, A., et al., (2025c): "Amazon precipitation under warming from the perspective of the moisture balance equation.", In: *preparation for submission*.

As a PhD student, I contributed to two other publications, one of which is a first-author publication based on the results of my master's thesis:

Yoon, A., et al., (2024a): "Factor analysis of recent major Heatwaves in East Asia.", In: *Geoscience Frontiers, 15(1), 101730.*.

Wijngaard, R. R., Oh, H., Khanal, S., **Yoon, A.**, van de Berg, W. J., & An, S. I., (2024b): "The associations of Tibetan Plateau spring snow cover with East Asian summer monsoon rainfall before and after 1990.", In: *Frontiers in Earth Science, 12, 1385657.*.

ACKNOWLEDGEMENTS

First and foremost, I would like to express my deepest gratitude to *Cathy Hohenegger* for her support and guidance to finish this thesis. I feel incredibly fortunate to have had her as my supervisor. I enjoyed every discussion we had, and her feedback was always helpful. I appreciate her patience, encouragement, and for challenging me to improve my research. Most of all, I am deeply inspired by her curiosity, dedication, and thoughtfulness as a scientist, which I hope to carry forward in my own career.

I thank the postdoctoral researchers I had the privilege of working with during my PhD—*Junhong Lee* and *Hans Segura*—for generously sharing their expertise, supporting my work, and encouraging me to enjoy the process of research. I also thank *Divya Praturi, Jiawei Bao*, and *Keno Riechers* for the insightful conversations that brought ideas and clarity during challenging moments.

I thank *Reiner Schnur* for patiently answering my numerous questions about JSBACH and for filling the gaps in my knowledge with his expertise. I thank *Martin Claussen* for his interest in my work and valuable feedback. I thank *Lukas Kluft* and *Tobias Kölling* for their invaluable help with running simulations and technical support.

I thank *Bjorn Stevens* for giving me the opportunity to join MPIM and for fostering such an inspiring scientific community. I also thank the IMPRS office—*Cornelia Kampmann, Michaela Born, Antje Weitz, Florian Mundt*—and *Angela Gruber* for their warm welcome and their constant, unconditional support, which made my life in Hamburg pleasant and comfortable.

To my all-time office mate *Abisha Gnanaraj*—I thank her for sharing the PhD journey with me, for her help and kindness. I thank *Quan Liu* and *Clara Bayley* for their thoughtful nature and honest feedback. And thanks to *Angel Peinado* for his insights and ever-present joy.

I thank *Moritz Epke*, *Janina Tschirschwitz*, and *Doseok Lee* for their valuable discussions and feedback that helped improve my thesis. Also, I thank friends here—*Paul Keil*, *Luca Schmidt*, *Hernan Campos*, *Anna-Luisa Sanchez*, *Maria-Jesus Rapanague*, *Lucas Casaroli*, *Zoe Kourkouraido*, *Kenneth Chan*, *Marius Schulz*, *Henning Franke*—and all my colleagues at MPI for creating memories and making my time here enjoyable.

I thank my friends in Korea and the USA—*Byeongjun Park*, *Minwoo Chun*, and *Hyeonji Oh*—for their support and for ensuring I never felt alone while living abroad. I thank *Jwooyeop Lee* for helping me through one of the most challenging times during my PhD and for his friendship.

Lastly, to my precious family—*Dad, Mom, and Chihoon*—thank you for always supporting my decision to follow this path and for believing in me every step of the way. 언제나 그립고 사랑하고, 진심으로 감사합니다.

CONTENTS

Part I

UNIFYING ESSAY

1

INTRODUCTION

When we excavate the remains of past civilizations, we rarely find any evidence that they made any attempts to adapt in the face of a changing climate. I view this inflexibility as the real reason for the collapse.

— Prof. Dr. Jason Ur, Archaeologist

Throughout recent history, humans have continually reshaped their environment through deforestation, mining, and urbanization, transforming land and even altering their climate. While these transformations of the land have enabled our lives to flourish, they raise a critical question: can land changes continue to benefit us, or might they trigger irreversible environmental consequences?

The collapse of the Maya civilization offers a cautionary tale. Once a flourishing society, civilization abruptly declined in the ninth century A.D, likely linked to regional hydrological shifts driven by widespread deforestation (McNeil et al., 2010; Oglesby et al., 2010). Of course, deforestation alone cannot cause the collapse of a civilization. But it is critical as massive deforestation can initiate a cascade of compounding risks. Altered rainfall reduces crop yields, leading to food insecurity and rising socio-political tensions, while extreme rainfall events erode infrastructure and overwhelm governance systems. Together, these pressures can converge into systemic collapse (Kemp and Cline, 2022; Lapola et al., 2023).

Today, history may be repeating itself. The Amazon Rainforest is at the center of it. Nearly 20% of the forest has already been cleared for croplands, cattle fields, and dams, with more projected to follow (Bullock et al., 2020). But deforestation is not the only threat. Amazon now faces another human-driven threat, CO2-induced warming. While our physical understanding of spatially averaged tropical precipitation responses to warming is well established (Held and Soden, 2006; Chou and Neelin, 2004; Seager et al., 2010), regional projections remain uncertain (Chadwick et al., 2013; Byrne and O'Gorman, 2015). Circulation change due to altered temperature gradients (Bayr and Dommenget, 2013), local humidity changes (Byrne and O'Gorman, 2015), and shifts of wet and dry regions (Muller and O'Gorman, 2011; Chadwick et al., 2013) contribute to these uncertainties. The lack of understanding of how precipitation will be projected regionally deepens our concern about the Amazon's future in a warming world.

Crucially, Amazon's fate is not confined to the region itself. A collapse of the forest will terminate one of Earth's largest carbon sinks (Phillips et al., 2017; Gatti et al., 2021), accelerating warming and intensifying extreme weather globally. It would threaten food security by disrupting rainfall patterns essential for agriculture across South America and beyond. It would also heighten outbreaks of zoonotic viruses, such as COVID-19, in fragmented ecosystems (Johnson et al.,

2020), and undermine access to medicinal biodiversity by destroying the forest's vast reservoir of pharmaceutical compounds (Newman, 1994). In short, Amazon's demise would not be a local tragedy, but a planetary crisis—one that could threaten the foundations of human civilization itself (Bradshaw et al., 2021).

However, unlike ancient societies, we now possess tools to anticipate the future. Decades of scientific advancement enabled us to simulate complex Earth system processes using Earth system models. Yet, at the same time, models continue to evolve, capturing physical processes better. As our modeling tools improve, so does our ability to understand the climate and prepare for the future under threats. In this thesis, I will use one of today's most advanced Earth system models to investigate how those human-induced disturbances – deforestation and CO_2-induced warming – are shaping the future climate of the Amazon.

2

BACKGROUND

I will first introduce the evolution of Earth system models in the context of the limitations that have driven the development of one of today's most advanced models used in this thesis.

Climate scientists have long developed numerical models grounded in fluid dynamics and thermodynamics to simulate the Earth system. These models serve as experimental platforms, so-called "digital Earths", to test hypotheses and explore the complex interplay of physical processes. The foundation of modern climate modeling can be traced back to the work of Smagorinsky, who introduced the primitive equation that forms the basis of General Circulation Models (Smagorinsky, 1963). These early models provided a robust framework for understanding large-scale atmospheric circulation. Over time, additional components were coupled into the atmospheric core, including the ocean, land surface, sea ice, and later the carbon cycle, transforming General Circulation Models into more comprehensive Earth System Models. Over time, these models are broadly referred to as Global Climate Models (GCMs).

Alongside the inclusion of more Earth system components, another direction of model development has been the enhancement of spatial resolution. Early GCMs, with typical horizontal grid spacings of around 100 km, could not resolve important regional or local processes. To address this, Regional Climate Models (RCMs) were introduced (Dickinson et al., 1989; Giorgi and Bates, 1989). These models "nest" a higher-resolution domain (typically 10–50 km) within GCM outputs, enabling better representation of features like coastlines, mountains, and mesoscale weather systems. Despite these advances, both GCMs and RCMs still rely on coarse resolutions that cannot resolve key small-scale processes such as deep convection, which is central to rainfall generation in the tropics. To compensate, they use convective parameterization schemes, which use empirical representations of unresolved sub-grid processes. However, this introduces persistent biases in the spatial and temporal structure of simulated precipitation as a side effect, limiting the model's ability to represent the underlying physical processes (Stevens and Bony, 2013).

To overcome this limitation, a new type of high-resolution model has emerged. With a grid spacing of 10 km or finer, a high-resolution global climate model that can explicitly resolve convection is called a 'global storm-resolving model' (Satoh et al., 2019). As it resolves convection, it can solve the systematic biases of convective parameterization and offer a more physically grounded representation of precipitation and cloud processes.

Based on this information, I will focus on one of the key parameterization-driven misrepresentations of precipitation from conventional models and how it simulates differently in a storm-resolving model, which is particularly relevant to this thesis.

2.1 REPRESENTATION OF LAND-ATMOSPHERE COUPLING IN CLIMATE MODELS

As we learned previously, convective parameterization introduces persistent biases in representing precipitation spatially and temporally, which undermines the models' ability to simulate the underlying physical mechanisms accurately (Stevens and Bony, 2013). One of the biases driven by parameterization is the misrepresentation of land-atmosphere coupling.

Land–atmosphere coupling describes the extent to which anomalies in land surface conditions influence precipitation, which in turn affects the land surface, creating a loop of mutual interactions (Koster et al., 2006). These two systems are coupled through evapotranspiration, and depending on the direction of the coupling, this loop can be positive (amplifying anomalies) or negative (stabilizing them). A positive feedback is explained based on moisture recycling that wetter soils lead to more evapotranspiration, which enhances rainfall (Eltahir, 1996). In contrast, planetary boundary layer (PBL) dynamics allow both positive and negative feedback as convection happens in different soil conditions. The PBL is the lowest atmospheric layer directly influenced by the surface. To trigger convection, PBL should reach the level of free convection (LFC), where the air parcel starts to rise freely. Over wet soils, higher evapotranspiration moistens the boundary layer, lowering the LFC and reducing inhibition to deep convection, thereby promoting convection (Findell and Eltahir, 2003). In contrast, dry soils enhance sensible heat flux, warming and deepening the PBL, which can bring the PBL closer to the LFC and trigger convection (Ek et al., 2004; Findell and Eltahir, 2003). Additionally, moisture convergence generated by heterogeneous soil conditions can transport moisture from wetter to drier regions, and it also enables a negative feedback (Findell and Eltahir, 2003; Segal et al., 2004; Guillod et al., 2015). Hence, both positive and negative feedback are physically plausible in the real world.

Despite the physical plausibility of both feedbacks, conventional climate models that rely on convective parameterization tend to show a positive feedback. This leads to a predominantly positive coupling between land and atmosphere in many GCMs (Koster et al., 2004; Koster et al., 2006; Guo et al., 2006; Dirmeyer et al., 2013). This positive feedback has been implicated in various phenomena, including intensified summer heatwaves following spring soil moisture deficit (Seneviratne et al., 2006; Hirschi et al., 2011; Miralles et al., 2019), local wetting effect from irrigation (DeAngelis et al., 2010; Lo and Famiglietti, 2013), and rainfall reduction after Amazon deforestation (Nobre et al., 1991; Lean and Warrilow, 1989). Because positive feedback amplifies the land surface anomalies, it can cause models to overestimate the influence of the land surface on precipitation. Hohenegger et al. (2009) is among the first studies to show that this sign of the land-atmosphere feedback de-

pends on the design of convective parameterization. In fact, earlier studies (Pan et al., 1996; Gallus Jr and Segal, 2000) had already noted that changing the convection scheme could reverse the sign of precipitation response to soil moisture anomalies. In contrast, Hohenegger et al. (2009) shows that a storm-resolving model, which no longer uses convective parameterization, shows a negative feedback. While that study was regional in scope, Lee and Hohenegger (2024) later confirmed this result using a global storm-resolving model, which consistently showed negative feedback. In fact, the storm-resolving model aligns more closely with observational evidence (Dirmeyer et al., 2013; Taylor et al., 2012; Lee and Hohenegger, 2024). Thus, it suggests that convective parameterization tends to misrepresent land and atmosphere coupling, particularly by overemphasizing the role of evapotranspiration in controlling precipitation.

This misrepresentation of land-atmosphere coupling in conventional models raises questions about earlier findings of Amazon deforestation and CO_2-induced warming, as local evapotranspiration plays a major role in determining precipitation over the region. This motivates my research questions to revisit Amazon's rainfall response using a new type of climate model that does not rely on convective parameterization. Let me now briefly introduce the key features of the Amazon rainfall system to provide context for understanding its system, before reviewing previous studies in order to assess the current state of knowledge and identify research gaps.

2.2 AMAZONIAN RAIN SYSTEM

The Amazon rainforest is one of the wettest lands on Earth, receiving between 1,500 and 3,000 mm of rainfall annually. Situated in the tropics, it benefits from strong trade winds that transport large volumes of moisture from the Atlantic Ocean (Hastenrath et al., 2004; Bosilovich, 2002). This oceanic moisture is intercepted by the Andes Mountains, which form a towering barrier along the western edge of South America, effectively trapping the moisture within the basin. Combined with abundant solar radiation, these conditions enable the development of the world's largest tropical forest. The forest also plays an active role in sustaining its own hydrological cycle. Through evapotranspiration, forest recycles water back into the atmosphere, contributing significantly to regional rainfall. This highlights that Amazon precipitation is sustained by two main moisture sources: land evapotranspiration and oceanic moisture convergence, encouraging the use of the moisture balance equation (precipitation = evapotranspiration + moisture convergence) to simplify the mechanisms driving changes in precipitation.

Pioneering observational studies have sought to quantify the contribution of local versus external moisture sources to Amazonian precipitation. These studies found that up to half of the rainfall in the Amazon Basin originates from local evapotranspiration (Molion, 1975; Salati et al., 1979; Lettau et al., 1979), underscoring the forest's critical role in sustaining its own hydrological cycle. This insight draws attention to the importance of forest-driven evapotranspiration as a key moisture

source for precipitation. Evapotranspiration is regulated by several environmental factors, including net surface radiation, vapor pressure deficit (VPD), wind speed, and soil moisture availability. In the tropics, conditions such as high radiation and VPD are generally favorable for evapotranspiration, provided that soil moisture is sufficient. In the Amazon, deep-rooted trees and broadleaf canopies enable access to deep soil moisture reservoirs, allowing forests to maintain high evapotranspiration rates even during the dry season or in the absence of oceanic moisture influx. This evaporated moisture contributes to moistening the boundary layer, increasing the likelihood of convective cloud formation and rainfall.

While evapotranspiration locally recycles moisture, precipitation over the Amazon is ultimately shaped by the broader atmospheric circulation. The seasonality of Amazon rainfall is primarily controlled by the position of the Intertropical Convergence Zone (ITCZ)—a band of converging trade winds near the equator that migrates north and south over the year (Fig. 1). This migration creates a distinct dry season (Jul–Sep, Fig. 1a) and wet season (Dec–Feb, Fig. 1b) in the Amazon, corresponding to the northward (dry) and southward (wet) shifts of the ITCZ as represented with green dots in Figure 1. During the wet season, the Amazon experiences northeasterly trade winds associated with the southward-displaced ITCZ. These winds are deflected by the Andes Mountains and redirected southward, forming the South American Low-Level Jet (SALLJ). The SALLJ combines with moisture convergence, whose direction is determined by the South Atlantic Subtropical Anticyclone (SASA), to form the South American Monsoon System. SASA is a semi-permanent high-pressure system which is located between 15° - 45° S and 45° W - 15° E over the Atlantic, as you can see a high-pressure system over the southeastern part of South America in Figure 1. As a result of these large-scale circulation features, the Amazon receives more than 20 cm of rainfall per month during the wet season, though with considerable spatial variability across the basin.

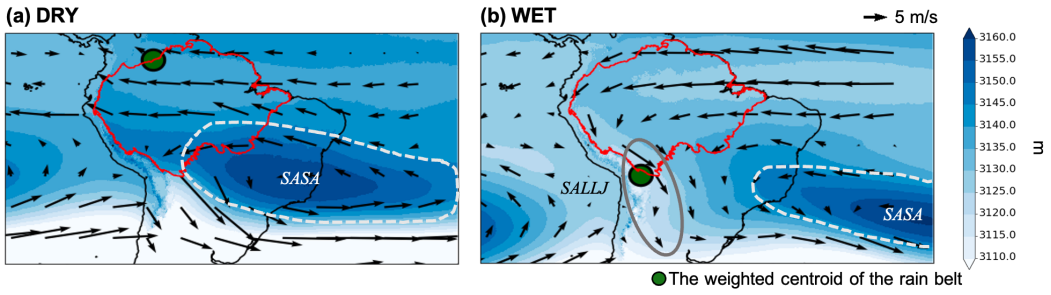

Figure 1: Seasonality of the Amazonian rainfall – Dry (JAS) and Wet (DJF). The wind and geopotential height (m) at 700 hPa are plotted with the location of the weighted centroid of the rain belt (green dot). 700 hPa is selected as it has the strongest trade wind, which converges to decide the location of the ITCZ. The high geopotential height in the southeastern region depicts the location of the South American Subtropical Anticyclone (SASA), and northerly wind in the wet season depicts SALLJ.

Particularly, the location and strength of SASA play an important role in shaping moisture convergence toward the Amazon (Reboita et al., 2018; Reboita et al., 2019; Degola, 2013; Gilliland and Keim, 2018). It exhibits pronounced seasonality, shifting westward during the dry season and eastward during the wet season. A westward anomaly has been linked to severe drought, like the severe drought in 2013/2014 (Rodrigues et al., 2019). On the other hand, the eastward anomaly contributes to the humidity transport, favoring more rainfall (Vianello and Maia, 1986; Reboita et al., 2019). The variability in SASA's position and intensity is influenced by multiple factors, including the subsidence branch of the Hadley cell (Rodwell and Hoskins, 2001; Richter et al., 2008), local thermal forcing (Miyasaka and Nakamura, 2010), monsoonal heating (Liu et al., 2004; Ji et al., 2014), and ENSO-related variability (Seager et al., 2003). These dependencies underscore the importance of understanding how pressure systems like SASA respond to climate change and land-use change, as shifts in any of these controlling factors could significantly alter the Amazonian rain system.

In the following sections, I will review how previous studies have explained changes in precipitation due to deforestation and CO_2-induced warming.

2.3 DEFORESTATION

In the 1960s, large-scale deforestation was initiated by the Brazilian government to promote the economy in the peripheral regions of the Amazon. The long highway was constructed to connect major cities in southern Brazil to the interior of the forest, promoting migration and settlement along the highway. As people cleared land for agriculture and settlement, deforestation widened, forming a fishbone pattern. The deforestation rate surged throughout the 1970s and 1980s, boosted by agriculture subsidies and infrastructure projects. In 1988, the satellite data from the newly launched PRODES monitoring system revealed that 10% of the Amazon forest had already been lost. Concerns have started to grow locally, but also internationally through the 1989 G7 summit in Paris and the Earth Summit in 1992. These attentions spurred scientific studies examining the consequences of deforestation for regional climate. Despite the growing awareness, deforestation did not slow significantly, increasing concerns about its impact. In parallel, scenario-based modeling studies gained momentum, inspired by earlier Salati's findings in the 1970s that suggested the Amazon recycles approximately half of its own rainfall through evapotranspiration (Salati et al., 1979). These findings raised a critical question about a threshold that deforestation disrupts the region's ability to generate enough rainfall to sustain the forest, and the forest collapses.

Following the very first modeling study that examine the change in precipitation after a complete deforestation using a global climate model (Henderson-Sellers and Gornitz, 1984), numerous studies employing coarse-resolution GCMs typically with horizontal resolutions of 2° - 5° have consistently shown a reduction of approximately 20% in annual mean Amazonian precipitation, yet with a large uncertainty (2 - 42%) (Lean and Warrilow, 1989; Nobre et al., 1991; Nobre

et al., 2009; Dickinson and Kennedy, 1992; Lean and Rowntree, 1993; Lean and Rowntree, 1997; Dirmeyer and Shukla, 1994; Hahmann and Dickinson, 1997; Costa and Foley, 2000; Kleidon and Heimann, 2000; Werth and Avissar, 2002; Da Silva et al., 2008; Medvigy et al., 2011; Hirota et al., 2011; Pires and Costa, 2013). The main reason for the reduction in annual mean precipitation is the reduction in evapotranspiration caused by changes to land surface properties. Deforestation in models is represented by modifying key biophysical parameters that define the land surface. These parameters include albedo, leaf area index, vegetation fraction, roughness length, root depth, and forest fraction, which regulate the surface water and energy fluxes. The loss of deep-rooted, broadleaf trees reduces evapotranspiration. Increased surface albedo and lower atmospheric water vapor enhance radiative cooling, promoting subsidence and further inhibiting convection. Mainly due to those local changes of evapotranspiration, a significant reduction in precipitation is prominently highlighted in previous global climate studies. A uniform reduction in precipitation across the Amazon also closely follows the spatial pattern of evapotranspiration changes (Nobre et al., 1991; Lean and Rowntree, 1993; Lean and Rowntree, 1997; Da Silva et al., 2008).

Counteracting these dominant local evapotranspiration effects, RCMs have revealed a possible compensation mechanism. The heated surface of the Amazon after complete deforestation generates a heat low, leading to stronger moisture transport at the surface from the Atlantic Ocean into the Amazon forest. This enhanced moisture transport further benefits from the lower roughness length of pasture relative to forest. As a consequence, RCMs tend to simulate a weaker reduction in annual mean precipitation than GCMs, with an average value of 0.60 mm, corresponding to a 7.9% reduction relative to the original annual mean over the Amazon (Moore et al., 2007; Da Silva et al., 2008; Correia et al., 2008; Lejeune et al., 2015; Llopart et al., 2018). Concerning the spatial distribution of precipitation, the enhanced moisture transport leads to a dipole pattern with precipitation enhanced over the eastern and reduced over the western Amazon. Compared to GCMs, the finer grid spacing of regional climate models enables them to better resolve topography, land–sea contrasts, and mesoscale circulations such as sea breezes, which can influence moisture transport and convection. However, the smaller domain size of RCMs introduces a critical limitation. They cannot capture large-scale feedbacks that operate beyond their boundaries. For example, a reduction in deep convection over the Amazon could weaken large-scale circulation patterns, further suppressing convection — a feedback that would not be represented in regional models with fixed boundary conditions (Lejeune et al., 2015; Medvigy et al., 2011). This limitation is particularly important given Amazon's location within the rainbelt in this region, where global-scale moisture convergence and atmospheric dynamics play an essential role in maintaining precipitation.

Given the importance of capturing large-scale feedback, GCMs appear more suitable than RCMs. While GCMs differ in their quantitative projections, they agree on a key mechanism: a reduction in evapotranspiration leads to a decline in precipitation. This simple water recycling mechanism even shows a linear response of precipitation to the extent of deforestation (Pires and Costa, 2013). Such feed-

back makes models prone to have low precipitation after deforestation, which may hinder forest regrowth. However, despite this apparent agreement, one important modeling limitation remains unresolved.

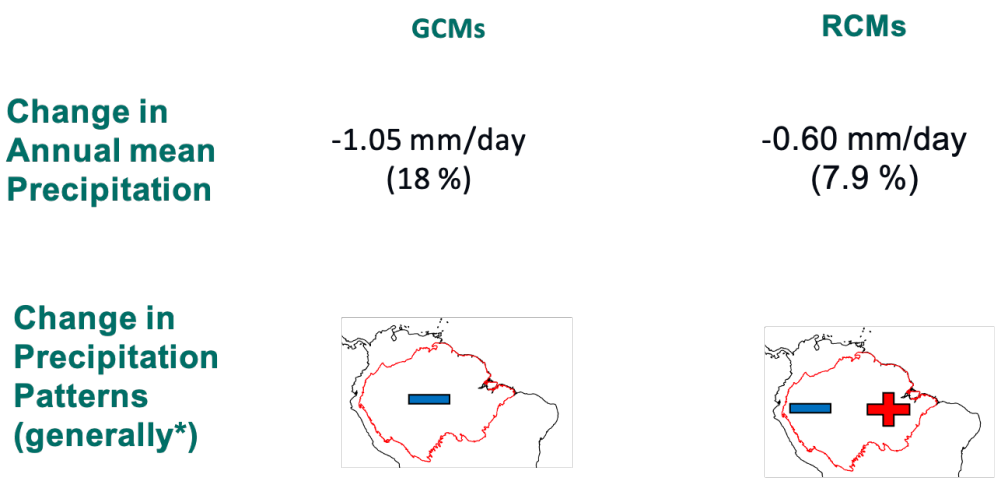

Figure 2: Summary of previous GCMs and RCMs studies showing the changes in annual mean precipitation averaged over the Amazon and spatial patterns in its change. The cited studies are listed in Tables S1 and S2 of Appendix A.

The unresolved limitation is that nearly all presented previous studies—both global and regional—have relied on climate models with convective parameterization to represent convection. As we already studied in section 2.1, convective parameterization tends to overemphasize the role of evapotranspiration on precipitation. Consequently, these models may inherently show a large reduction in mean precipitation following evapotranspiration, often considered an indicator of potential irreversibility of the disturbed forest. Through literature reviews (Fig. 2), we now suspect that both GCMs and RCMs may misrepresent the response of precipitation to deforestation due to inherent model biases. Therefore, it necessitates revisiting the impacts of deforestation using a global storm-resolving model, which overcomes biases of both convective parameterization and boundary conditions.

Alongside model deficiencies, there is another reason we need to revisit using a storm-resolving model. Annual mean precipitation has been the most widely used metric for assessing the Amazon's sustainability after deforestation. It is indeed a useful metric for assessing the ecosystem. For instance, Malhi et al. (2009) used annual precipitation and dry season intensity to classify vegetation types and identify climatic thresholds for vegetation transitions. However, focusing solely on annual mean precipitation can obscure critical information about extreme precipitation events. In many ecosystems, extreme rainfall events exert a stronger influence on the ecosystem than average conditions, as increased drought and runoff alter significantly biological processes (Knapp et al., 2008; Smith, 2011; Thompson et al., 2013). Beyond precipitation, other climatic variables also influence the stability of disturbed forests. Reduced evapotranspiration after deforestation increases sensible heat and raises surface temperatures. Additionally, lowered surface roughness

suppresses turbulent mixing, further warming the surface (Baldocchi and Ma, 2013; Winckler et al., 2019) and enhancing horizontal near-surface winds (Lawrence and Vandecar, 2015; Sampaio et al., 2007; Spracklen and Garcia-Carreras, 2015). Given that tropical species are adapted to a stable climate within a narrow temperature range (Janzen, 1967; Wright et al., 2009; Perez et al., 2016), both elevated mean temperature and temperature variability can heighten their vulnerability. Strong winds may also hinder forest regrowth, as young trees with shallow roots and fragile stems are particularly susceptible to wind damage. Despite their ecological significance, extremes have not been a focus in past studies for two main reasons. First, conventional climate models rely on convective parameterizations that are inappropriate to capture the fast, small-scale processes associated with extremes (Kendon et al., 2017; Jones and Randall, 2011). Second, the substantial decrease in annual mean precipitation simulated by these models, as I presented before, has overshadowed the need to explore extremes. This further highlights the need for a storm-resolving model to assess how deforestation reshapes not only average conditions but also the extremes.

2.4 CO_2-INDUCED WARMING

Another major threat to the Amazon comes from rising atmospheric CO_2 concentrations, which have led to significant regional warming. During the dry season, the Amazon has warmed at an average rate of 0.27°C per decade since the 1980s, exceeding 2°C over the past 40 years (Flores et al., 2024). If current trends continue, the region could experience more than 4°C of warming by 2050 (Marengo et al., 2018; Gatti et al., 2023). While changes in precipitation are expected to have accompanied this warming, no basin-wide trend has yet been detected (Marengo, 2004; Espinoza Villar et al., 2009; Satyamurty et al., 2010; Almeida et al., 2017). Nonetheless, concerns about an abrupt biome transition in the Amazon are intensifying as CO_2-induced warming may trigger a self-amplifying feedback in which reduced rainfall leads to lower evapotranspiration, which in turn suppresses rainfall even further. This feedback can be initiated by a weakening of oceanic moisture inflow into the basin. When the supply of oceanic moisture declines, less water is available for recycling through evapotranspiration, amplifying the reduction in precipitation (Zemp et al., 2017). It underscores the importance of understanding how Amazonian rainfall responds to changes in moisture convergence, particularly in the context of ongoing global warming.

To address these changes, modeling studies have been widely conducted. Although our understanding of large-scale tropical precipitation changes under warming is well established (Held and Soden, 2006; Chou et al., 2009; Seager et al., 2010; Muller and O'Gorman, 2011), regional projections, such as over the Amazon, remain highly uncertain (Joetzjer et al., 2013; Li et al., 2006). For example, under the RCP8.5 scenario, half of the 36 CMIP5 models project wetter conditions in the Amazon, while the other half predict drying (Boisier et al., 2015). This divergence is often attributed to differences in simulated oceanic-atmosphere feedbacks—particularly those related to internal variability and SST patterns (Joetzjer

et al., 2013; Kent et al., 2015). Such variability strongly affects moisture convergence, which in turn drives rainfall changes. While CMIP6 models exhibit a more consistent drying signal over the Amazon (Cook et al., 2020; Ukkola et al., 2020), concerns remain about the reliability of this agreement. Much of the projected drying stems from a consistent El Niño–like SST warming pattern across the tropical Pacific (Parsons, 2020). However, CMIP6 models continue to exhibit systematic sea surface temperature (SST) biases—especially in regions crucial for Amazon rainfall, such as the tropical Pacific (Ying et al., 2024). This raises a question of whether the drying consensus reflects a real climate signal or merely a common model bias (Tierney et al., 2015). Additional uncertainties arise from structural limitations in the models themselves, particularly their reliance on convective parameterizations (Stevens and Bony, 2013; Richter et al., 2012), which influence both rainfall amount and spatial distribution.

These challenges highlight the need for next-generation models that can reduce structural uncertainties. Storm-resolving models, which explicitly simulate convection without relying on parameterization, offer a promising path forward. To my best knowledge, only two studies have used a storm-resolving model to investigate Amazon precipitation under increased CO_2, but not yet sufficient to fully address the question. For example, Rehbein and Ambrizzi (2023) focuses on the changes in the frequency of mesoscale convections under warming, missing the information about how total precipitation changes. Another study, Kahana et al. (2024), projects drying Amazon with a regional climate model, but their model is constrained by boundary conditions from a conventional global model that also simulates drying. As a result, their findings are not entirely independent of the parameterization biases it aims to overcome. All in all, it highlights the need to examine changes in annual mean precipitation using a global storm-resolving model.

Complementary to global storm-resolving models, atmosphere-only simulations (AMIP) provide a valuable framework for isolating the atmospheric response to CO_2-induced warming. By prescribing SSTs, AMIP experiments eliminate ocean and atmosphere feedbacks, thereby reducing uncertainties associated with SST pattern changes (Bony et al., 2013; Shaw and Voigt, 2016; Chadwick et al., 2019; Mutton et al., 2024). These simulations are also particularly well-suited for decomposing the CO_2-induced warming into two key components that influence precipitation over the land: radiative effects from increased CO_2 and remote ocean warming. Before the ocean is mediated to increase CO_2, local radiative warming affects atmospheric stability and reduces relative humidity (Joshi et al., 2008; Lambert et al., 2011; Byrne and O'Gorman, 2013) to influence regional rainfall. In a longer time-scale, land precipitation can be influenced by ocean warming, as enhanced temperature gradient between land and ocean (Joshi et al., 2008) modifies the large-scale circulation. Hence, these radiative and SST warming effects can be separated not only by their physical origins, but also by their response times: radiative effects correspond to a fast adjustment of the atmosphere, while SST warming represents a slower, ocean-mediated response. To disentangle two aspects of CO_2-induced warming, we compare two AMIP simulations: (1) one with quadrupled CO_2 and prescribed present-day SSTs (4CO2) to isolate the fast radiative response,

and (2) another with uniform +4 K SST warming under fixed preindustrial CO_2 (P4K) to capture the slow ocean-mediated response. These simulations enable us to identify the dominant physical mechanisms driving land precipitation between these two CO_2-induced warmings. While it has been successfully applied in regions such as West Africa (Mutton et al., 2024) and South Asia (Endo et al., 2018), it remains unexplored over the Amazon.

All in all, we bring together these two methodological advances—global storm-resolving coupled simulations and AMIP experiments with separated fast and slow responses—to investigate the changes in Amazonian rainfall under different warming by elevated CO_2 concentration. The feedback loop triggered with moisture convergence needs to be considered to explain precipitation changes under warming through changes in two primary components of the Amazonian rainfall: evapotranspiration and moisture convergence (see Section 2.2). This framework allows us to assess whether rainfall changes are amplified by changes in moisture convergence in a warm world, and to what extent these processes govern the overall precipitation response.

2.5 RESEARCH QUESTIONS

Based on literature reviews, we first hypothesize that results under deforestation might be highly influenced by deficiencies in conventional models. In addition, our understanding of how the rainfall over the Amazon responds to CO_2-induced warming remains unclear. One of the main limitations in previous studies is the wrong representation of convective processes stemming from convective parameterization. To tackle this common limitation, we need a global storm-resolving model that no longer uses convective parameterization. For this, I use the ICOsahedral Nonhydrostatic model, one of the global storm-resolving models developed by the German Weather Service and the Max-Planck-Insitute for Meteorology (ICON, Giorgetta et al., 2018). With this powerful tool, I am going to tackle three research questions.

- RQ1. Does Amazonian annual mean precipitation decrease until it hinders forest regrowth after complete deforestation in a storm-resolving global model?
- RQ2. How do Amazonian extreme events change under complete deforestation?
- RQ3. How does CO_2-induced warming alter the hydrological balance of the Amazon, and what physical processes are responsible?

3

MUTED AMAZON RAINFALL RESPONSE TO DEFORESTATION IN A GLOBAL STORM-RESOLVING MODEL

Does Amazonian annual mean precipitation decrease until it hinders forest regrowth after complete deforestation in a storm-resolving global model?

As I summarized in Figure 2, GCMs tend to show a large reduction with a uniform spatial pattern, and RCMs show less reduction with a dipole pattern. However, these are results based on climate models with convective parameterization and/or fixed large-scale circulation, which may misrepresent physical processes. I will present here the results answering the first question with ICON, a global storm-resolving model, which overcomes these limitations.

Simulations are done in a configuration of an atmosphere-only with 5 km horizontal resolution and 90 vertical levels up to an altitude of 75 km same as Hohenegger et al. (2023). Convective parameterization is switched off, but it still uses parameterizations for turbulence, cloud microphysics, and radiation. The land model is the Jena Scheme for Biosphere-Atmosphere Coupling in Hamburg version 4 with "lite" configuration, which has five soil layers, as in Hohenegger et al. (2023). With this setup, I run a control (CTL) and a completely deforested (DEF) experiment to investigate the effect of deforestation. The complete deforestation scenario is implemented by switching the biophysical parameters of the land surface from forest to pasture (Table 1) within the Amazon forest, reproducing previous studies on Amazon deforestation. The deforested values for the biophysical parameters were chosen according to those past studies. The experiments are initialized on 20 January 2020 from the European Center for Medium Range Forecasting (ECMWF) Integrated Forecasting Model (IFS) (Malardel et al., 2016; Wedi, 2014) analysis and integrated for 3 years. This work is published in Geophysical Research Letter (Yoon and Hohenegger, 2025, see Appendix A).

Parameters	Forest → Pasture
Albedo	0.12 → 0.18
Leaf Area Index	8.40 → 2.70
Vegetation fraction	0.92 → 0.85
Roughness length (m)	1.80 → 0.05
Root depth (m)	1.33 → 0.60
Forest fraction	0.86 → 0.00

Table 1: The values for the forest are an average of the grid point values from JSBACH over the Amazon, and the values for pasture are taken from a table in Gandu et al. (2004), which is based on their values from multiple previous studies. The value for the root depth is from Correia et al. (2008), as this gives a larger difference to the forest case given the small root depth of the forest in JSBACH (1.3 m against 4.0 m in Gandu et al. (2004)). The table only includes the values of the parameters that we directly changed, not all the parameters that could potentially be changed by these changes, such as stomatal conductance.

3.1 LESS SENSITIVE TO EVAPOTRANSPIRATION

The ICON simulation shows a markedly different response to Amazon deforestation compared to previous studies. I update Figure 2 with ICON results (Fig. 3). First, ICON shows a much smaller reduction of -0.27 mm day^{-1} – corresponding to 4% of the pre-deforested value – than the GCM and RCM studies. This difference is even more pronounced in the spatial pattern, showing opposite patterns. Most previous studies show a homogeneous precipitation reduction in GCM studies or a drier-west and wetter-east pattern in RCM studies. In contrast, ICON exhibits the opposite – wetter-west and drier-east pattern.

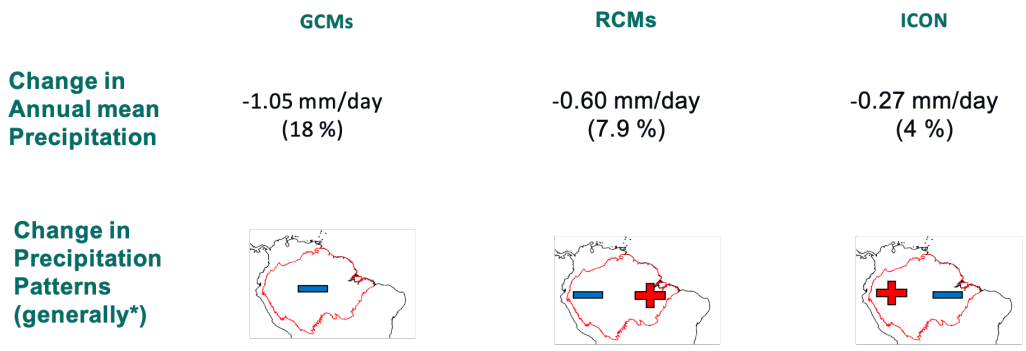

Figure 3: Summary of GCMs, RCMs, and ICON studies.

To further examine these differences, we look at the relationship between changes in evapotranspiration and precipitation from available previous GCM, RCM studies, and ICON (Fig. 4). While previous GCMs and RCMs show a linear relationship between evapotranspiration loss and precipitation loss, ICON lies outside this range. Despite a large reduction in evapotranspiration, precipitation changes are minimal, suggesting that precipitation simulated from the ICON is less sensitive to evapotranspiration. But what compensates for the large reduction from evapo-

transpiration?

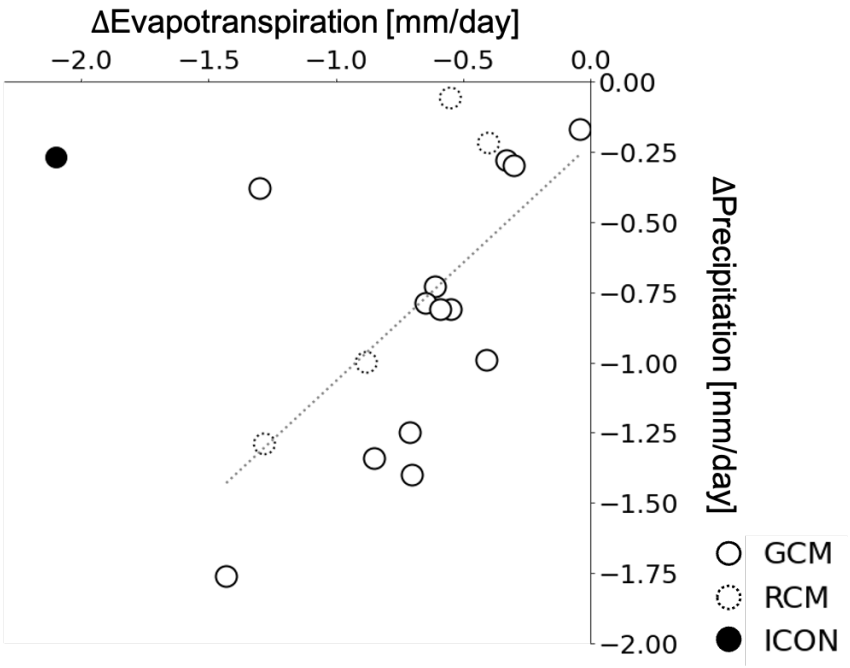

Figure 4: Scatter plot of changes in mean evapotranspiration versus changes in mean precipitation from available previous studies, distinguishing between GCMs and RCMs, and ICON. The linear regression derived from past studies is represented by a dashed line. Studies without evapotranspiration information (see Table S1 in Appendix A) are omitted. Spatial averages over the Amazon only.

3.2 INCREASED MOISTURE CONVERGENCE

According to the moisture balance equation, a weaker precipitation response can be explained by increased moisture convergence. In ICON, increased moisture convergence offsets reduced evapotranspiration, maintaining near-constant annual precipitation. This is evident in the spatial distribution of the moisture balance components (Fig. 5). Precipitation exhibits a seasonal dipole pattern: increased rainfall over the northwestern Amazon during the dry season, and over the southern Amazon during the wet season. Among the sources of moisture, only moisture convergence mirrors this dipole as evapotranspiration declines uniformly across the basin. What explains this dipole in moisture convergence?

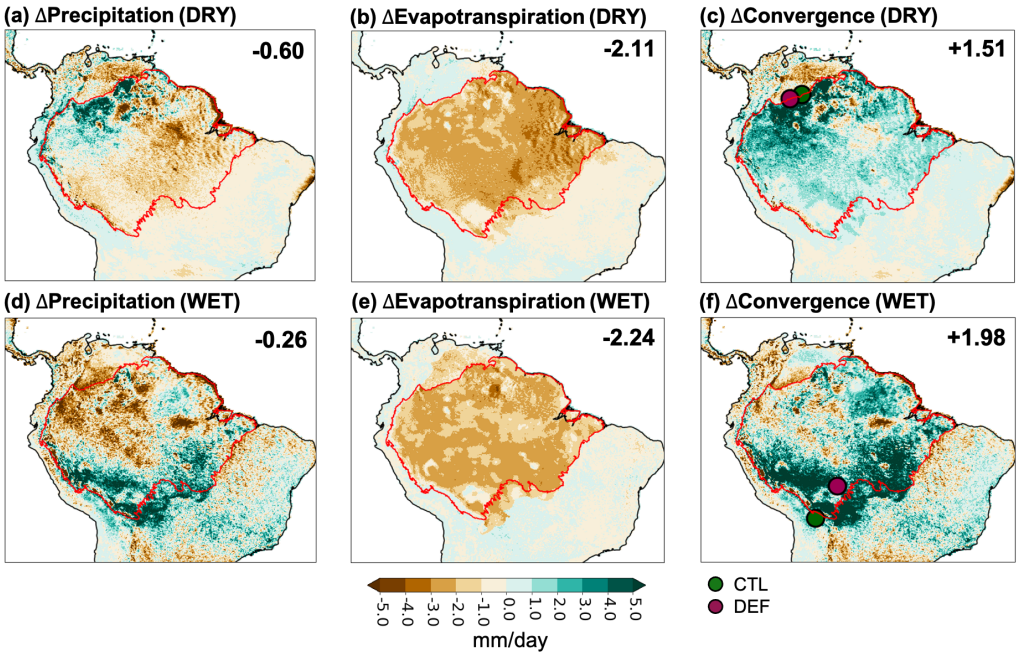

Figure 5: Maps (all in mm day^{-1}) of the changes in each component of the atmospheric moisture budget after deforestation (DEF-CTL) for (a–c) dry (JAS), and (d–f) wet (DJF) seasons. The filled circles in (c, f) indicate the location of the center of the rainbelt in CTL (dark green) and DEF (dark magenta). Numbers (mm day^{-1}) denote the mean changes over the Amazon region.

Looking back at Figure 5c and f, moisture convergence increases over regions aligned with the climatological rainbelt, as indicated by dots showing the centroid of the top 10% of rainfall over the tropical South America (30°S-13°N, 82°W-30°W). These locations correspond to the seasonal ITCZ position, suggesting that the convergence increase is tied to shifts or intensification of the ITCZ. In short, precipitation increases where convergence strengthens along the existing rainbelt, indicating a reinforcement of the pre-deforestation convergence pattern.

To explore the circulation changes underlying this convergence, we analyzed winds and geopotential height at 1,000 hPa and 700 hPa. Near the surface (Fig. 6a, b), reduced evapotranspiration raises the mean 2 m temperature by 4.57 K in the dry and 3.33 K in the wet season. This induces a surface heat low, enhancing moisture advection from the Atlantic and vertical motion over the Amazon. Additionally, reduced roughness length due to deforestation also leads to an enhancement of the horizontal 10 m winds. The surface response is consistent with previous RCM studies (Hahmann and Dickinson, 1997; Nobre et al., 2009; Da Silva et al., 2008; Lejeune et al., 2015) and explains the drier-west and wetter-east pattern, but not the zonally elongated and strong anomalies in the northern and southern Amazon.

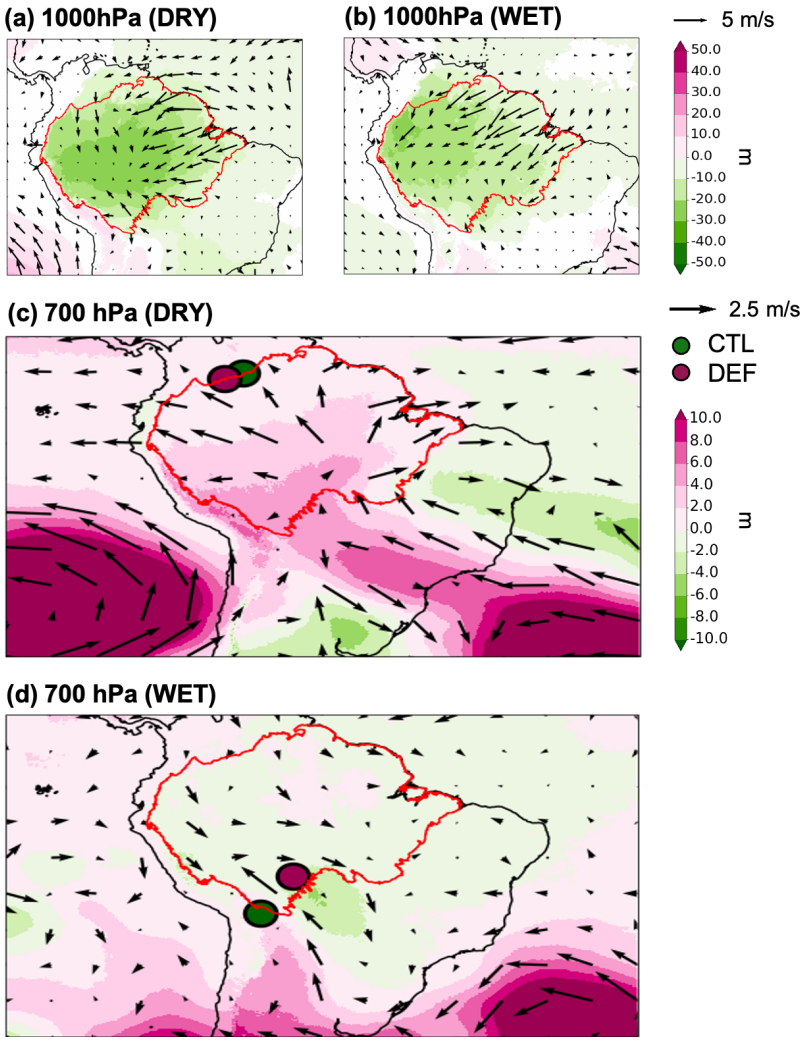

Figure 6: Maps of changes in geopotential height (m) and wind ($m\,s^{-1}$) in dry (JAS) and wet (DJF) seasons after deforestation (a), (b) at 1000 hPa, and (c), (d) at 700 hPa. The filled circles show the location of the centroid of the rainbelt in each simulation.

At 700 hPa, changes in large-scale circulation become more apparent. During the dry season, the easterly flow develops a stronger northward component, enhancing convergence over the northern Amazon (Fig. 6c). This shift is linked to changes in geopotential height and a westward displacement of the SASA (compare with SASA in Fig. 1a), creating a stronger pressure gradient inside the Amazon, accelerating the wind. Meanwhile, the SASA's subsidence suppresses convection over the southeastern Amazon, despite enhanced surface inflow. During the wet season (Fig. 6d), convergence strengthens over the southeastern Amazon and along the Andes. While displacement of SASA is less pronounced in the wet season, an expanded high-pressure area over the southern Amazon blocks the southward flow (Fig. 1b) and induces a northward anomaly, enhancing convergence in the southern Amazon.

In sum, the large-scale circulation response at 700 hPa—driven by surface heating and modified pressure gradients—explains the spatial pattern of increased moisture convergence and precipitation in ICON. This mechanism differs from that proposed by RCM studies and emphasizes the role of remote, dynamically driven convergence rather than solely local land–atmosphere feedbacks, which is the only mechanism in conventional GCM studies. Therefore, my results suggest that a global storm-resolving model allows other processes, which are often masked out by the strong impact of evapotranspiration due to convective parameterization.

4

EXTREME EVENTS IN THE AMAZON AFTER DEFORESTATION

How do Amazonian extreme events change under complete deforestation?

The insignificant reduction in the Chapter 3 contradicts the classification of the Amazon rainforest as a climate tipping element. Does it mean that Amazon is unharmed after a complete deforestation? Using the same simulation as the first study, I check the changes in the tail of hourly precipitation in response to deforestation and analyze the underlying mechanisms. Additionally, I will also address temperature changes and wind changes. I addressed the results in detail in a manuscript submitted to the Earth System Dynamics (Yoon et al., 2025, see Appendix B).

4.1 VIOLENT RAINS

To assess changes in rainfall intensity following deforestation, we examine hourly precipitation over the Amazon. Figure 7 shows the distribution of hourly precipitation in the Amazon basin for both the CTL and DEF simulations. Across three simulation years, intense hourly precipitation occurs more frequently in the deforested case (Fig. 7a). To better visualize, we categorize hourly preciptiation into five intensity levels based on the WMO classification (2018): "No rain", "light" rain (0-2.5 $\mathrm{mm\,hr^{-1}}$), "moderate" rain (2.5–10 $\mathrm{mm\,hr^{-1}}$), "heavy" rain (10–50 $\mathrm{mm\,hr^{-1}}$), and "violent" rain (more than 50 $\mathrm{mm\,hr^{-1}}$). After deforestation, the frequency of both "no rain" and "violent rain" increases substantially – nearly tripling and rising by 1.5 times, respectively (Fig. 7b). On the other hand, light rain, which constitutes the majority of rainfall events, remains largely unchanged, explaining why mean precipitation does not significantly differ (Chapter 3).

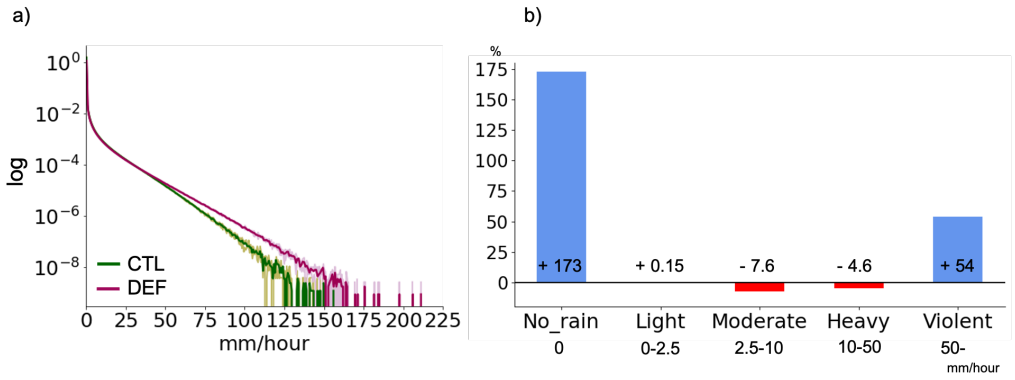

Figure 7: Distribution of hourly precipitation [mm hr^{-1}] over the Amazon basin before and after deforestation. (a) The logarithmic probability density function of hourly precipitation rates across all Amazonian grid points. Dark green and dark magenta for CTL and DEF, respectively, using all three years (2020-2022), lighter colors for each year separately. (b) Percentage change (written in numbers, %) in frequency for different intensity categories.

To investigate the mechanisms behind the increase in violent rain events, we follow a schematic framework (Fig. 8) that attributes changes in extreme rainfall (> 50 mm hr^{-1}) to two key factors: atmospheric moisture (total column water vapor, TCW) and vertical ascent (updraft strength at 500 hPa, W_{500}) (Trenberth, 1999; O'Gorman and Schneider, 2009; Allan and Soden, 2008; Lenderink and Van Meijgaard, 2008; Liu et al., 2009; Muller et al., 2011). Figure 9a shows the distribution of violent hourly precipitation in the control simulation (CTL), binned by TCW and W_{500}. As expected, more intense rainfall is associated with higher TCW and stronger updrafts. To assess what drives the intensification of violent rain after deforestation, Figure 9b presents the differences in TCW and W_{500} between CTL and DEF. The results show that enhanced vertical velocity primarily explains the increase in precipitation intensity, while TCW remains largely unchanged within the 50–60 mm range.

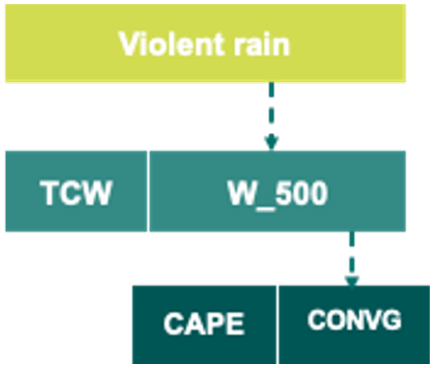

Figure 8: Schematic for the mechanism of increased violent rain events. Total column water vapor (TCW) and vertical velocity at 500hPa (W_{500}). Convective Available Potential Energy (CAPE) and moisture convergence (CONVG). The arrows show the flow of the mechanism that causes violent rain.

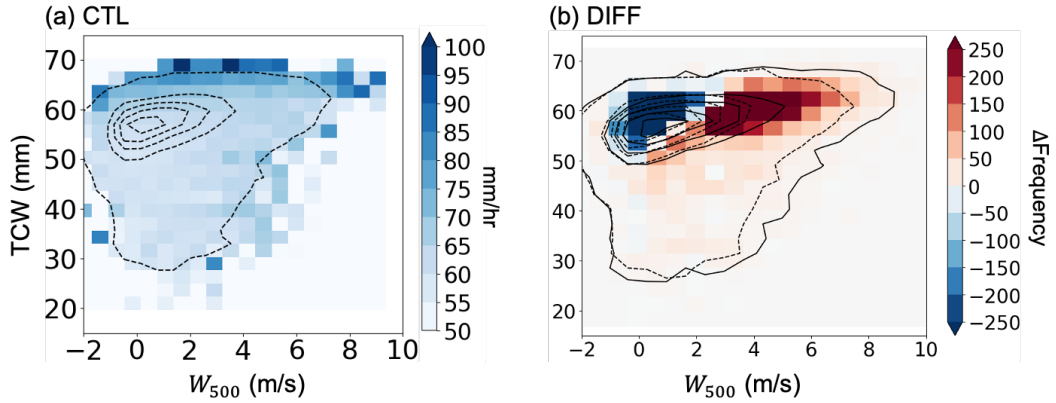

Figure 9: The mean intensity of hourly precipitation [mm hr^{-1}] only in violent events, averaged within each bin (shaded) ordered by Total Column Water (TCW) and vertical velocity at 500hPa (W_{500}) for (a) CTL. Dashed contours represent the frequency of TCW and W_{500} occurrences, with contour levels at 100, 500, 1000, 1500, and 2000; the innermost contour corresponds to the highest frequency. (b) Shading shows the difference in frequency (DEF minus CTL) for TCW and W_{500} within each bin. Dashed (CTL) and solid (DEF) lines indicate the frequency distributions overlaid for comparison.

We then, following Figure 8, investigate whether stronger updrafts result from changes in local atmospheric instability and/or in large-scale convergence (Davies et al., 2013; Loriaux et al., 2017). To assess local instability, we used Convective Available Potential Energy (CAPE) conditioned on violent rain events. After deforestation, CAPE values decrease (Fig. 10a), indicating that the enhancement in updraft strength is not driven by an increase in local atmospheric instability. This reduction in CAPE is linked with drier near-surface conditions, which raise the lifting condensation level and level of free convection, thereby suppressing instability. On the other hand, Convective Inhibition (CIN) increases, with the mean value rising from 27 J kg^{-1} to 111 J kg^{-1} (Fig. 10b). The more inhibited environment makes convective initiation less likely, helping to explain the rise in no-rain events.

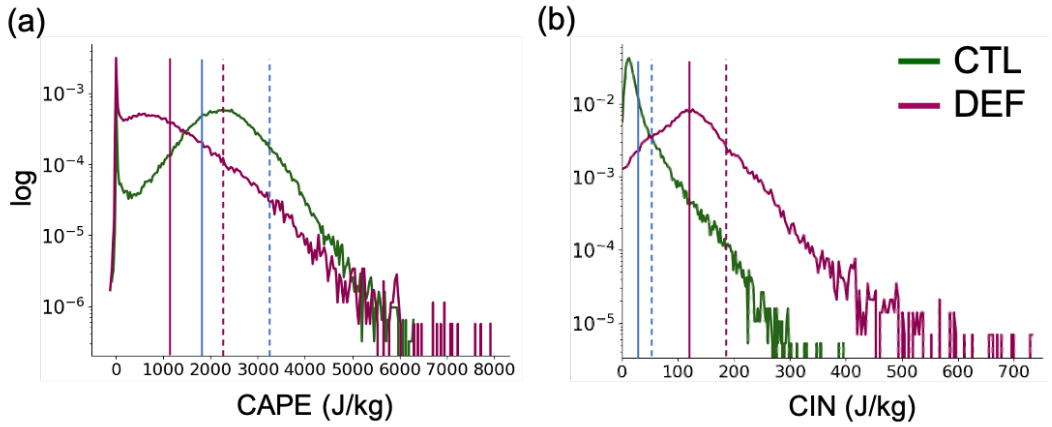

Figure 10: CAPE [J kg^{-1}] one hour before violent precipitation over the Amazon and CIN [J kg^{-1}] from all events. The logarithmic probability density function of (a) CAPE and (b) CIN is represented with the mean (solid vertical lines) and the 99th percentile (dashed vertical lines). The PDF is derived from all grid cells and all time steps. CTL is in dark green, and DEF is in dark magenta.

We now attribute the increase in updraft strength to enhanced moisture convergence. The strength of convergence one hour before violent rain events increases after deforestation (Fig. 11a). Also, the regions experiencing more violent rains (shading in Fig. 11b, c) coincide with regions of stronger convergence (contours in Fig. 11b, c), separating in dry (JAS) and wet (DJF) seasons respectively (Fig. 11b, c). Given that the spatial pattern of stronger moisture convergence aligns with the location of the rainbelt in the corresponding season, violent precipitation appears to be more closely linked to large-scale moisture convergence. All in all, the environment becomes less favorable to convect thermodynamically, requiring a stronger dynamical driver to precipitate (see flows of arrows in Fig. 8).

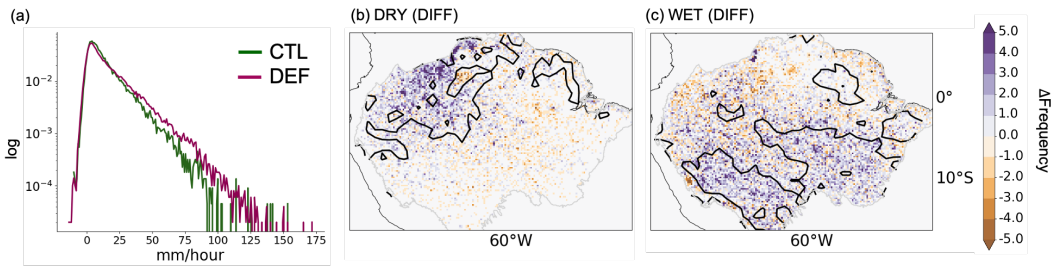

Figure 11: (a) Logarithmic probability density function of moisture convergence one hour before violent precipitation events over the Amazon, shown for CTL (dark green) and DEF (dark magenta). (b, c) Differences in the frequency of violent precipitation events between DEF and CTL (DEF minus CTL) at each grid point (shading). The area with a positive anomaly of convergence is defined as the grid points where moisture convergence exceeds the same threshold, 90th percentile of CTL values, and shows a positive anomaly in DEF (contour lines) in (b) the dry season and (c) the wet season.

4.2 HEAT STRESS

Deforestation leads to an annual mean increase of 3.84 °C in 2 m temperature across the Amazon, with warming occurring throughout the day and an enhanced diurnal temperature range. This warming is primarily driven by increased sensible heat flux and reduced latent heat flux, despite a net decrease in surface radiation due to its increased albedo. As a result, the deforested surface remains warmer than the control throughout the day, consistent with findings in tropical regions (Schultz et al., 2017). Additionally, day-to-day temperature variability increases by an average of 0.4 °C, indicating more pronounced fluctuations in daily mean temperature after deforestation.

Based on its temperature change, we further evaluate thermal stress on humans using seven heat stress indices (see Methods in Appendix B): apparent temperature (AT), NOAA heat index (HI), humidex (Hu), simplified wet-bulb globe temperature (T_{WBG_s}), indoor wet-bulb globe temperature (T_{WBG}), wet-bulb temperature (T_{WB}), universal thermal climate index (UTCI). We calculate indices with full spatiotemporal data over the Amazon, six out of seven indices show a clear shift toward higher stress levels (Fig. 12). Median values of AT, HI, Hu, and UTCI all rise from moderate to strong discomfort, while T_{WBG_s} indicates an increase in required rest periods from 50% to 75% per hour, implying reduced work capacity. Only T_{WB} shows a slight decrease, as lower humidity partially offsets higher temperatures. Overall, the results consistently point to heightened thermal discomfort, increased health risks, and reduced labor productivity due to deforestation.

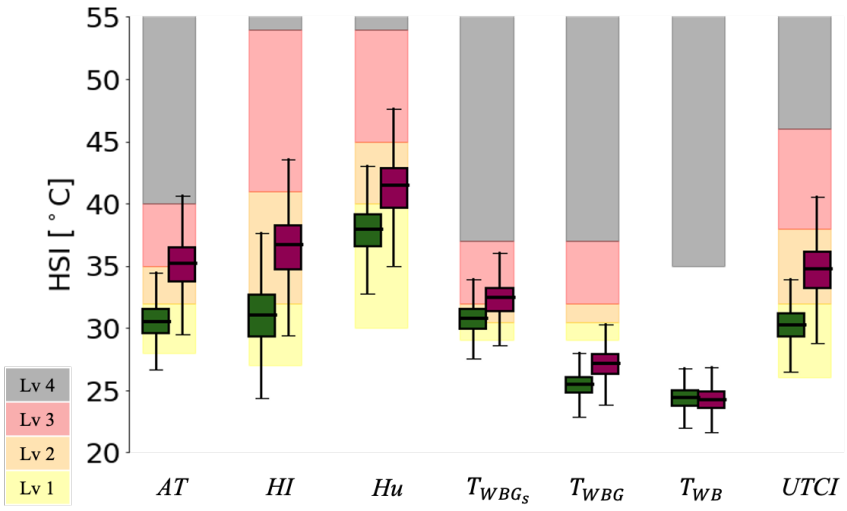

Figure 12: Box-and-whisker plots of heat stress indices (HSI), showing the mean, interquartile range (25-75th percentiles), and whiskers (10-90th percentiles): AT, HI, Hu, T_{WBG_s}, T_{WBG}, T_{WB}, UTCI. The background colors show the range of discomfort for each level following Table S1 from Schwingshackl et al. (2021). Yellow shows the range between levels 1 and 2, orange is between 2 and 3, red shows between 3 and 4, and grey is above level 4. Descriptions of indices and levels are given in the Method section (Appendix B).

4.3 DAMAGING WINDS

Lastly, we investigate how near-surface wind changes after deforestation. The 10 m wind speed increases from a mean value of 0.93 $m\,s^{-1}$ to 3.12 $m\,s^{-1}$, and in particular the 99th percentile rises from 3.36 $m\,s^{-1}$ to 8.45 $m\,s^{-1}$. Previous studies have shown that the increase in mean wind speed is a direct result of the decrease in roughness length (Sud et al., 1988) and an intensification of the large-scale circulation after deforestation (Yoon and Hohenegger, 2025). However, beyond that, the increase in hourly precipitation, identified in section 4.1, opens up the possibility of having additional strong winds due to the downdrafts associated with violent rain (Garstang et al., 1998; Windmiller et al., 2023).

To isolate the contribution of downdrafts from that of surface roughness and background circulation to the increase in 10 m wind speeds after deforestation, we apply the Alpert–Stein factor separation method (Stein and Alpert, 1993). Since we lack simulations with fixed surface roughness, we group background circulation and roughness effects together as R/C, and denote downdraft-related effects as D. We classify events into 'no-light rain' (no rain + light rain) and 'violent rain' for both CTL and DEF simulations (Table 2). Wind changes during no-light rain primarily reflect R/C, while changes during violent rain in DEF include R/C, D, and their synergy (R/C & C).

Table 2: The categories of simulations and rain types to disentangle the impact of Roughness length/ background Circulation (R/C), Downdraft (D), and its synergy impact (R/C & D) on windspeed in DEF compared to CTL. The impact of each component is represented with f(0): CTL, f(R/C): roughness length/ background circulation, f(D): downdraft, and f(R/C & D): synergy between R/C and D. Values are in units of $m\,s^{-1}$.

Simulation	Rain type	Abbrv.	value
CTL	No-Light rain	f(0)	0.92
DEF	No-Light rain	f(0)+f(R/C)	3.11
CTL	Violent rain	f(0)+f(D)	1.40
DEF	Violent rain	f(0)+f(R/C)+f(D)+f(R/C,D)	4.56

The mean wind speed in CTL during no-light rain is 0.92 $m\,s^{-1}$, whereas it is 3.11 $m\,s^{-1}$ in DEF, indicating a contribution of 2.19 $m\,s^{-1}$ from changes in R/C due to deforestation (f(R/C) in Table 2). In CTL, during violent rain, the mean wind speed is 1.40 $m\,s^{-1}$. The difference to the no-light rain case is 0.48 $m\,s^{-1}$, and this represents the contribution from D (f(D)) in an unchanged environment. This comparison indicates that the impact of R/C alone due to deforestation is significantly larger than the impact of downdrafts under control conditions. The wind speed of violent rain is 4.56 $m\,s^{-1}$ in DEF, and it contains both the effect of R/C and of the synergy of R/C and D compared to the violent rain in CTL. This gives a synergy effect of 0.97 $m\,s^{-1}$. In summary, the relative contributions to the total wind speed anomaly (f(R/C)+f(D)+f(R/C,D)) are 60% R/C, 13% D, and 27%

synergy. These results suggest that deforestation enhances surface wind not only by altering surface properties and circulation but also by intensifying downdrafts during violent rain.

5

AMAZON PRECIPITATION UNDER WARMING FROM THE PERSPECTIVE OF THE MOISTURE BALANCE EQUATION

How does CO_2-induced warming alter the hydrological balance of the Amazon, and what physical processes are responsible?

Previous studies show weak agreement on how precipitation over the Amazon responds to CO_2-induced warming, and the underlying mechanisms remain poorly understood. Although CMIP6 models exhibit a stronger consensus—projecting drying over large parts of the Amazon—this agreement is often attributed to a common tropical Pacific SST response resembling an El Niño–like pattern. However, it remains unclear whether this consistent response arises from a robust physical mechanism or shared structural biases across models, such as similar convective parameterizations. To address these limitations, I use the ICON model simulations configured in two different ways: (1) fully coupled atmosphere-ocean simulations, and (2) atmospheric-only simulations following the AMIP protocols.

Coupled simulation belongs to the fourth cycle of model development within the Next Generation of Earth Modelling Systems (Segura et al., 2025). It uses 5 km resolution in the ocean, and 10 km resolution in the atmosphere and land, with 90 vertical levels. The land surface model is the Jena Scheme for Biosphere-Atmosphere Coupling in Hamburg (JSBACH, Reick et al., 2021). JSBACH includes five vertical soil layers, of which we consider only the top three in our Amazon-focused analysis, only including the root zone. Biogeochemical processes, including dynamic vegetation, photosynthesis, and carbon and nitrogen cycles, are not included in the simulations. The ocean model is ICON-O (Korn et al., 2022) for the coupled simulation. Further information about model settings can be found in Segura et al. (2025) Appendix A. Simulations follow the SSP3-7.0 warming scenario from 2020 to 2049. After excluding a spin-up period (2020-2023), we analyze two periods to assess the impact of increasing CO_2: averaged value in the beginning of five years from 2024-2028, and the end of five years from 2045-2049.

The AMIP simulations are run at 10 km horizontal resolution over the atmosphere and land, with 90 vertical levels. They span 14 years in common (1980-1993). Prescribed SST and sea ice are from a merged product based on HadISST1 and NOAA OI.v2 datasets. With this setup, three simulations are conducted: 1) CTL, the control simulation with prescribed monthly SST and pre-industrial CO_2 levels, 2) 4CO2, a simulation with quadrupled CO_2 with prescribed SST. Direct CO_2 effect includes both the direct atmosphere heating by increased CO_2 and part of land warming due to direct response to increased CO_2, 3) P4K, an experiment with a uniform SST warming by 4K, with preindustrial CO_2, to isolate the ocean warming effect. I addressed further details in Appendix C.

5.1 DRIER AMAZON IN A COUPLED, WETTER AMAZON IN AMIP SIMULATIONS

We begin by analyzing annual mean precipitation over the Amazon. In the present-day climate, the first five years of the coupled simulation produce lower precipitation (4.76 mm day^{-1}) compared to the AMIP CTL (6.73 mm day^{-1}). Under elevated CO_2 conditions, the coupled simulation shows a reduction of 0.3 mm day^{-1} (–6.21% relative to the first five years), with a 1.08 K surface warming over the Amazon. Precipitation generally declines throughout the year, except for slight increases in February, August, and September, though these are not statistically significant as precipitation changes are still within the standard deviation (Fig. 13). On the other hand, both AMIP simulations show an increase in annual mean precipitation by 0.27 mm day^{-1} (+4%) for 4CO2 and 0.14 mm day^{-1} (+2%) for P4K with 0.42 K and 4.71 K of warming, respectively. On a monthly scale, 4CO2 shows consistent precipitation increases year-round, while P4K exhibits stronger seasonality—enhanced precipitation during the wet (DJF) season and reduced rainfall during the dry (JAS) season.

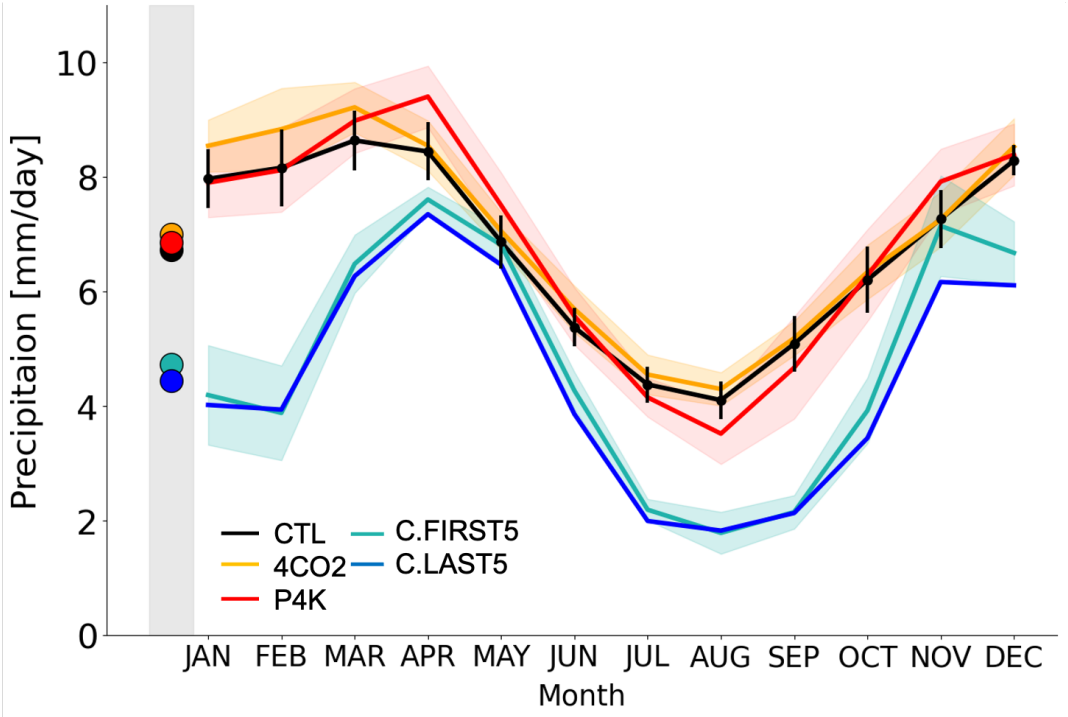

Figure 13: Monthly mean precipitation (mm day^{-1}) averaged over the Amazon region. Coupled simulations are represented in light blue (the first 5-year average, C.FIRST5) and dark blue (the last 5-year average, C.LAST5). AMIP simulations are represented by black (CTL), orange (4CO2), and red (P4K) lines. To account for the internal variability, the standard deviation range from CTL is shown with black vertical lines. Shaded areas indicate the corresponding variability ranges for the first 5-year average (blue), 4CO2 (orange), and P4K (red).

Using the atmospheric moisture balance, we separate the contributions of evapotranspiration and moisture convergence to precipitation changes. We also quantify

each contribution by normalizing the moisture budget terms by control precipitation written in numbers on the Table 3. The coupled simulation shows drying over the Amazon (-6.21%), mainly due to reduced evapotranspiration (-3.76%), with additional contribution from weaker moisture convergence (-2.45%). In contrast, both AMIP simulations show increased precipitation (+4.04% and +2.01%, respectively). In 4CO2, this is primarily driven by enhanced moisture convergence (+2.66%), while in P4K, increased evapotranspiration (+3.64%) dominates despite a reduction in moisture convergence (-1.64%). Overall, the AMIP simulations produce more rainfall over the Amazon, highlighting different underlying mechanisms depending on the different CO_2-induced warming.

Table 3: A table of percentage changes (%) in each component of the atmospheric moisture budget, normalized by precipitation from the control simulations ($\frac{\Delta Pr}{Pr} \times 100 = \frac{\Delta CONVG}{Pr} \times 100 + \frac{\Delta EVP}{Pr} \times 100$, Pr: precipitation, CONVG: moisture convergence, EVP: evapotranspiration). Values are expressed in percentages (%) and averaged over the Amazon region.

components	coupled	4CO2	P4K
ΔPr	-6.21	+4.04	+2.01
ΔCONVG	-2.45	+2.66	-1.64
ΔEVP	-3.76	+1.37	+3.64

5.2 FEEDBACK LOOPS IN THE MOISTURE BALANCE EQUATION

To explain the observed precipitation changes, we propose a feedback framework based on the moisture balance equation (precipitation = moisture convergence + evapotranspiration), initiating the loop from moisture convergence rather than evapotranspiration (Fig. 14). This choice reflects the fact that moisture supplied by moisture convergence directly affects precipitation and soil moisture, which then regulate evapotranspiration, whereas moisture supplied by evapotranspiration does not influence convergence. In the coupled simulation, reduced moisture convergence triggers a decline in precipitation, lowering soil moisture and further reducing evapotranspiration, reinforcing the initial drying through a positive feedback loop. A similar pattern is seen in 4CO2, where increased convergence enhances precipitation and maintains soil moisture and evapotranspiration. However, this feedback breaks in the P4K simulation: despite reduced moisture convergence, evapotranspiration and precipitation both increase. This broken feedback in P4K suggests a missing mechanism between soil moisture and evapotranspiration, which we explore next.

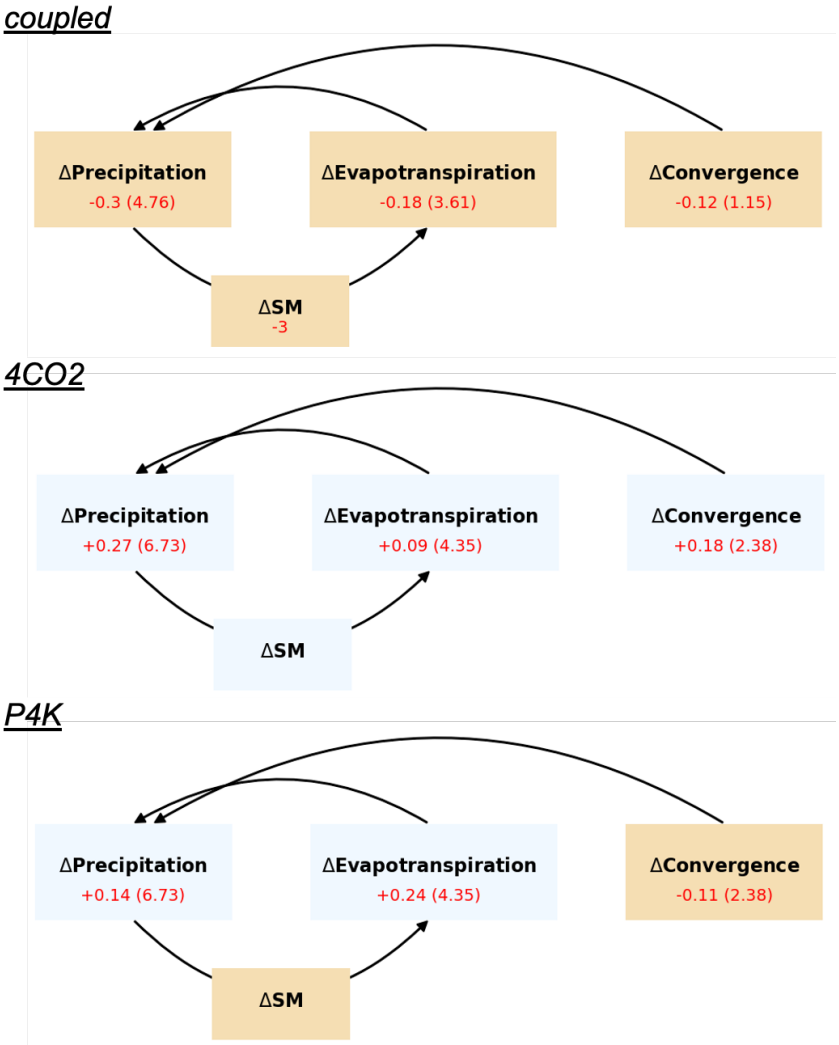

Figure 14: Schematic of feedbacks in the moisture balance equation for each simulation. Brown boxes indicate a decrease relative to their control condition, while blue boxes indicate an increase. Amazon-averaged changes in values (mm day^{-1}) are written in red, with corresponding control values provided in parentheses. Soil moisture (m) represents root-zone soil moisture averaged over the Amazon basin.

In the coupled simulation, root zone soil moisture declines by 3 mm. Since soil moisture outputs are unavailable for AMIP experiments (except CTL), we use evaporative fraction (EF, $\frac{\mathrm{LatentHeat}}{\mathrm{SensibleHeat+LatentHeat}}$) as a proxy, based on its Budyko-like relationship with root-zone soil moisture (Fig. 15). EF and soil moisture show a linear relationship within the transitional regime (EF in the range of 0.3–0.8), where the coupled simulation lies. Over time, EF in the coupled run decreases from 0.68 (a light blue dot) to 0.63 (a dark blue dot), indicating that evapotranspiration is sensitive to declining soil moisture and linked to reduced moisture convergence (Fig. 14). In contrast, both 4CO2 and P4K maintain high EF values (>0.8), suggesting that soil moisture remains sufficiently abundant to avoid limiting evapotranspiration. The slight EF increase in 4CO2 (a black →an orange dot in Fig. 15) supports the positive feedback loop involving increased moisture con-

vergence and evapotranspiration, while the small EF decrease in P4K (a black →a red dot in Fig. 15) aligns with modest soil moisture loss. However, in P4K, this reduction is not enough to constrain evapotranspiration, which is maintained—or even enhanced—through sufficient atmospheric drivers such as net radiation, vapor pressure deficit (VPD), and wind, which shows +11.4 $W\,m^{-2}$, +2.67 K, and -0.09 $m\,s^{-1}$ compared to CTL.

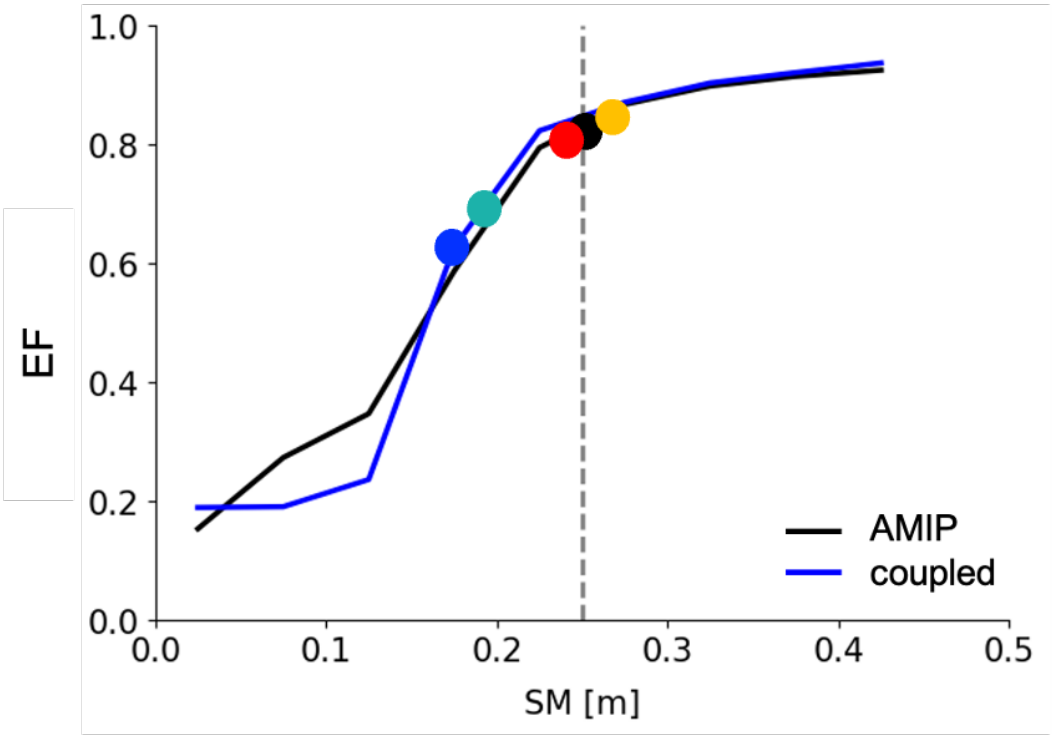

Figure 15: Relationship between evaporative fraction (EF) and root-zone soil moisture (m) for AMIP CTL (black line) and the first 5-year average of coupled simulation (blue line). The line represents the median EF within each bin with an interval of 0.05, based on daily values over the Amazon basin in the range of 0 to 0.5. Each dot shows the EF averaged over the Amazon from different simulations: light blue: C.FIRST5, dark blue: C.LAST5, black: CTL, orange: 4CO2, red: P4K.

Through these results, we learn that the level of soil moisture constrains the impact of moisture convergence on precipitation and differentiates the two feedback loops: when soil moisture is sufficient, evapotranspiration and precipitation can increase despite a reduction in moisture convergence.

6 CONCLUSIONS

What we observe is not nature itself,
but nature exposed to our method of questioning.

— Werner Heisenberg, 1958

As Heisenberg noted, "What we observe is not nature itself, but nature exposed to our method of questioning.", climate models define the lens through which we question complex processes. The shift from parameterized to storm-resolving models is not merely a technical advance, but a fundamental change in how we understand precipitation responses over the Amazon to deforestation and warming, as summarized below. Here, I will first answer three questions posed in section 2.4.

6.1 ANSWERING THE RESEARCH QUESTIONS

Does Amazonian annual mean precipitation decrease until it hinders forest regrowth after complete deforestation in a storm-resolving global model?

No, annual mean precipitation over the Amazon doesn't decrease enough to hinder forest regrowth. This weak sensitivity of precipitation to Amazon deforestation supports the general idea that conventional global climate models tend to overestimate land-atmosphere coupling, whereas a global storm-resolving model exhibits much weaker coupling strengths (see section 2.1). Our results show that the annual mean precipitation over the Amazon remains stable due to a strong negative circulation feedback. Deforestation alters the pressure system at 700 hPa, enhancing moisture convergence that compensates for reduced evapotranspiration. These circulation changes indicate that the induced annual mean precipitation changes do not necessarily render the system irreversible. Our results suggest that previous studies may have overestimated the risk of such a substantial rainfall drop due to model biases in their representation of land-atmosphere coupling.

How do Amazonian extreme events change under complete deforestation?

Hourly precipitation becomes more extreme, with both an increase in no rain and violent rain events. This shift is accompanied by a 4°C rise in average temperature, greater diurnal and seasonal variability, and a windier Amazon with the 99th percentile wind values more than doubled. These changes in hourly precipitation can increase the risk of droughts and floods. These changes pose serious challenges not only to the ecosystem but also to infrastructure and agriculture, ironically, the very sectors driving deforestation. The increased variability in temperature further exacerbates the vulnerability of tropical tree species, which are evolutionarily

adapted to stable climate conditions within a narrow temperature range (Janzen, 1967; Wright et al., 2009; Perez et al., 2016). In addition to ecological impacts, the increased temperature extremes increase human heat stress and low work productivity. Similarly, stronger surface winds may create unfavorable conditions for forest recovery and agriculture. Altogether, these findings highlight the need to examine the extremes, tails of precipitation, temperature, and wind distributions, which offer a stark warning about the escalating impacts of ongoing Amazon deforestation.

How does CO_2-induced warming alter the hydrological balance of the Amazon, and what physical processes are responsible?

The hydrological response of the Amazon varies depending on the type of CO_2-induced warming. An ocean-atmosphere coupled simulation under a warming scenario reveals a positive feedback: reduced moisture convergence leads to lower soil moisture, lower evapotranspiration, and ultimately decreased rainfall. In contrast, atmosphere-only simulations isolating the fast radiative and slow ocean warming effects both show increased precipitation, but through different feedback mechanisms. The fast radiative warming has a positive feedback: enhanced moisture convergence increases soil moisture, increases evapotranspiration, and further increases rainfall. This positive feedback is absent in the slow ocean warming simulation. In the ocean warming simulation, ample soil moisture sustains high evapotranspiration despite weaker moisture convergence. Answering the question, the hydrological balance and responsible physical processes differ by warming type. In atmosphere-only simulations that isolate warming according to its response time, precipitation is primarily driven by moisture convergence before the ocean warms, whereas evapotranspiration—sustained by sufficient soil moisture—becomes the key component to determine precipitation after ocean warming. These results highlight that the mechanisms controlling rainfall can shift with the timescales of the system's adjustment to increased CO_2.

These three works contribute to having a new perspective of the Amazon basin as the tipping element in response to two different human-induced disturbances. Regarding deforestation, I showed its impact from a global storm-resolving model for the first time. It uncovers the response to large-scale circulation feedback that enhances moisture convergences, compensating for reduced evapotranspiration. Increased moisture convergence has not been shown in previous studies, resulting in opposite conclusions about its annual mean precipitation. As a result, it flips our long-held belief that cutting down trees makes a deforested region irreversible, as precipitation decreases substantially following reduced evapotranspiration after complete deforestation. Yet it also encourages new questions about the resilience of the Amazon, moving beyond the conventional focus on annual mean precipitation to the tail of hourly precipitation, temperature, and winds. A storm-resolving model is also beneficial as it is finally able to capture the fast, small-scale processes related to extreme events. Regarding the impact of a warming world, we ex-

plored how Amazonian precipitation responds to different effects of CO_2-induced warming, using a feedback loop within the moisture balance equation. This study marks a step toward understanding Amazonian rainfall under warming by using a global storm-resolving model and separating the effects of radiative forcing and ocean warming based on their response times, alongside a coupled simulation. The feedback mechanism used for understanding Amazonian rainfall changes not only deepens our understanding of the processes driving precipitation changes but also suggests a potential tipping behavior, which I will explain in the outlook.

6.2 OUTLOOKS

Beyond my results, what questions can be asked further? I will close my thesis by raising three questions motivated by my findings.

First, Figure 4 shows that ICON has the largest reduction in evapotranspiration. However, this reduction is offset by increased moisture convergence, driven by large-scale atmospheric feedbacks. In contrast, most previous global climate model studies report little to no change in moisture convergence. This may suggest that conventional global climate models, unlike ICON, may fail to capture the same large-scale feedbacks. A key distinction between these model types is the use of convective parameterization. Hence, one may ask whether convective parameterization distorts the large-scale atmospheric response to land use change, such as pressure anomalies at 700 hPa. To investigate this, a useful approach would be to conduct a sensitivity experiment using ICON with convective parameterization enabled. This would allow a controlled comparison to evaluate how parameterization affects the strength and structure of large-scale circulation in response to land surface changes.

Next, in the third study, we separate the impact of CO_2-induced warming into two components based on response time: a fast radiative effect and a slow ocean warming effect. Our results show that moisture convergence shifts from a positive anomaly in the fast response to a negative anomaly in the slow response. Nevertheless, precipitation increases in both cases, sustained by increased evapotranspiration. This is possible because ample soil moisture allows evapotranspiration to remain high, even when moisture convergence declines in the ocean warming condition. However, this buffering capacity may not persist under continued ocean warming. If convergence continues to decline with progressive ocean warming (i.e., P4K, P5K, P6K, and so on), evapotranspiration could eventually decline. As less moisture is supplied by convergence, soil moisture may fall below a critical threshold, triggering an abrupt decline in precipitation. This hypothesis suggests that the land surface has a limited ability to buffer atmospheric drying. It raises an interesting question about whether continued ocean warming shows a nonlinear response, where declining moisture convergence eventually reverses the precipitation feedback?

Lastly, in reality, the Amazon faces simultaneous deforestation and CO_2-induced warming. Hence, one could wonder about their combined impacts. Based on my results, we can estimate the combined impact. To make it comparable among simulations, let's focus on atmosphere-only simulations. In response to the fast radiative CO_2 effect, moisture convergence increases. It has a positive feedback in the moisture balance equation that increases precipitation. Deforestation also increases moisture convergence, despite causing a substantial decline in evapotranspiration. This suggests that reduced evapotranspiration might be compensated by increased moisture convergence, preventing a significant drop in precipitation. However, under ocean warming, decreased moisture convergence may be offset by increased moisture convergence from the effect of deforestation. In such a case, the net change in moisture convergence might be negligible, and the resulting precipitation decline would be primarily driven by reduced evapotranspiration due to deforestation. This raises a question: can the effects of warming and deforestation be linearly combined? If so, does this imply that the combined response may initially show little change in precipitation, but eventually lead to a substantial decline as ocean warming progresses?

In closing my thesis, I hope these questions will inspire future studies using a range of different storm-resolving models, enabling us not only to explore the physical consistency through these questions but also the robustness between different storm-resolving models. Ultimately, the goal of better predicting the future Amazon should not stop at understanding its mechanism, but extend to meaningful action. As our tools improve and our knowledge deepens, so too does our responsibility to keep Amazon healthy—before it is too late.

Part II

APPENDIX

A

MUTED AMAZON RAINFALL RESPONSE TO DEFORESTATION IN A GLOBAL STORM-RESOLVING MODEL

The work in this appendix is published as:

Yoon, A., Hohenegger, C. (2025a): "Muted Amazon rainfall response to deforestation in a global storm-resolving model", In: *Geophysical Research Letters, 52(4), e2024GL110503.*

Author contributions:
AY: conceptualization; data curation; formal analysis; investigation; methodology; software; visualization; writing – original draft; writing – review and editing. **CH**: conceptualization; funding acquisition; investigation; project administration; resources; supervision; review and editing

Muted Amazon rainfall response to deforestation in a global storm-resolving model

Arim Yoon[1,2], Cathy Hohenegger[1]

[1]Max-Planck-Institut für Meteorologie, Hamburg, Germany
[2]International Max Planck Research School on Earth System Modelling, Max-Planck-Institut für Meteorologie, Hamburg, Germany

ABSTRACT

Ongoing Amazon deforestation has raised concerns about forest dieback via induced precipitation changes. Previous studies have found that complete deforestation reduces evapotranspiration, contributing to low precipitation rates that would limit the regrowth of the forest, but such studies have used climate models with convective parameterization and/or fixed large-scale circulation. For the first time, we simulate a complete Amazon deforestation scenario without convective parameterization, allowing full interaction between convection and large-scale circulation, for 3 years. Our results show no significant reduction in annual mean precipitation. Changes in the 700 hPa circulation and associated moisture convergence compensate for the reduction in evapotranspiration. These changes also lead to a north-south dipole pattern in the precipitation response during the dry and wet seasons. The uncovered dynamics suggest that Amazon mean precipitation may be more resilient to land surface perturbations than previously thought.

INTRODUCTION

Completely deforesting the Amazon forest is expected to lead to a significant reduction in Amazon precipitation (see references and numbers in Table S1). Although estimates vary among studies, the collective finding from previous Global Climate Models (GCMs) is an average reduction of 1.05 mm day^{-1}, equivalent to a reduction of 18% in annual mean precipitation. This reduction has led to the notion that past a certain deforestation threshold, not enough precipitation would fall to sustain the Amazon forest and the forest would die (Nobre et al., 1991; Lenton et al., 2008; Pires and Costa, 2013; Flores et al., 2024). The amount of deforestation required to reach such a tipping point is a matter of continuous debate (Avissar et al., 2002; Spracklen and Garcia-Carreras, 2015; Lejeune et al., 2015) and has led more recent studies on Amazon deforestation to focus on partial deforestation rather than complete deforestation (Sampaio et al., 2007; Pires and Costa, 2013; Swann et al., 2015; Alves et al., 2017; Wongchuig et al., 2023), combined with the effect of global warming (Ruv Lemes et al., 2023; Commar et al., 2023). Interpretation from observations also appears inconclusive (Tao et al., 2023; Boulton et al., 2022).

The main physical cause for the reduction in precipitation is the reduction in evapotranspiration. Replacing the rainforest uniformly with pasture leads to a uniform reduction in evapotranspiration and a uniform reduction in precipitation (Lean and Warrilow, 1989; Nobre et al., 1991; Dickinson and Kennedy, 1992; Lean and Rowntree, 1997; Gedney and Valdes, 2000; Da Silva et al., 2008). In addition,

from an energetic perspective, both the higher albedo of pasture and the reduction in water vapor in the atmosphere lead to a radiative heat loss. This favors subsiding motions over the Amazon forest, making it harder to convect (Neelin and Held, 1987; Eltahir, 1996).

Counteracting these effects, regional climate models (RCMs) have revealed a possible compensation mechanism (see references in Table S2). The increased warming over the Amazon following complete deforestation generates a heat low, leading to stronger moisture transport at the surface from the Atlantic Ocean into the Amazon forest. This enhanced moisture transport further benefits from the lower roughness length of pasture versus forest. As a consequence, precipitation reductions are weaker in RCMs than in GCMs, with an averaged value of 0.60 mm day^{-1}, about 7.88%. Concerning the spatial distribution of precipitation, the enhanced moisture transport leads to a dipole pattern with precipitation enhanced over the eastern and reduced over the western Amazon. Compared to GCMs, the finer grid spacing of RCMs allows them to better resolve topography and surface-induced mesoscale circulations, including sea breezes. However, the weaker precipitation reduction in RCMs has been called into question: it has been hypothesized to be an artifact related to the failure of RCMs to account for large-scale feedback due to their limited domain of integration (Lejeune et al., 2015; Medvigy et al., 2011). A reduction of convection over the Amazon could lead to a weakening of the large-scale circulation, further weakening convection, a feedback that would be absent in RCMs. This note of caution is understandable as the Amazon sits in the region where the trade winds converge. It is thus tied to the position of the intertropical convergence zone as well as of the large-scale circulation and of the pressure systems associated with it (Nobre and Shukla, 1996; Santos et al., 2017; Reboita et al., 2019).

The aforementioned results, including both GCM and RCM studies, have been obtained with climate models that represent convection using statistical-empirical approaches, often referred to as 'convective parameterization'. This is a consequence of their grid spacing being too coarse to explicitly represent convective storms by solving the underlying fluid-dynamical equations. There is a growing body of literature showing that precipitation in models using convective parameterizations may be overly sensitive to evapotranspiration, both compared to observations and to models that explicitly resolve convection (Hohenegger et al., 2009; Taylor et al., 2013; Hohenegger and Stevens, 2022; Lee and Hohenegger, 2024). Thus, the effect of reduced evapotranspiration on precipitation following deforestation may have been too strong in previous studies and may have masked the effect of other compensating mechanisms such as circulation — moisture transport — changes.

For the first time, we study the effect of complete Amazon deforestation on Amazon precipitation with neither the limitation of a convective parameterization nor of a regionally limited domain of integration. We use a storm-resolving configuration of the ICOsahedral Nonhydrostatic (ICON) model (Hohenegger et al., 2023) integrated with a horizontal grid spacing of 5 km, over the full globe for three years. We follow early studies on Amazon deforestation and run a control (CTL) and a complete deforestation (DEF) scenario, where the Amazon forest is replaced by pasture (see Methods and Table S3).We focus on the Amazon region and do not

discuss remote effects of Amazon deforestation, which, at least in coarse-resolution GCM studies, have been shown to exist (e.g. Medvigy et al., 2013).

METHODS

Model and simulations

We use the Sapphire configuration of the ICON model run in an atmosphere-only mode with 5 km horizontal resolution and 75 km model top (Hohenegger et al., 2023). The minimum and maximum tropospheric layer thicknesses are 25 m and 400 m. Schmidt et al. (2024) showed that there is no significant sensitivity to the chosen vertical grid spacing, whereas Hohenegger et al. (2020) showed no strong sensitivity of mean precipitation to the horizontal grid spacing. The ICON-Sapphire configuration allows us to resolve convection explicitly without using any convective parameterization and is called storm-resolving. The remaining needed physical parameterizations are the same as in Hohenegger et al. (2023), except that we don't use an ocean model. Sea surface temperature is prescribed with the climatology of PCMDI-AMIP 1.1.2 averaged from 1979 to 2016 (Taylor et al., 2000). The land model is the Jena Scheme for Biosphere-Atmosphere Coupling in Hamburg (JSBACH) version 4 with "lite" configuration, which has five soil layers, as in Hohenegger et al. (2023). CO_2 is prescribed to a value of 414 ppm to represent current conditions.

We run a CTL and a DEF experiment to investigate the effect of deforestation. The complete deforestation scenario is implemented by switching the biophysical parameters of the land surface from forest to pasture (Table S3) within the Amazon forest, reproducing previous studies on Amazon deforestation. We do so as we want to investigate the potential maximum effect of deforestation. The deforested values for the biophysical parameters were chosen according to those past studies (Table S3). Pasture has a higher albedo, which reduces the available net energy at the surface. The reduced root depth and leaf area index increase the stomata resistance and lead to reduced evapotranspiration. As a consequence, planetary boundary layer moisture decreases, whereas sensible heat flux and surface temperature increase. Reduced roughness especially allows winds to be accelerated through reduced friction. The experiments are initialized on 20 January 2020 from the European Center for Medium Range Forecasting (ECMWF) Integrated Forecasting Model (IFS) (Wedi, 2014; Malardel et al., 2016) analysis and integrated for three years. The first 11 days of the simulations are discarded as spin-up. This is sufficient to allow soil moisture to equilibrate over the Amazon region, both in CTL and DEF (see Fig. S1).

To get an estimate of internal variability, we make use of an available 30-y simulation of ICON-Sapphire. Compared to our set-up, the grid spacing is 10 km, the simulation is coupled to an ocean, and it uses a different turbulence scheme. We calculate the standard deviation of the 30-y simulation to assess whether the changes due to deforestation are out of the range of its internal variability or not. Hence, we implicitly assume that the standard deviation does not vary too much with model choices, which is not ideal, but this was the only simulation that had been run long enough to estimate internal variability.

Determination of rain belt center

To validate and interpret the results, we will determine the center of the rainbelt over South America. The latter is defined as the weighted centroid of the biggest precipitation object found in South America (30°S-13°N, 82°W-30°W). A precipitation object is defined by continuous grid points with precipitation larger than the 90th percentile of precipitation over the considered region. The selected area and method follow Segura et al. (2022), whereby the method is inspired by the structure-amplitude-location (SAL) method, first proposed by Wernli et al. (2008).

RESULTS

No significant reduction in mean precipitation despite a large reduction in evapotranspiration

Using the same model version, but coupled to an ocean, Segura et al. (2022) already documented that the ICON model can reproduce precipitation and its seasonal migration over South America extremely well (see Fig. 3 from their paper). This evaluation remains true for CTL (see Fig. S2, S3). We observe a tendency for CTL to produce higher precipitation amounts than the 20-y mean of the IMERG observational dataset (Huffman et al., 2019). Nonetheless, this overestimation is within one standard deviation of the year-to-year variability in observations except for the four months of March, April, June, and October (Fig. S2a). We also observe generally larger discrepancies in the location of the rainbelt center during the rainier months, which can be explained by the larger internal variability combined with the limited integration period. But all in all, CTL reproduces the spatial distribution of the annual mean precipitation, the observed mean location of the center of the rainbelt (Fig. S2b-d) and its seasonal migration (Fig. S3) remarkably well.

Our global storm-resolving simulation reveals insignificant change in annual mean precipitation when averaged over the entire Amazon following deforestation (see filled circles close to the y-axis in Fig. A.1). We consider a change to be significant if the amount of change lies outside one standard deviation of a 30-y control climate, see section 2.1. Deforestation leads to a reduction in annual mean precipitation of 0.27 mm day^{-1}, which is within the standard deviation of 0.66 mm day^{-1}. This represents a 4% reduction in annual mean precipitation, to be compared to an average reduction of 18% from previous GCMs with convective parameterizations (Table S1). Monthly, only August and October exhibit a significant precipitation reduction (Fig. A.1). Seasonally, the precipitation responds differently between the dry (JAS) and the wet (DJF) seasons. The precipitation reduction during the dry season, of 0.60 mm day^{-1}, is larger than its standard deviation (0.41 mm day^{-1}) and thus significant. In contrast, the reduction in the wet season, with a reduction of 0.26 mm day^{-1}, is well within its standard deviation of 1.07 mm day^{-1}.

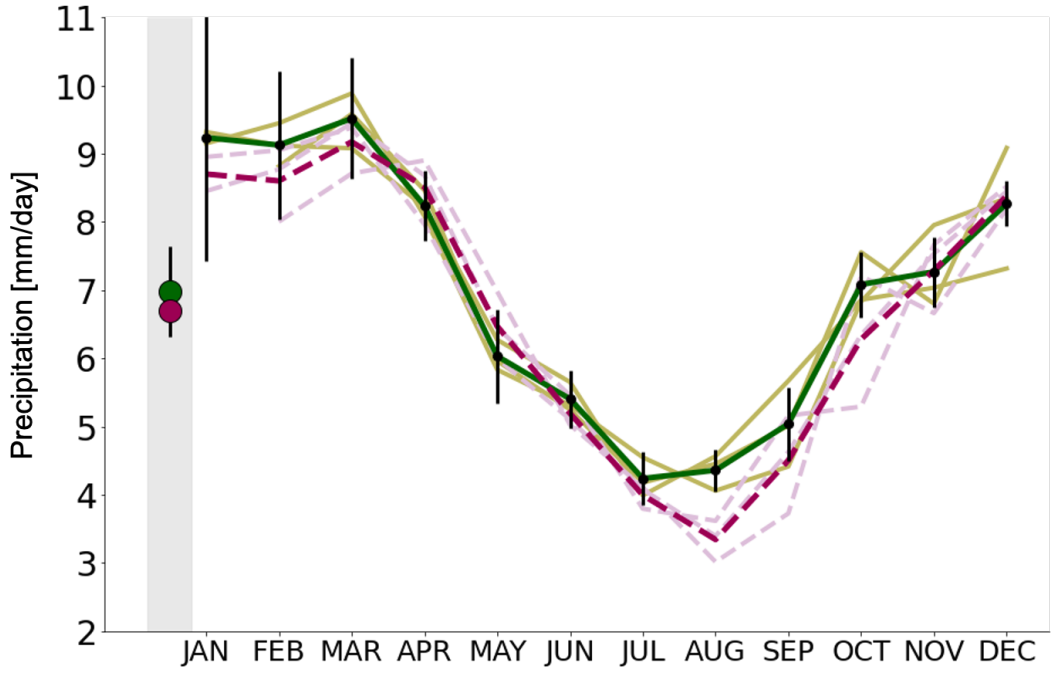

Figure A.1: Monthly mean precipitation (mm day^{-1}) averaged over the Amazon (see red outline in Fig A.3a). The 3-y mean from CTL is plotted in a solid dark green line and DEF is in a dashed dark magenta line. Individual three years are in lighter colors with solid (CTL) and dashed (DEF) lines. The filled circles inside the grey box represent the annual mean precipitation (CTL=6.97, DEF=6.70 mm day^{-1}), and the black vertical lines are the standard deviations of a 30-yr CTL simulation conducted with a 10-km grid spacing (see Methods) and used to estimate internal variability.

As past studies attributed reduced precipitation to decreased evapotranspiration, we look in Fig. A.2 at the relationship between changes in evapotranspiration and changes in precipitation. Our global storm-resolving simulation falls out of expectation. The simulated precipitation change from ICON (-0.27 mm day^{-1}) is about a quarter of the estimate from fitting a linear regression through the values of past GCM studies (-1.13 mm day^{-1}). Moreover, besides ICON, only one (Kleidon and Heimann, 2000) of the 13 past GCM studies and two (Lejeune et al., 2015; Llopart et al., 2018) of the RCM studies exhibit a precipitation change smaller than the evapotranspiration change. Kleidon and Heimann (2000) attributed their precipitation response to cloud feedbacks that enhance net surface solar radiation, counteracting albedo effects following deforestation. This contrasts with most other studies. Lejeune et al. (2015) and Llopart et al. (2018) explained their precipitation response by increased surface moisture convergence due to the generation of a heat low over Amazon. Their change in moisture convergence is stronger than in other past RCM studies. Studying global deforestation, Luo et al. (2022) also found a near 1:1 linear relationship between precipitation and evapotranspiration in CMIP6 models, at odds with our results. Given the uncovered smallness of the Amazon's mean precipitation changes, our results challenge the existence of a tipping point. Flores et al. (2024) mentioned an annual precipitation of 1,000 mm and a rainfall seasonality intensity of -400 mm as critical thresholds. These are much smaller than the

values obtained from DEF based on the same calculation as Flores et al. (2024), namely 2,445 mm and -195 mm, respectively.

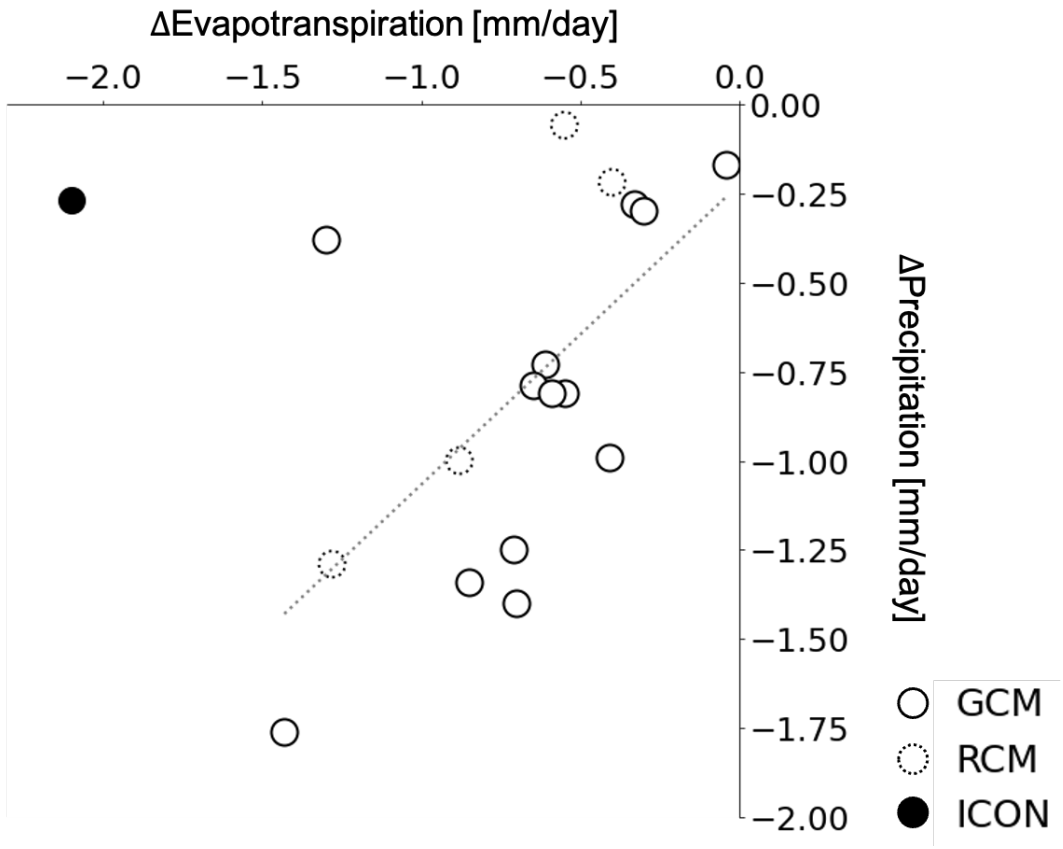

Figure A.2: Scatter plot of changes in mean evapotranspiration versus changes in mean precipitation from available previous studies, distinguishing between GCM and RCMs, and ICON. The linear regression derived from past studies is represented by a dashed line. Studies without evapotranspiration information (see Tab.S1) are omitted. Spatial averages over the Amazon only.

The obtained reduction in evapotranspiration by broadly similar annual mean precipitation amount in DEF implies changes in soil moisture and runoff. Soil moisture increases in DEF in the second and third soil layers and slightly decreases in the first layer (Fig. S1), as expected from the absence of the deep forest roots. The increase in soil moisture is accompanied by an increase in runoff, allowing the terrestrial water balance to find a new equilibrium. The runoff increases from 2.78 mm day^{-1} in CTL to 4.40 mm day^{-1} in DEF.

A North-to-South dipole pattern emerges in the dry and wet seasons due to interactions with the large-scale circulation

We focus now on the spatial pattern of precipitation change (Fig. A.3). Given the distinct significance between the dry and the wet seasons, we start by focusing on these two seasons. In both seasons, the spatial pattern of the precipitation response is not uniform. In contrast, the evapotranspiration response is uniform. This further confirms that precipitation in our global storm-resolving simulation

is not strongly coupled to evapotranspiration, including potential changes in soil moisture. Given the spatial uniformity of the evapotranspiration change and the constraint of the atmospheric moisture budget, the pattern of the precipitation response reflects in Fig. A.3 the change in column-integrated horizontal moisture convergence. The latter is simply referred to as column moisture convergence hereinafter.

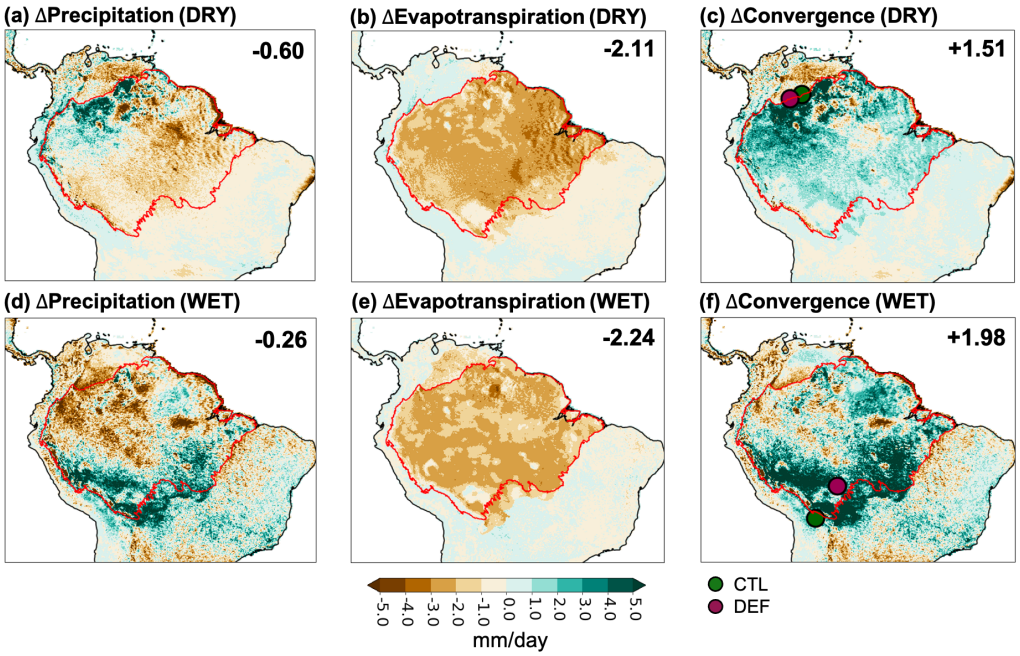

Figure A.3: Maps (all in mm day^{-1}) of the changes in each component of the atmospheric moisture budget after deforestation (DEF-CTL) for (a-c) dry (JAS) and (d-f) wet (DJF) seasons. The filled circles in (c,f) indicate the location of the center of the rainbelt in CTL (dark green) and DEF (dark magenta). Numbers (mm day^{-1}) denote the mean changes over the Amazon region.

The column moisture convergence averaged over the Amazon region increases by 1.51 mm day^{-1} in the dry and 1.98 mm day^{-1} in the wet season, compensating for the reduction in evapotranspiration. During both seasons, the column moisture convergence exhibits a North-South dipole pattern. Column moisture convergence is strongly enhanced over the northern Amazon during the dry season after deforestation, whereas it is enhanced over the southern Amazon during the wet season. In agreement, precipitation is primarily enhanced over the northern Amazon during the dry season, and over the southern Amazon during the wet season. This pattern is distinct from what was found with previous RCMs, which reported an East-West pattern with precipitation enhanced over the eastern Amazon and reduced over the western Amazon (Da Silva et al., 2008; Lejeune et al., 2015; Llopart et al., 2018). What explains this spatial pattern in the response to column moisture convergence?

From Fig. A.3c and f, the area of enhanced column moisture convergence coincides with the location of the rainbelt center. The latter is indicated by the colored dots in Fig. A.3c and f. In other words, the precipitation response to deforestation can simply be understood by a strengthening of the pre-existing convergence pat-

tern, thereby increasing precipitation over the core region of the rainbelt. To further understand these changes, we look at how the circulation changes.

At 1000hPa (Fig. A.4a, b), reduced evapotranspiration raises the mean 2m temperature by 4.57K in the dry and 3.33K in the wet season. This induces a strong surface heat-low, spinning up a sea-breeze like circulation with enhanced advection from the Atlantic and upward motion over the Amazon. The reduction in roughness length due to deforestation also leads to an enhancement of the horizontal 10-m winds. The surface response is consistent with previous RCM studies (Hahmann and Dickinson, 1997; Nobre et al., 2009; Da Silva et al., 2008; Lejeune et al., 2015) and should have caused increased precipitation over the eastern Amazon and decreased precipitation over the western Amazon.

This mechanism could explain the small area of enhanced precipitation over the north-eastern Amazon during the dry season, for instance, but it cannot explain the main, zonally elongated and strong enhancement of precipitation over the northern and southern Amazon during the dry and wet seasons respectively. In contrast, the change in the circulation at 700 hPa (Fig. A.4c, d) is consistent with the pattern of the precipitation response. During the dry season (Fig. A.4c), the easterly flow (see Fig. S4c) takes on a stronger northward component, enhancing convergence over the northern Amazon. The alteration of the flow direction is linked to a displaced geopotential height (Fig. A.4c and Fig. S5a, b). Here, we only show the geopotential height at 700 hPa from the third year due to output availability. However, based on the fact that the wind at 700 hPa shows a consistent response to deforestation every year, we assume that the response of geopotential is the same from year to year. At 700 hPa, the South Atlantic Subtropical Anticyclone (SASA, see Miyasaka and Nakamura, 2010; Reboita et al., 2019) largely impacts the wind distribution (Fig. S4c). The SASA is strengthened and shifts westward within the Amazon after the deforestation. This displacement creates a larger pressure gradient inside the Amazon, accelerating the wind (Fig. A.4c). The proximity of the SASA and its associated subsidence prevents convection from developing on the southeastern Amazon, despite enhanced surface advection from the Atlantic. During the wet season (Fig. A.4d), convergence is enhanced over the southeastern Amazon and along the Andes, near the rainbelt center. Although the displacement of the SASA is less pronounced compared to the dry season, partly due to the anticyclone's distance from the land, we observe an expansion of a higher pressure area near the La Plata river basin along the Andes. This expanded area with higher pressure blocks the flow of the southward trade wind (Fig. S4d) replacing it with a northward flow (Fig. A.4d), enhancing moisture convergence. Thus, the large-scale circulation response at 700 hPa mostly makes the circulation changes resulting from the generated surface heat low over the Amazon and explains the precipitation response. This is distinct from the mechanism advanced in RCM studies to explain the enhanced moisture convergence in such simulations.

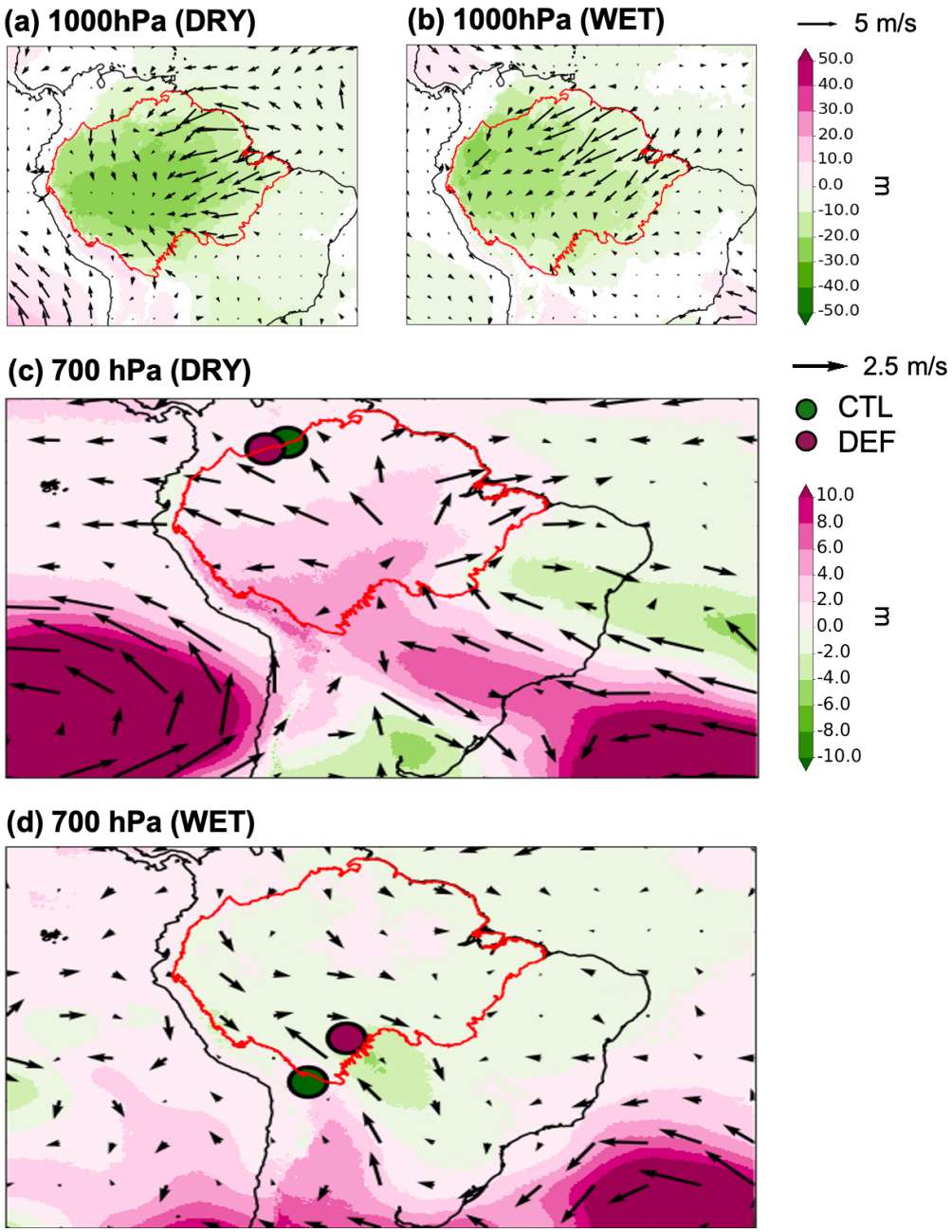

Figure A.4: Maps of changes in geopotential height (m) and wind (m/s) in dry (JAS) and wet (DJF) seasons after deforestation at 1000hPa (a), (b), and at 700hPa (c), (d). The filled circles show the location of the centroid of the rainbelt in each simulation.

Disentangling the cause of the changes in the large-scale pressure pattern is difficult. The location of the pressure systems around Amazon is controlled by local thermal forcing (Seager et al., 2003; Liu et al., 2004; Miyasaka and Nakamura, 2010). As such, the enhanced warming over South America following deforestation could displace the SASA. In addition, the location of the pressure systems also responds to the presence of convection over South America (Espinoza et al., 2021). The convection, due to its diabatic heating, generates its own circulation (Gill, 1982) and reinforces subsidence over the ocean and south of the Amazon, a region known as

the La Plata River basin (Nielsen et al., 2019). This diabatic forcing excites a Rossby wave west and a Kelvin wave east of convection, impacting the strength of the South Pacific anticyclone on the West and of the SASA on the East (Rodwell and Hoskins, 2001). Thus, part of the changes in the pressure systems may result from altered convective activity over land following deforestation. As shown by Findell and Eltahir (2003), under certain thermodynamical conditions, warming, and not moistening, can be more efficient at triggering convection.

Although we cannot fully disentangle cause and effect in the interactions between the SASA, the 700-hPa large-scale flow, and convection, these interactions have not been mentioned in previous studies of complete Amazon deforestation based on coarse-resolution GCMs. If anything, Kleidon and Heimann (2000), the only GCM study with a low precipitation sensitivity, mentioned a general weakening of the tropical circulation, and not strengthening as in our case.

We have seen that, from a moisture budget perspective, the enhanced moisture convergence compensates for the reduced evapotranspiration and explains the spatial pattern of the precipitation response. From an energy budget perspective, past studies have argued that the reduced energy input at the surface due to the increased albedo would disfavor convection. In our simulation, surface net energy decreases by 14.44 Wm^{-2} and 26.59 Wm^{-2} in the wet and dry seasons, respectively. The albedo change is responsible for a ~14 Wm^{-2} decrease, the rest mainly comes from an increased surface upward longwave radiation due to the warmer temperatures. However, as shown by Jalihal et al. (2019), the convection response is rather determined by the change in total column energy as well as in Total Gross Moist Stability, TGMS (see his Eq. 10). TGMS quantifies changes in lateral transport of moist static energy, which can be important over small regions to maintain the heating of the column. Following Equation 15 from Jalihal et al (2019), we quantify changes in total column energy and TGMS for both seasons. In both seasons, the contribution from changes in TGMS dominates, with a value of around 80%. This further confirms the importance of circulation changes in determining the precipitation response, rather than direct surface latent heating. In our global storm-resolving simulation, the increased moisture convergence and the interactions with the large-scale circulation stabilize precipitation.

While the dry and wet seasons have a North-South dipole pattern, the annual mean precipitation response exhibits a West-East dipole pattern (Fig. S6a) embedded in a waning crescent of enhanced precipitation. Notably, the combination of the monthly changes leads to a wetter western and drier eastern Amazon after deforestation, opposite to the drier western and wetter eastern Amazon from past studies on total Amazon deforestation (see Tabs S1 and S2). To get the shape of the waning crescent, the transitional period (May and June) needs to be considered on top of the dry and wet seasons (Fig. S6b, c). The remaining months (March, April, October, and November) display a uniform increase in precipitation and thus are irrelevant. Like in the dry and wet seasons, the transitional period's precipitation pattern is also driven by changes in mid-level circulation at 700 hPa rather than at 1000hPa (Fig. S7). Whereas the 10-m winds are enhanced over the eastern Amazon, the 700-hPa winds show a diverging circulation over the eastern Amazon, disfavorable for convection.

CONCLUSIONS

The response of precipitation to Amazon deforestation depends on the sensitivity of precipitation to local evapotranspiration, modulated by changes in the moisture transport from the Atlantic Ocean into the Amazon, either through large-scale circulation and/or through a heat low generated over the Amazon by deforestation. Investigating these interactions for the first time using a global domain and an explicit representation of convection, we find that: (i) the reduction in the annual mean precipitation over the Amazon following deforestation is insignificant; (ii) there is no enhancement of precipitation over the eastern Amazon; rather, the precipitation exhibits a North-South dipole pattern in the dry and wet seasons, with an increase over the core region of the rainbelt; (iii) neither reduced evapotranspiration nor the enhanced moisture transport at the surface from the Atlantic Ocean into the Amazon explains the main features of the spatial pattern of the precipitation response; rather, it is explained by changes in the wind at 700hPa associated with displaced large-scale pressure systems. Compared to 17 past studies on complete Amazon deforestation, only two RCM studies and one GCM study also exhibited a low precipitation sensitivity, however with a distinct spatial pattern and no mention of large-scale circulation change. It remains unclear why past GCM studies on complete Amazon deforestation did not observe such large-scale circulation changes. From studies on the soil moisture-precipitation feedback (e.g. Pan et al., 1996; Gallus Jr and Segal, 2000; Hohenegger et al., 2009), it is known that the design of a convection scheme can make the feedback switch from generally positive to negative. The use of a convection scheme thus may explain the generally too strong sensitivity of precipitation to evapotranspiration in coarse-resolution GCMs. Other aspects of the model set-up, such as boundary layer schemes (e.g. Langenbrunner et al., 2019) or the way the biophysical parameters are altered (e.g. Lean and Rowntree, 1997; Kleidon and Heimann, 2000), can further affect the precipitation sensitivity to evapotranspiration. RCMs with explicit convection may instead be able to reproduce our results as long as their domain of integration is large enough to include shifts in the position of the South Atlantic Subtropical Anticyclone following deforestation.

All in all, the uncovered weak sensitivity of precipitation to Amazon deforestation in our global storm-resolving simulation is consistent with the general idea that the land couples too strongly to the atmosphere in traditional coarse-resolution GCMs (e.g. Ferguson et al., 2012; Levine et al., 2016) and that the soil moisture-precipitation feedback is much weaker in a GCM with explicit than with parameterized convection (Lee and Hohenegger, 2024). The uncovered strong negative circulation feedback stabilizes annual mean precipitation in the Amazon to land surface perturbations. These dynamics indicate that the induced precipitation changes do not necessarily render the system irreversible. However, these dynamics may also exacerbate extremes, intensifying the wet-dry contrast by making wet regions wetter and dry regions drier. Given the relevance of such negative feedback, while computational resources limited our investigation to a few years, with one model, and without ocean interactions, this experiment should be repeated with other global storm-resolving models when they are capable of running multi-

year integrations with ocean coupling. Obtaining a consensus on how the large-scale circulation responds to regional land surface perturbations will be the key.

ACKNOWLEDGEMENTS

AY acknowledges funding by the CLICCS centre of excellence subproject A3 funded by DFG. We thank the German Climate Computing Center DKRZ for providing computing resources and the Integrated Climate Data Center (ICDC), the Center for Earth System Research and Sustainability (CEN), University of Hamburg for supporting the IMERG data. In addition, we want to acknowledge Lukas Kluft and Tobias Kölling for commenting on technical issues, Hans Segura for sharing codes for calculating the center of the rainbelt, Junhong Lee and Reiner Schnur for having a valuable discussion about land processes, and Bjorn Stevens for an internal review of the initial manuscript at the Max Planck Institute for Meteorology. We also thank the reviewers for their careful feedback to improve and refine the manuscript.

OPEN RESEARCH

The source code of the ICON model is freely available at `http://icon-model.org`. The simulations were done with the ICON branch nextgems_cycle2. The IMERG data was downloaded from the Integrated Climate Data Center website (`https://www.cen.uni-hamburg.de/en/icdc/data/atmosphere/imerg-precipitation-amount.html`). The scripts used to process data and plot the figures in this paper are available in the repository via Yoon and Hohenegger (2024).

SUPPLEMENTARY

Table S1: The GCMs and land surface scheme, resolution, and the use of an ocean model (A for atmosphere-only, C for coupled-ocean-atmosphere) are indicated together with the resulting spatial pattern of the precipitation change, the change in the annual mean evapotranspiration (ET, mm day^{-1}) and precipitation (P, mm day^{-1} and %). The average precipitation reduction from past GCM studies is 1.05 mm/day (17.82%). For the spatial pattern, the first cardinal direction has more precipitation after deforestation (e.g., E/W = East becomes wetter and West becomes drier after deforestation), and '-' is used if there is no mention of spatial pattern. The format is similar to the supplementary table from Spracklen and Garcia-Carreras (2015). *Hirota et al (2011) showed a similar pattern to our study, but no details about the underlying mechanism can be found.

Reference	Model	Resolution	Ocean	Pattern	ET	P (%)
Lean and Warrilow (1989)	UKMO	2.5×3.75	A	-	-0.85	-1.34 (-20)
Nobre et al. (1991)	NMC/SiB	1.8×2.8	A	Uniform	-1.43	-1.76 (-26.1)
Dickinson and Kennedy (1992)	NCAR CCM1 BATS	4×7.5	A	-	-0.7	-1.4 (-25.5)
Lean and Rowntree (1993)	UKMO	2.81×2.81	A	Uniform	-0.55	-0.81 (-14.2)
Dirmeyer and Shukla (1994)	COLA/SSiB	4.5×7.5	A	NE/SW	-0.33	-0.28 (-11.4)
Lean and Rowntree (1997)	UKMO	2.5×3.75	A	Uniform	-0.3	-0.3 (-5)
Hahmann and Dickinson (1997)	NCAR CCM2 BATS1e	2.81×2.81	C	E/W	-0.41	-0.99 (-16.6)
Costa and Foley (2000)	GENESIS IBIS	4.5×7.5	C	S/N (JFM,JAS)	-0.61	-0.73 (-11.8)
Gedney and Valdes (2000)	ECMWF IFS	3×3	C	-	-0.65	-0.79 (-15.6)
Kleidon and Heimann (2000)	ECHAM4	5.6×5.6	A	E/W	-1.30	-0.38 (-7.7)
Werth and Avissar (2002)	GISS-II	4×5	A	-	-0.59	-0.81 (-21.7)
Da Silva et al. (2008)	GISS	5×4	A	Uniform (JF)	-0.71	-1.25 (-19.0)
Nobre et al. (2009)	CPETC SSiB	1.85×2.85	C	E/W	-	-3.3 (-42)
Medvigy et al. (2011)	OLAM	Variable, 25km over Amazon	A	SE/NW	-0.04	-0.17 (-2.3)
Hirota et al. (2011)	CPTEC	1×1	A	W/E*	-	-1.38 (-27.6)
Pires and Costa (2013)	CCM3/IBIS	2.81×2.81	A	-	-	-1.15 (-18.6)

Table S2: Same as Table S1 but for RCM studies. The average decrease in precipitation is 0.60 mm day^{-1} (7.88%). *Correia et al. (2008) showed a significant precipitation decrease in the eastern and northeastern Amazon and a narrow increase in the extreme western part along the Andes. Compared to our obtained spatial pattern, they miss the increase over the northern and southern Amazon and their increase over the western Amazon is narrower.

Reference	Model	Resolution	Ocean	Pattern	ET	P (%)
Moore et al. (2007)	RAMS4.4	20 km	A	Band (E to W)	-	-0.41 (-8.2)
Da Silva et al. (2008)	RAMS	20 km	A	E/W	-0.88	-1.00 (-12.5)
Correia et al. (2008)	ETA/SSiB	40 km	A	W/E*	-1.28	-1.29 (-12.6)
Lejeune et al. (2015)	COSMO-CLM	0.44×0.44	A	E/W	-0.4	-0.22 (-5.3)
Llopart et al. (2018)	RegCM4/CLM4.5	50 km	A	E/W	-0.55	-0.06 (-0.8)

B

EXTREME EVENTS IN THE AMAZON AFTER DEFORESTATION

The work in this appendix has been submitted as:

Yoon, A., Hohenegger, C., Bao, J., Brunner, L. (2025b): "Extreme events in the Amazon after deforestation", In *review in Earth System Dynamics*

Author contribution:
AY: conceptualization; data curation; formal analysis; investigation; methodology; software; visualization; writing – original draft; writing – review and editing. **CH**: conceptualization; funding acquisition; investigation; project administration; resources; supervision; review and editing, **JB**: investigation; review and editing, **LB**: visualization; review and editing.

Extreme events in the Amazon after deforestation

Arim Yoon[1,2], Cathy Hohenegger[1], Jiawei Bao[3], Lucas Brunner[4]

[1]Max Planck Institute for Meteorology, Bundesstraße 53, 20146 Hamburg, Germany [2]International Max Planck Research School on Earth System Modeling (IMPRS-ESM), Bundesstraße 53, 20146 Hamburg, Germany [3]Institute of Science and Technology Austria, Am Campus 1, 3400 Klosterneuburg, Austria [4]Research Unit Sustainability and Climate Risk, Center for Earth System Research and Sustainability (CEN), University of Hamburg, Hamburg, Germany

ABSTRACT

Potential self-perpetuating dieback of the Amazon rain forest has been a topic of concern. The concern is that initial deforestation could critically impair the forest's water recycling capacities, further harming the remaining forest through reduced annual precipitation. Many studies have focused on annual mean precipitation changes, due to its widespread perception as a central control on the Amazon rain forest's stability. However, the impact of deforestation goes beyond changes in the annual mean precipitation. Yet, global coarse-resolution climate models are not well suited to investigate changes in short-duration and localized events due to their coarse resolution. Here, we circumvent these issues by analyzing a full-deforestation scenario simulated by a global storm-resolving model. We focus on changes in the tail of the hourly distribution of precipitation, temperature, and wind. Hourly precipitation becomes more extreme in the absence of the forest than in an intact forest, with an increased occurrence of both no rain and intense rainfall. These changes are driven by enhanced moisture convergence that strengthens vertical velocity. On average, the near-surface temperature rises significantly by about 3.84 °C, and the daily minimum temperature after deforestation becomes similar to the daily maximum temperature before deforestation. Most human heat stress indicators shift to more severe levels, with implications for health and a significant reduction in work productivity. Finally, the mean 10 m wind speed intensifies by a factor of four, with the 99th percentile wind speed doubling. To summarize, our findings, while based on an idealized case, provide a stark warning of the effects of continuing deforestation of the Amazon.

INTRODUCTION

The Amazon is home to unparalleled biodiversity and a major carbon sink, making its preservation vital. However, more than 20% of the Amazon forest has already been cleared, and 6% has degraded, with further deforestation expected (RAISG, 2022). As forests shape the local energy balance, the water cycle, and the atmospheric dynamics (Bonan, 2008), their removal will change environmental conditions, potentially in a way that is unfavorable for forest regrowth. Among environmental conditions, precipitation has been a primary focus. Annual mean precipitation, the most broadly used indicator, is indeed a useful metric for assessing ecosystem structure. For instance, Malhi et al. (2009) used annual precipitation

and dry season intensity to classify vegetation types and identify climatic thresholds for vegetation transitions. However, annual mean precipitation can obscure important details about short-duration precipitation events. In fact, extreme precipitation is often more influential on ecosystem processes than mean conditions (Heisler-White et al., 2009; Smith, 2011; Thompson et al., 2013). Beyond ecological impacts, intense precipitation also poses significant challenges to infrastructure and agriculture (Wang et al., 2013; Gao et al., 2018; Guerreiro et al., 2024; Brown et al., 2020; Fowler et al., 2021). Moreover, forest loss often entails elevated heat stress, and intense winds can damage the forest and alter forest regrowth (Quine and Gardiner, 2007; Zhan et al., 2017; Kotz et al., 2021). In our previous study, we investigated the mean annual precipitation response to full Amazon deforestation in a storm-resolving global climate model (Yoon and Hohenegger, 2025). Unlike previous studies, we found that annual mean precipitation remains almost unchanged under the deforestation scenario. These findings contradict the classification of the Amazon rainforest as a climate tipping element. However, the impacts of deforestation go well beyond changes in the annual mean. Thus, the goal of this study is to investigate changes in extreme precipitation, temperature extremes, and gust winds following complete Amazon deforestation using the same simulations of Yoon and Hohenegger (2025).

Past studies using coarse-resolution global and regional models, with parameterized convection, have found a reduction in mean precipitation following deforestation (Nobre et al., 1991; Lejeune et al., 2015; Spracklen and Garcia-Carreras, 2015; Llopart et al., 2018). To the best of our knowledge, no study has so far investigated the impact of full Amazon deforestation on precipitation extremes. Extreme precipitation is generated by two essential factors (Johns and Doswell III, 1992; O'Gorman and Schneider, 2009; Muller et al., 2011; Schumacher and Rasmussen, 2020): the availability of atmospheric moisture (Trenberth et al., 2003; Lenderink and Attema, 2015), supplied by evapotranspiration and moisture convergence, and the strength of updrafts (Trenberth et al., 2003; Emori and Brown, 2005; Brown et al., 2020; Loriaux et al., 2017). Regarding the first factor, there is strong agreement among previous studies that evapotranspiration uniformly decreases after complete deforestation, leading to a reduction in mean precipitable water (Gedney and Valdes, 2000; Medvigy et al., 2011; Hirota et al., 2011; Pires and Costa, 2013). However, past studies inconsistently reported both increases and decreases in mean moisture convergence.

Concerning the second factor, strong updrafts, the amount of convective available potential energy (CAPE) is often used as a proxy for it. Some studies have shown that CAPE decreases after deforestation (Wang et al., 2009; Swann et al., 2015; Lemes et al., 2023), although none of the studies focused on hourly precipitation. In addition to CAPE, the vertical uplifts over the Amazon basin are predominantly observed in conjunction with moisture convergence, as indicated by observational data (Viscardi et al., 2024). Therefore, moisture convergence constitutes a second proxy candidate for the identification of enhanced updrafts and convection (Crook and Moncrieff, 1988; Tiedtke, 1989; Schaefer and Doswell III, 1980; Davies et al., 2013; King et al., 2022).

Besides precipitation, forests interact with multiple environmental variables in complex ways. Temperature is one of them, particularly in tropical forests. Tropical

species are adapted to stable climate conditions within a narrow temperature range (Janzen, 1967; Wright et al., 2009; Perez et al., 2016), making them particularly vulnerable not only to an increase in mean temperature but also to greater variability. There is a strong consensus that deforestation increases the mean temperature due to biophysical changes. Reduced evapotranspiration results in more net surface energy being redistributed as sensible heat flux (Perugini et al., 2017; Duveiller et al., 2018; Butt et al., 2023) and lowered surface roughness length weakens turbulence heat transport, resulting in near-surface heat accumulation (Baldocchi and Ma, 2013; Winckler et al., 2019). Some studies reported that deforestation shifts the daily maximum distribution toward higher values and the daily minimum toward lower values, increasing overall variability (Voldoire and Royer, 2004). To further quantify the effect of temperature changes, especially on humans, heat stress indicators can be used, derived from meteorological variables (e.g., Morabito et al., 2014; Spangler et al., 2022; Wang et al., 2009). For instance, Oliveira et al. (2021) have reported that complete deforestation can cause the same level of heat stress as several degrees of global warming. Their investigation was based on the wet-bulb global temperature index, which is used in military training, work safety, and outdoor activities.

The wind is another representative cause of disturbance after deforestation. Frequent damaging winds can prevent a full regrowth of the forest, as young trees with shallow roots and fragile stems that regrow after deforestation may be more vulnerable to stronger winds. Deforestation is expected to increase surface winds by lowering roughness length (Lawrence and Vandecar, 2015; Sampaio et al., 2007; Spracklen and Garcia-Carreras, 2015; Lejeune et al., 2015) and increasing near-surface wind due to enhanced land and ocean temperature gradient (Good et al., 2008; Llopart et al., 2018; Mu et al., 2023). Moreover, potentially stronger downdrafts from convective storms may pose a further threat. However, studies have focused on averaged features, not on the distribution of changes in hourly wind speed, including changes in downdraft, after deforestation.

Beyond the fact that only a handful of studies have investigated changes in short-duration precipitation, temperature, and wind events after deforestation over the Amazon, the models used were coarse resolution. Their coarse resolution and their use of convective parameterizations make them unsuitable to represent fast processes and small scales. Therefore, we use the same simulations as Yoon and Hohenegger (2025), who used a global storm-resolving model with a 5 km horizontal resolution, and investigate changes in hourly rainfall, diurnal and seasonal temperature, hourly surface wind speed, and heat stress after deforestation.

METHOD

We used the ICON-Sapphire simulation presented in Yoon and Hohenegger (2025). The horizontal resolution is 5 km with a convective parameterization switched off, and a 75 km model top with 90 height levels. The domain is global, and simulations are run for 3 years. Two simulations are conducted with and without the Amazon forest, prescribing different biophysical parameters in the land surface model (Table B1). The two simulations are named CTL (without deforestation) and DEF (with complete deforestation). For the analysis presented here, precipitation,

temperature, and surface wind are hourly averaged, and we focus on the Amazon basin (see black contour in Fig. B.7a). The moisture convergence is computed from the residuals of the moisture balance equation, including the time tendency of total column water vapor (TCW, Moisture Convergence $= P - E - \frac{d(TCW)}{dt}$). This is done because the direct calculation of moisture convergence is too inaccurate with the available ourpur frequency. 3D instantaneous data are saved in 6-hourly intervals.

Table B1: The values for CTL are an average of the grid point values from JSBACH over the Amazon, and the values for DEF are taken from a table in Yoon and Hohenegger (2025), which is based on their values from multiple previous studies.

Parameters	CTL $\rightarrow$ DEF
Albedo	0.12 $\rightarrow$ 0.18
Leaf Area Index	8.40 $\rightarrow$ 2.70
Vegetation fraction	0.92 $\rightarrow$ 0.85
Roughness length (m)	1.80 $\rightarrow$ 0.05
Root depth (m)	1.33 $\rightarrow$ 0.60
Forest fraction	0.86 $\rightarrow$ 0.00

For the analysis, convective Available Potential Energy (CAPE) and Convective Inhibition (CIN) were computed based on outputs using the MetPy v1.3.1 Python package May et al. (2022). Parcel ascent was modeled with dry adiabatic lifting to the level of free convection and pseudo-adiabatic moist ascent thereafter, following the approximations of Bolton (1980). CAPE and CIN are calculated at pressure levels using hourly air temperature and dewpoint temperature starting from the surface.

Daily temperature variability is quantified using day-to-day temperature variation (DTDT) index (Karl et al., 1995), defined as the mean absolute difference in daily mean temperature between successive days ($\delta T = T_{i+1} - T_i$) within a given period (Eq. 1 in Ge et al., 2022).

$$DTDT = \frac{1}{n-1} \sum_{i=1}^{n-1} |T_{i+1} - T_i| \tag{B.1}$$

n: Total days

To diagnose the impact of deforestation on human discomfort due to changes in temperature and humidity, we use seven heat stress indices as described by Schwingshackl et al. (2021): apparent temperature (AT), NOAA heat index (HI), humidex (Hu), simplified wet-bulb globe temperature (T_{WBG_s}), indoor wet-bulb globe temperature (T_{WBG}), wet-bulb temperature (T_{WB}), universal thermal climate index (UTCI). These indices serve different purposes, leading to a wide range of formulations, with no single index universally regarded as superior (Barnett et al., 2010; Burkart et al., 2011; Schwingshackl et al., 2021). Therefore, to better estimate

the impact of deforestation on heat stress, it is required to analyze the overall characteristics of these indices.

HI and Hu are primarily used as heat warning indices. HI, widely applied for assessing heat stress based on temperature and relative humidity, categorizes heat risk into four levels: caution (27 °C, fatigue possible), extreme caution (32 °C, heat stroke, cramps, or exhaustion possible), danger (41 °C, heat stroke, cramps, or exhaustion likely), and extreme danger (54 °C, heat stroke, cramps, or exhaustion highly likely). Hu, developed in Canada, combines temperature and vapor pressure to evaluate thermal discomfort, with threshold indicating some discomfort (30 °C), great discomfort (40 °C), dangerous heat stroke (45 °C), and imminent heat stroke (54 °C). T_{WB} is a physiologically relevant heat stress index that defines the adaptability limits to extreme heat. It represents the lowest temperature an air parcel can reach through evaporative cooling, incorporating temperature, humidity, and pressure. A threshold of 35°C is considered intolerable for humans and likely lethal. T_{WBG} and T_{WBG_s} are widely used for occupational health assessments, as they account for heat stress levels at different work intensities and rest/work ratios for acclimatized workers. T_{WBG} is a weighted combination of T_{WB} and air temperature, while T_{WBG_s} provides a computationally efficient alternative of T_{WBG} using a linear combination of temperature and vapor pressure. Both indices have the same thresholds, where increasing heat stress requires 25%, 50%, and 75% rest per hour for levels 1 (29 °C), 2 (30.5 °C), and 3 (32 °C), respectively, while level 4 (37°C) indicates conditions where no work is permitted. UTCI and AT are indices designed to assess thermal comfort. UTCI, a model-based index incorporating air temperature, radiant temperature, wind speed, and humidity, is commonly used in studies evaluating heat-related mortality. Here we use the polynomial approximation based on temperature and vapor pressure introduced by Bröde et al. (2012). Its thresholds classify conditions as moderate (26 °C), strong (32 °C), very strong (38 °C), and extreme heat stress (46 °C). AT, derived from temperature and vapor pressure, is commonly used in epidemiological studies to assess heat-related health risks. Its severity levels range from slight discomfort (28 °C) to moderate (32 °C), strong (35 °C), and extreme discomfort (40 °C). A detailed description of the heat stress levels associated with these indices is summarized in Tables S1 and S2 of Schwingshackl et al. (2021).

RESULTS

Violent Rain

We start by investigating the intensity of hourly precipitation after deforestation. Figure B.1a shows the distribution of hourly precipitation in the Amazon basin for both CTL and DEF. Across all three simulation years, the probability of intense hourly precipitation is consistently higher after deforestation, as indicated by the lighter color lines (Fig. B.1a). To better visualize changes, the hourly precipitation rates are categorized into five intensity levels based on the WMO classification (2018): "No rain", "light" rain (<0-2.5 $\mathrm{mm\,hr^{-1}}$), "moderate" rain (2.5–10 $\mathrm{mm\,hr^{-1}}$), "heavy" rain (10–50 $\mathrm{mm\,hr^{-1}}$), and "violent" rain (more than 50 $\mathrm{mm\,hr^{-1}}$). Figure B.1b illustrates the percentage changes in each category after deforestation. Impor-

tantly, the two extreme categories – no rain and violent rain– exhibit a substantial relative increase in frequency after deforestation. No rain almost triples, and violent rain increases by a factor of 1.5. In contrast, light to heavy rainfall remains largely stable, and because light rainfall dominates the frequency of events, the overall mean precipitation remains unchanged as found in Yoon and Hohenegger (2025).

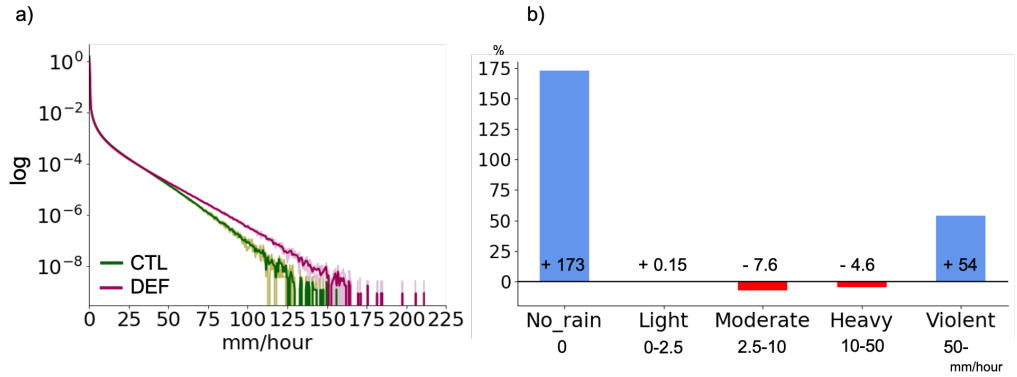

Figure B.1: Distribution of hourly precipitation [mm hr^{-1}] over the Amazon basin before and after deforestation. (a) The logarithmic probability density function of hourly precipitation rates across all Amazonian grid points. Dark green and dark magenta for CTL and DEF, respectively, using all three years (2020-2022), lighter colors for each year separately. (b) Percentage change (written in numbers, %) in frequency for different intensity categories.

We hypothesize that the changes in the tails of the precipitation distribution can be attributed to the fact that it is more difficult to trigger convection in DEF, leading to more violent outbursts when convection does happen. To confirm this, we first examine the mechanisms leading to increased violent rain: the availability of atmospheric moisture and strong updrafts (Trenberth, 1999; O'Gorman and Schneider, 2009; Allan and Soden, 2008; Lenderink and Van Meijgaard, 2008; Liu et al., 2009; Muller et al., 2011). Figure B.2 shows the intensity of hourly violent precipitation, binned by Total Column Water vapor (TCW) and vertical velocity at 500 hPa (W_{500}). Not surprisingly, Figure 2 shows that the intensity of violent rain is stronger with higher TCW and/or stronger W_{500} in both simulations. These links become more pronounced after deforestation, and more violent rains are simulated in DEF together with higher W_{500} and TCW (Fig. B.2b). However, the overall relation between precipitation intensity, TCW and W_{500} remains largely unchanged. More importantly, Figure B.2c indicates that the increase in the frequency of violent rain after deforestation comes from a shift towards stronger W_{500}, whereas TCW remains in the same range of 50 to 60 mm. Hence, the increase in violent rain is primarily driven by stronger updrafts and not by enhanced TCW (Fig. B.2c).

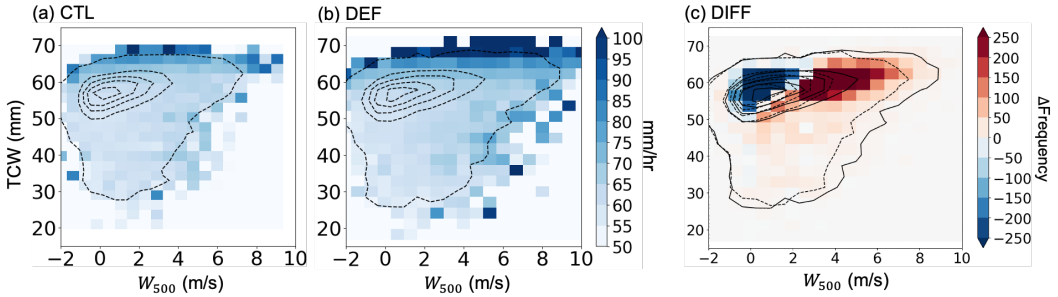

Figure B.2: The mean intensity of hourly precipitation [mm hr^{-1}] only in violent events, averaged within each bin (shaded) ordered by Total Column Water (TCW) and vertical velocity at 500hPa (W_{500}) for (a) CTL and (b) DEF. Dashed contours represent the frequency of TCW and W_{500} occurrences, with contour levels at 100, 500, 1000, 1500, and 2000; the innermost contour corresponds to the highest frequency. (c) Shading shows the difference in frequency (DEF minus CTL) for TCW and W_{500} within each bin. Dashed (CTL) and solid (DEF) lines indicate the frequency distributions already shown in (a) and (b), overlaid for comparison.

Having established that the increase in violent rainfall is mainly due to stronger updrafts, we now investigate the factors responsible for the updraft enhancement. Updraft strength is related to local atmospheric instability and convergence that forces ascent (Davies et al., 2013; Loriaux et al., 2017). Early studies consider moisture convergence as a dynamic variable determined by the circulation (Dai and Trenberth, 2004; Back and Bretherton, 2009). Although moisture convergence mixes the TCW signal, we use it as a proxy for convergence, given that TCW remains unaffected for violent rains after deforestation (Fig. B.2c).

First, atmospheric instability is assessed using Convective Available Potential Energy (CAPE). We calculate CAPE one hour prior to the violent rain events in order to relate it to the prerequisites for strong updrafts (Figs. B.3). The probability distribution of CAPE values shifts toward lower values after deforestation. The 99th percentile decreases from 3148 J kg^{-1} to 2138 J kg^{-1} (Fig. B.3a), and mean CAPE values decrease from 1950 J kg^{-1} to 1058 J kg^{-1}. This reduction suggests that the increase in updraft strength is not driven by an increase in local atmospheric instability, as measured by CAPE. To understand why CAPE decreases under deforested conditions, we examine its dependence on near-surface temperature and humidity, as CAPE is directly influenced by both factors (Figs. B.3b-c). We take both values from the lowest atmospheric layer to calculate CAPE. While higher temperatures generally increase CAPE, this effect is restricted by the availability of atmospheric moisture. Before deforestation, the highest occurrence of near-surface temperature and humidity is within 24-26 °C and 16-19 g kg^{-1}, respectively, where CAPE values range from 1500 to 3000 J kg^{-1}. After deforestation, this distribution shifts in the range of 27-30 °C and below 15 g kg^{-1}, leading to mean CAPE values around 1000 J kg^{-1}. The increase in drier near-surface conditions is a direct consequence of the decrease in evapotranspiration following deforestation, whereas the reduction in CAPE follows from the raised lifting condensation level and level of free convection. In line with our findings, Abramian et al. (2023) also indicated that CAPE is not a good predictor of the strength of updrafts in their study of squall

lines. Hence, increased instability cannot explain the stronger updrafts observed after deforestation.

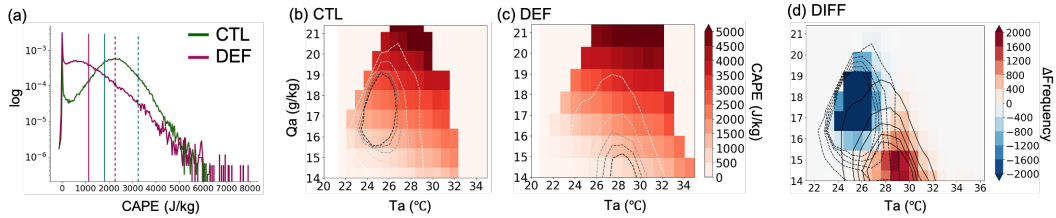

Figure B.3: CAPE [J kg^{-1}] one hour before violent precipitation over the Amazon. (a) The logarithmic probability density function of CAPE is represented with the mean (solid vertical lines) and the 99th percentile (dashed vertical lines). The PDF is derived from all grid cells and all time steps. CTL is in dark green, and DEF is in dark magenta. CAPE intensity one hour before intense precipitation, binned by near-surface temperature and near-surface specific humidity for (b) CTL and (c) DEF. Colors indicate the average CAPE in each bin. Dashed lines show the frequency of near-surface temperature and specific humidity at levels 100, 500, 1000, 1500, and 2000 times (from white to black). Panel (d) shows the change in the frequency of near-surface temperature and humidity in shading. Dashed (CTL) and solid (DEF) lines indicate the frequency distribution (i.e., the same lines as in Figures b and c).

We now attribute the increase in updraft strength to enhanced moisture convergence. How does moisture convergence change after deforestation, and how does it relate to the occurrence of violent rain events? Figure B.4a shows the probability distribution function of moisture convergence strength one hour before violent precipitation in both CTL and DEF. The tails of the convergence distribution are heavier after deforestation, aligning with the simulated increase in violent precipitation. Now, to answer whether violent rain occurs preferentially in regions with stronger moisture convergence, we examine the spatial patterns of these two variables, separately for dry (Jul-Sep) and wet (Dec-Feb) seasons, given the distinct seasonal circulation patterns in the Amazon region (Marengo, 1992; Leite-Filho et al., 2020; Reboita et al., 2019; Yoon and Hohenegger, 2025). Figures B.4b and c depict regions of stronger moisture convergence in the DEF simulation than in CTL (blue contours in Fig. B.4b,c). The frequency change in violent rain is defined as the difference in the number of violent rain occurrences between DEF and CTL for each grid point (shading in Fig. B.4b,c). Notably, regions with enhanced convergence largely overlap with those experiencing more violent rains, supporting the hypothesis that enhanced convergence leads to stronger updrafts and, consequently, more violent precipitation. These results are similar to an observation-based study by Davies et al. (2013), which showed a strong correlation between mechanical updraft and violent precipitation due to moisture convergence rather than CAPE in their study of convective precipitation over the tropical region at Darwin, Australia. Additionally, given that the spatial pattern of stronger moisture convergence aligns with the location of the rainbelt in the corresponding season, violent precipitation appears to be more closely linked to large-scale moisture convergence.

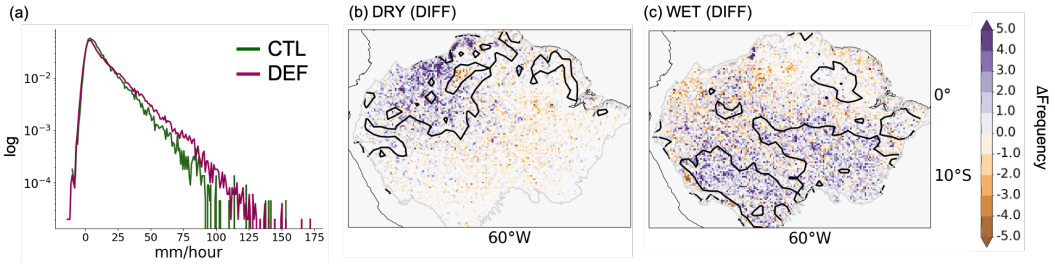

Figure B.4: (a) Logarithmic probability density function of moisture convergence one hour before violent precipitation events over the Amazon, shown for CTL (dark green) and DEF (dark magenta). (b, c) Differences in the frequency of violent precipitation events between DEF and CTL (DEF minus CTL) at each grid point (shading). The area with a positive anomaly of convergence is defined as the grid points where moisture convergence exceeds the same threshold, 90th percentile of CTL values, and shows a positive anomaly in DEF (Blue contour lines) in (b) the dry season and (c) the wet season.

While our results suggest that increased updrafts are attributed to increased violent rains through convergence, one might wonder why we see more no-rain events. Alongside the decrease in CAPE, Convective Inhibition (CIN) increases, with the mean value rising from 27 $\mathrm{J\,kg^{-1}}$ to 111 $\mathrm{J\,kg^{-1}}$ (Fig. B.5a). The environment is more inhibited for convection, and this explains why more no-rain events appear. After all, the environment, in general, becomes less favorable to convect thermodynamically, requiring a stronger dynamical driver to precipitate.

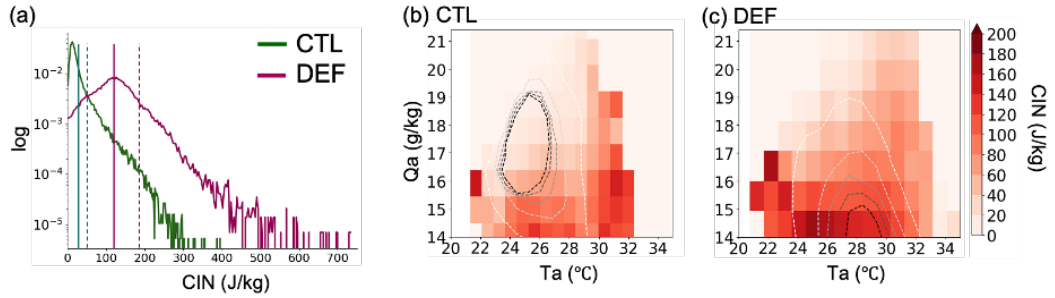

Figure B.5: Same as Figure 3(a-c) but for CIN [$\mathrm{J\,kg^{-1}}$].

Heat Stress

The mean 2 m temperature increases by 3.84 °C in the annual mean averaged over the Amazon region. Looking at the diurnal cycle (Fig. B.6a), we can see warm temperatures at all times and an increased diurnal temperature range. The post-deforestation nighttime temperatures become comparable to pre-deforestation daytime values. The temperature changes are significant in the sense that the difference between DEF and CTL is larger than the interannual variability in temperature in CTL. The temperature distribution of daily mean, daily minimum, and

maximum constantly shifts to higher values after deforestation (Fig. B.6b)

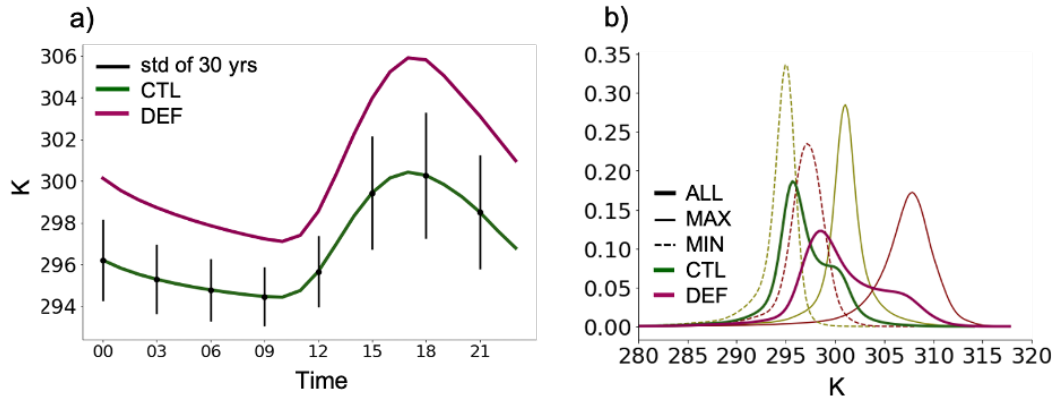

Figure B.6: Changes in 2 m temperature [K] over the Amazon region after deforestation. (a) The mean diurnal cycle of 2 m temperature in CTL (dark green) and DEF (dark magenta) with the vertical black lines representing internal variability. The internal variability is computed from the standard deviations of 2 m temperature from a 30 year CTL simulation conducted with a 10 km grid spacing. (b) Temperature distributions of the daily mean (thick solid), daily maximum (thin solid), and daily minimum (thin dashed) temperatures for every grid point in the Amazon.

To understand the temperature changes, we analyze the surface energy budget. The total net surface shortwave radiation increases due to an increase in downwelling shortwave radiation by 30.93 $W\,m^{-2}$, which results from reduced overall cloud cover in DEF. However, the higher albedo partly offsets this increase, reducing it by 16.48 $W\,m^{-2}$. On the other hand, surface energy loss by longwave radiation increases from 29.25 $W\,m^{-2}$ to 61.84 $W\,m^{-2}$ due to both enhanced upwelling longwave radiation by warmer surface temperature and reduced downwelling longwave radiation at the surface. Although the combined effects of shortwave and longwave radiation lead to a net surface radiation decrease of 18.14 $W\,m^{-2}$, the redistribution of energy favors sensible heat flux (+38.21 $W\,m^{-2}$) over latent heat flux (-59.37 $W\,m^{-2}$), resulting in higher 2 m mean temperature. This also explains the larger daytime temperature. At night, the temperature in DEF is still higher than the temperature in CTL. This occurs because daytime heating sets a warmer initial condition at the start of nighttime cooling. Although nighttime surface longwave cooling is stronger in DEF, the nighttime period is too short for radiative cooling in DEF to fully offset the temperature difference with CTL. As a result, before DEF can cool to the same extent as CTL, the warming resumes at sunrise, maintaining a consistently higher 2 m temperature throughout the diurnal cycle. This is consistent with studies that have shown that in the tropical region, open lands tend to be still warmer than forests at night, unlike in boreal regions (Schultz et al., 2017).

We further examine day-to-day variability to understand how temperature fluctuates between days. We use the day-to-day temperature variation (DTDT), which measures the absolute difference in daily mean temperature between consecu-

tive days within a given period (see Methods). Following deforestation, the mean DTDT increases across the Amazon by, on average, 0.4 °C (Fig. B.7a), indicating higher day-to-day temperature variability in the deforested case. In Figure B.7b, we look at the full distribution of daily δT between successive days ($T_{i+1} - T_i$), not just the absolute value between consecutive days (Fig. B.7b). The distribution broadens, both on the positive and negative sides. The increase is slightly stronger on the positive side. We find a fourfold increase in the probability of having between -3 and -1 °C changes in temperature between days and an eightfold increase in the probability of having between 1 and 3 °C changes between days. Together with the documented increase in the diurnal temperature cycle and day-to-day variability, seasonality also increases after deforestation: the range between the yearly maximum and minimum changes from 11.98 to 12.27°C.

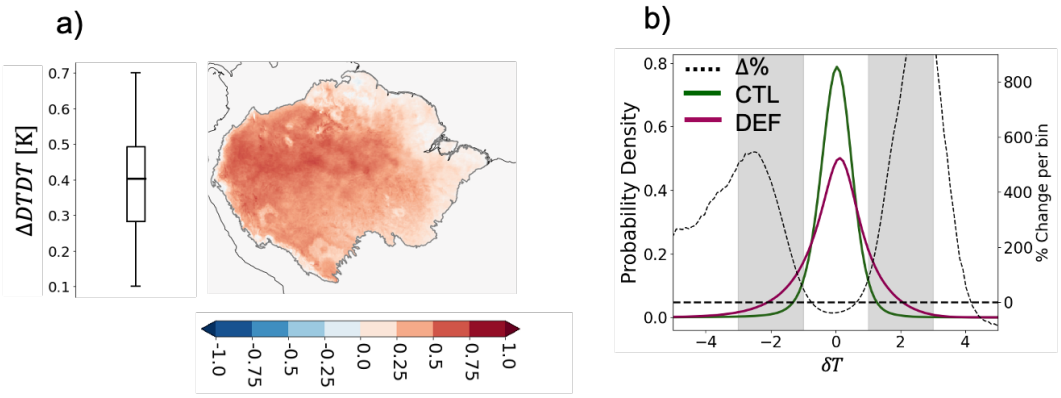

Figure B.7: (a) Differences in day-to-day temperature variability (DTDT) over the Amazon basin, assessed over the 3-year simulation period. The box-and-whisker plot shows the interquartile range (25th–75th percentiles) as the box, with the horizontal line inside the box indicating the mean. The whiskers extend to the 10th and 90th percentiles. (b) The probability density function of δT in CTL (dark green) and DEF (dark magenta) is shown on the left y-axis. Percentage changes between CTL and DEF are represented by the black dashed line on the right y-axis. The grey range is for temperature changes between (-3 K, -1 K) to (1 K, 3 K).

Given these changes, we assess their impact on human thermal stress using seven heat stress indices (see Methods for index explanation). We calculate indices from the full spatio-temporally pooled distribution and show the distribution through the box and whisker plot (Fig. B.8). Each index has four heat stress thresholds, represented by color-shading in Figure B.8, except T_{WB}, which has a single threshold. Although each index categorizes thermal stress levels differently based on its intended application, we standardized the descriptions for AT, HI, Hu, and UTCI as follows: 'level1: slight discomfort', 'level2: moderate discomfort', 'level3: strong discomfort', and 'level4: extreme discomfort'. For T_{WBG_s} and T_{WBG}, which are used in occupational health assessments, the levels are defined as 'level1: 25%rest/hour', 'level2: 50%rest/hour', 'level3: 75%rest/hour', and 'level4: 100%rest/hour'. All indices, except T_{WB}, consistently indicate a shift toward higher stress levels (Fig. B.8). The median AT increases from slight discomfort

to strong discomfort. Similarly, the median HI, Hu, and UTCI shift from moderate discomfort to strong discomfort. The T_{WBG_s} suggests that required rest periods increase from 50%rest/hour to 75%rest/hour, indicating a substantial decline in work capacity. Moreover, the number of stressed days increases. In the DEF, 70% of days exceed level 2 across all indices, compared to only 10-30% in CTL. Notably, for level 3, T_{WBG_s} shows a sharp increase, with 63% of days exceeding this threshold in DEF compared to just 13.2% in CTL. In contrast, T_{WB} exhibits a slight reduction after deforestation, as the decrease in humidity offsets the temperature increase. Indoor T_{WBG} increases but does not yet shown any days above level 2 after deforestation, which is not surprising as it is a weighted mean of T_{WB} and near-surface air temperature. Overall, most heat stress indices indicate increased thermal discomfort, higher health risks, and reduced work productivity after deforestation.

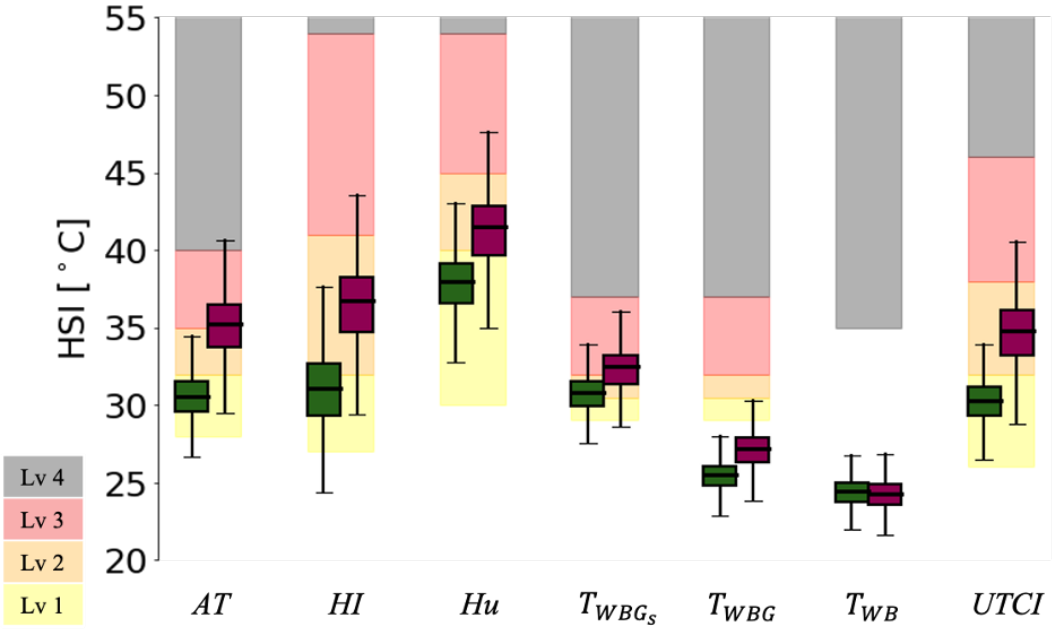

Figure B.8: Box-and-whisker plots of heat stress indices (HSI), showing the mean, interquartile range (25-75th percentiles), and whiskers (10-90th percentiles): AT, HI, Hu, T_{WBG_s}, T_{WBG}, T_{WB}, UTCI. The background colors show the range of discomfort for each level following Table S1 from Schwingshackl et al. (2021). Yellow shows the range between levels 1 and 2, orange is between 2 and 3, red shows between 3 and 4, and grey is above level 4. Descriptions of indices and levels are given in the Method section.

Damaging Winds

Lastly, we investigate how near-surface wind changes after deforestation. The 10 m wind speed increases from a mean value of 0.93 $m\,s^{-1}$ to 3.12 $m\,s^{-1}$, and in particular the 99th percentile rises from 3.36 $m\,s^{-1}$ to 8.45 $m\,s^{-1}$ (shading in Fig. B.9). Previous studies have shown that the increase in mean wind speed is a direct result

of the decrease in roughness length (Sud et al., 1988) and an intensification of the large-scale circulation after deforestation (Yoon and Hohenegger, 2025). However, beyond that, the increase in hourly precipitation, identified in section 3.1, opens up the possibility of having additional strong winds due to the downdrafts associated with violent rain (Garstang et al., 1998; Windmiller et al., 2023).

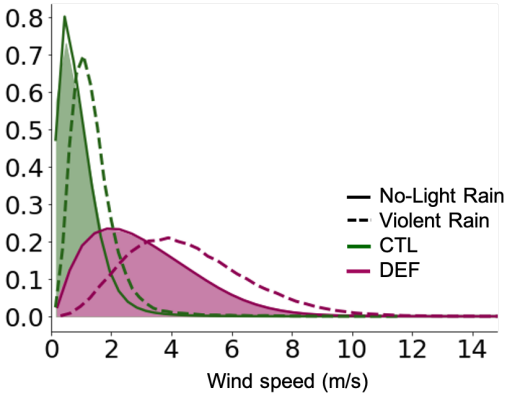

Figure B.9: Normalized probability density function of 10 m wind speed. Hourly winds from all cases are shaded, with solid lines representing no-light rain cases and dashed lines representing violent rain cases. Wind speeds are collected from all grid cells within the Amazon basin at any time when no-light/ violent rain occurs, and then pooled to construct the probability density function.

We aim to quantify the additional increase in 10 m wind speeds after deforestation that is due to downdrafts associated with violent rain, separating this effect from changes caused by surface roughness and background circulation. We cannot distinguish between the effect of surface roughness and of background circulation, as we do not have simulations with unchanged roughness at hand. We refer to this factor as R/C and to the downdraft effect as D. To achieve this, we use the Alpert-Stein factor separation method (Stein and Alpert, 1993). We categorize cases into 'no-light rain' (including no rain and light rain) and 'violent rain' in both the CTL and DEF simulations (B2). We then assume that wind changes in light rain events primarily reflect the influence of R/C, whereas changes in violent rain events after deforestation reflect three components: R/C, D, and synergy between R/C and D, see B2.

The mean wind speed in CTL during no-light rain is 0.92 $\mathrm{m\,s^{-1}}$, whereas it is 3.11 $\mathrm{m\,s^{-1}}$ in DEF (solid lines in Fig. B.9), indicating a contribution of 2.19 $\mathrm{m\,s^{-1}}$ from changes in R/C due to deforestation (f(R/C) in Table **??**). In CTL, during violent rain (dashed lines in Fig. B.9), the mean wind speed is 1.40 $\mathrm{m\,s^{-1}}$. The difference to the no-light rain case is 0.48 $\mathrm{m\,s^{-1}}$, and this represents the contribution from D in an unchanged environment. This comparison indicates that the impact of R/C alone due to deforestation is significantly larger than the impact of downdrafts under control conditions. The wind speed of violent rain is 4.56 $\mathrm{m\,s^{-1}}$ in DEF, and it contains both the effect of R/C and of the synergy of R/C and D compared to the violent rain in CTL. This gives a synergy effect of 0.97 $\mathrm{m\,s^{-1}}$. In summary, the relative contributions to the total wind speed anomaly are 60% R/C,

13% D, and 27% synergy. This indicates that deforestation amplifies wind speed not only by modifying surface roughness and circulation but also by strengthening the contribution of downdrafts during violent rain events. Note that the time resolution of outputs, hourly average value, may fail to capture downdrafts, which last for less than 30 minutes (Windmiller et al., 2023).

Table B2: The categories of simulations and rain types to disentangle the impact of Roughness length/ background Circulation (R/C), Downdraft (D), and its synergy impact (R/C & D) on windspeed in response to deforestation compared to CTL. The impact of each component is represented with f(0): CTL, f(R/C): roughness length/ background circulation, f(D): downdraft, and f(R/C & D): synergy between R/C and D. Values are in units of $m\,s^{-1}$. O: included/ X: not included

Simulation	Rain type	R/C	D	R/C & D	Abbrv.	value
CTL	No-Light rain	X	X	X	f(0)	0.92
DEF	No-Light rain	O	X	X	f(0)+f(R/C)	3.11
CTL	Violent rain	X	O	X	f(0)+f(D)	1.40
DEF	Violent rain	O	O	O	f(0)+f(R/C)+f(D)+f(R/C,D)	4.56

CONCLUSION

In this study, we investigated the effect of Amazon deforestation on short-duration events by looking at changes in hourly precipitation, temperature, and winds. We are particularly interested in the changes in the tails of the distributions, given the threats they pose. To do so, we use global simulations of Amazon deforestation conducted with a grid spacing of 5 km and explicit convection. In contrast to coarse-resolution simulations, such simulations are better suited to investigate changes in extremes.

The main findings are:

- From the five categories of rain events, major changes are only in the tails of the distributions: Violent rain increases by 54% and no-rain by 174%.
- daily minimum and maximum temperatures increase by 2.7 and 5.4°C. Day-to-day temperature becomes more variable, and all heat stress indicators, except for the wet-bulb temperature, point toward higher heat stress.
- the 99th percentile wind values more than doubled.

The increase in violent rains is due to stronger moisture convergence, not stronger CAPE and not stronger TCW, while the increase in no-rain results from increased CIN. The strong warming directly reflects the decrease in evapotranspiration following deforestation, whereas the increase in T_{WB} is mitigated by a strong decrease in near-surface humidity. Finally, we attributed the increase in mean wind speed during violent rain events to changes in roughness length and circulation (60%), downdraft intensification (13%), and synergistic interactions among the two

factors (27%). The documented changes would have impacts on human and forest regrowth. Increased diurnal and seasonal temperature variability will exacerbate the vulnerability of tropical trees, slowing their regeneration. Likewise, the elevated surface wind speeds are expected to create unfavorable conditions for forest regrowth and agriculture. In conclusion, we show that even if annual mean precipitation may remain stable after deforestation, the tail of temperature, precipitation, and wind distribution broadens, making conditions more unfavorable.

ACKNOWLEDGEMENTS

AY acknowledges funding by the CLICCS centre of excellence subproject A3 funded by DFG. We thank the German Climate Computing Center DKRZ for providing computing resources and the Integrated Climate Data Center (ICDC), the Center for Earth System Research and Sustainability (CEN), University of Hamburg, for supporting the IMERG data. In addition, we would like to thank Jana Sillmann for suggesting the analysis of heat stress indices and Keno Riechers for providing a thorough internal review of the initial manuscript at the Max Planck Institute for Meteorology. Open Access funding is enabled and organized by Projekt DEAL.

CODE AVAILABILITY

The source code of the ICON model is freely available at http://icon-model.org. The simulations were done with the ICON branch nextgems_cycle2. The IMERG data was downloaded from the Integrated Climate Data Center website (https://www.cen.uni-hamburg.de/en/icdc/data/atmosphere/imerg-precipitation-amount.html). The scripts used to process data and plot the figures in this paper are available in the repository via https://doi.org/10.17617/3.NYLGAN.

C

AMAZON PRECIPITATION UNDER WARMING FROM THE PERSPECTIVE OF THE MOISTURE BALANCE EQUATION

The work in this appendix has been prepared for submission:

Yoon, A., Hohenegger, C., Segura, H (2025c): "Amazon precipitation under warming from the perspective of the moisture balance equation", In: *preparation for submission*.

Author contributions:
AY: conceptualization; data curation; formal analysis; investigation; methodology; software; visualization; writing – original draft; writing – review and editing. **CH**: conceptualization; funding acquisition; investigation; project administration; resources; supervision; review and editing, **HS**: discussion, provide a code for calculating SAL

Amazon precipitation under warming from the perspective of the moisture balance equation

Arim Yoon[1,2], Cathy Hohenegger[1], Hans Segura[1]

[1]Max Planck Institute for Meteorology, Bundesstraße 53, 20146 Hamburg, Germany [2]International Max Planck Research School on Earth System Modeling (IMPRS-ESM), Bundesstraße 53, 20146 Hamburg, Germany

ABSTRACT

Despite its importance, the impact of increased atmospheric CO_2 on Amazonian precipitation remains unclear, as does its underlying mechanism. In this study, we use a global storm-resolving model better to understand the mechanisms of Amazon precipitation changes under warming. For that, both coupled under SSP3-7.0 and idealized warming with prescribed SST, a quadrupling CO_2 (4CO2) and 4K plus SST (P4K), are used. We find that the response of precipitation follows different feedback loops between precipitation, moisture convergence, and evapotranspiration in the moisture balance equation, initiated by the moisture convergence. Coupled and 4CO2 simulations show a positive feedback where moisture convergence, evapotranspiration, and precipitation follow each other. As moisture convergence decreases, evapotranspiration decreases, and precipitation decreases in the coupled and all terms increase in the 4CO2 simulation. In contrast, P4K doesn't show the same positive feedback where moisture convergence decreases, evapotranspiration increases, and precipitation increases. The difference in P4K is due to its abundant soil moisture, which could sustain enough moisture for evapotranspiration. To understand how the feedback loop is initiated, the energy framework is applied to attribute the changes in moisture convergence in either total column energy or changes in vertical stability.

INTRODUCTION

Under increasing atmospheric CO_2 concentration, Amazon has warmed at an average rate of 0.27 °C per decade since the 1980s, exceeding 2 °C of warming over the past 40 years (Flores et al., 2024). While shifts in precipitation have accompanied this warming, there is no consistent, basin-wide trend that has been observed (Marengo, 2004; Espinoza Villar et al., 2009; Satyamurty et al., 2010; Almeida et al., 2017). Although southern Amazonia shows a consistent drying trend (Alves et al., 2016; Espinoza et al., 2019; Feron et al., 2024), which is largely attributed to land-use change rather than direct CO_2-induced warming. Consequently, the direct impact of warming on Amazonian rainfall remains poorly understood.

To isolate the effects of CO_2-induced warming from other anthropogenic disturbances, modeling studies have been conducted. Although our understanding of large-scale tropical precipitation changes under warming is well established (Held and Soden, 2006; Chou et al., 2009; Seager et al., 2010; Muller and O'Gorman, 2011), regional projections over the Amazon remain highly uncertain (Joetzjer et al., 2013;

Li et al., 2006). For example, under the RCP8.5 scenario, half of the 36 CMIP5 models project wetter conditions in the Amazon, while the other half predict drying (Boisier et al., 2015). This divergence is often attributed to biases introduced by convective parameterizations (Stevens and Bony, 2013; Richter et al., 2012). Additionally, oceanic feedbacks—especially related to internal variability and sea surface temperature (SST) patterns—have been identified as major sources of uncertainty (Joetzjer et al., 2013; Kent et al., 2015). While CMIP6 models exhibit a more consistent drying response (Cook et al., 2020; Ukkola et al., 2020), it raises concerns about their reliability on rainfall projection over the Amazon. Drying Amazon under warming in the CMIP6 is largely due to their consistently projected 'El Niño-like' SST pattern (Parsons, 2020). However, these models often exhibit systematic biases in present-day SST patterns, especially in key regions such as the tropical Pacific (Ying et al., 2024). This raises concerns about whether the agreement on Amazon drying in CMIP6 reflects a true climate signal or merely a shared systematic bias (Tierney et al., 2015), thereby limiting confidence in their projections.

These challenges highlight the need for next-generation models that can overcome structural uncertainties. Storm-resolving models (SRMs), which explicitly simulate convection without relying on parameterization, offer a promising path forward. To date, two studies are using a storm-resolving regional climate model to investigate Amazon precipitation under increased CO_2. Rehbein and Ambrizzi (2023) reports that the frequency of mesoscale convections decreases under warming, without reporting changes in total precipitation, which does not stem from mesoscale convections. Another study Kahana et al. (2024) projects drying Amazon, but their model depends on boundary conditions provided by a conventional global model that itself simulates drying. As a result, the simulation is not fully independent of the parameterization biases it aims to avoid. This underscores the need for global storm-resolving simulations.

Complementary to storm-resolving models (SRMs), atmosphere-only simulations (AMIP) provide a valuable framework for isolating the atmospheric response to CO_2-induced warming. By prescribing sea surface temperatures (SSTs), AMIP experiments eliminate ocean–atmosphere feedbacks, thereby reducing uncertainties associated with SST pattern changes (Bony et al., 2013; Shaw and Voigt, 2016; Chadwick et al., 2019; Mutton et al., 2024). These simulations are also particularly well-suited for decomposing the drivers of land warming into two key components that influence land precipitation: radiative effects from increased CO_2 and remote ocean warming. A central factor shaping precipitation over land is the land–ocean temperature contrast as land warms more (Joshi et al., 2008), which can alter large-scale circulation. Additionally, local land warming by radiative warming affects atmospheric stability, circulation by temperature gradient, and lowered relative humidity (RH) (Joshi et al., 2008; Lambert et al., 2011; Byrne and O'Gorman, 2013). Reduced RH can influence rainfall—either directly by limiting available moisture (Chadwick et al., 2013; Byrne and O'Gorman, 2015) or indirectly through increased cloud-base height and changes in convective dynamics (Fasullo, 2012). To disentangle these effects, we compare two AMIP simulations: (1) one with quadrupled CO_2 and prescribed present-day SSTs (4CO2) to isolate the fast radiative response, and

(2) another with uniform +4 K SST warming under fixed preindustrial CO_2 (P4K) to capture the slow ocean-mediated response. This approach enables us to identify the dominant physical mechanisms driving land precipitation between these two CO_2-induced warming, corresponding to different time scales. While it has been successfully applied in regions such as West Africa (Mutton et al., 2024) and South Asia (Endo et al., 2018), it remains largely unexplored over the Amazon.

In this study, we bring together these two methodological advances—global storm-resolving coupled simulations and AMIP experiments with separated fast and slow responses—to investigate the changes in Amazonian rainfall under different warming by elevated CO_2. To enable direct comparison across these simulations, we apply the moisture balance equation, which decomposes precipitation into two primary components of the Amazonian rainfall: evapotranspiration and moisture convergence. This diagnostic framework allows us to assess whether changes in rainfall are governed predominantly by local land–atmosphere processes (i.e., reduced evapotranspiration) or by large-scale dynamic factors such as changes in atmospheric moisture transport.

METHODS

We use the ICOsahedral Non-hydrostatic model with Sapphire configuration Hohenegger et al., 2023, ICON, a global storm-resolving global climate model that explicitly resolves convection and parameterizes only turbulence, cloud microphysics, and radiation. Two types of simulations are performed with ICON, each with slight differences in configuration: 1) atmospheric-only simulations following the AMIP protocols, and 2) fully coupled atmosphere-ocean simulations.

Coupled simulation belongs to the fourth cycle of model development within the Next Generation of Earth Modelling Systems (Segura et al., 2025). It uses 5 km resolution in the ocean, and 10 km resolution in the atmosphere and land, with 90 vertical levels. The land surface model is the Jena Scheme for Biosphere-Atmosphere Coupling in Hamburg (JSBACH; Reick et al., 2021). JSBACH includes five vertical soil layers, of which we consider only the top three in our Amazon-focused analysis, only including the root zone. Biogeochemical processes, including dynamic vegetation, photosynthesis, and carbon and nitrogen cycles, are not included in the simulations. The ocean model is ICON-O (Korn et al., 2022) for the coupled simulation. Further information about model settings can be found Segura et al. (2025) Appendix A. Simulations follow the SSP3-7.0 warming scenario from 2020 to 2049. After excluding a spin-up period (2020-2023), we analyze two periods to assess the impact of increasing CO_2: averaged value in the beginning of five years from 2024-2028, and the end of five years from 2045-2049.

The AMIP simulations are run at 10 km horizontal resolution over the atmosphere and land, with 90 vertical levels. They span 14 years in common (1980-1993). Prescribed SST and sea ice are from a merged product based on HadISST1 and NOAA OI.v2 datasets. With this setup, three simulations are conducted: 1) CTL,

the control simulation with prescribed monthly SST and pre-industrial CO_2 levels, 2) 4CO2, a simulation with quadrupled CO_2 with prescribed SST. CO_2 change is only applied to the radiation scheme to isolate the direct radiative effect, 3) P4K, an experiment with a uniform SST warming by 4K, with preindustrial CO_2, to isolate the ocean warming effect.

All simulation outputs are written on the Hierarchical Equal Area isoLatitude Pixelization (HEALPix) grid with 10 different zoom levels. This study uses zoom level eight, which corresponds to a resolution of approximately 25.5km, with a daily mean output.

RESULTS

How does Amazon mean precipitation change?

We begin by analyzing the mean precipitation averaged over the Amazon. In the present-day climate, the coupled simulation averaged over the first five years shows an annual mean precipitation of 4.76 mm day^{-1}, which is notably lower than that of the AMIP-CTL, at 6.73 mm day^{-1}. These values are compared with the IMERG satellite dataset, which provides a 20-year climatology (2001-2021). Among the two simulations, AMIP-CTL closely reproduces both the annual mean and the seasonality of the Amazonian rain (Fig. C.1a). In contrast, the coupled simulation deviates from observations, primarily due to a broader latitudinal migration of the rainbelt. It causes the seasonal peak of precipitation to shift outside the Amazon basin (Fig. C.1b). As a result, the wet-season rainfall is underestimated within the basin itself, leading to a lower annual mean. Nevertheless, as both the coupled and AMIP simulations capture the general seasonal migration of precipitation shown through the movement of the centroid of the rainbelt over South America (82°W-30°W, 30°S-13°N) (Fig. C.1b, c), the large-scale circulation is well captured from both setups of simulations.

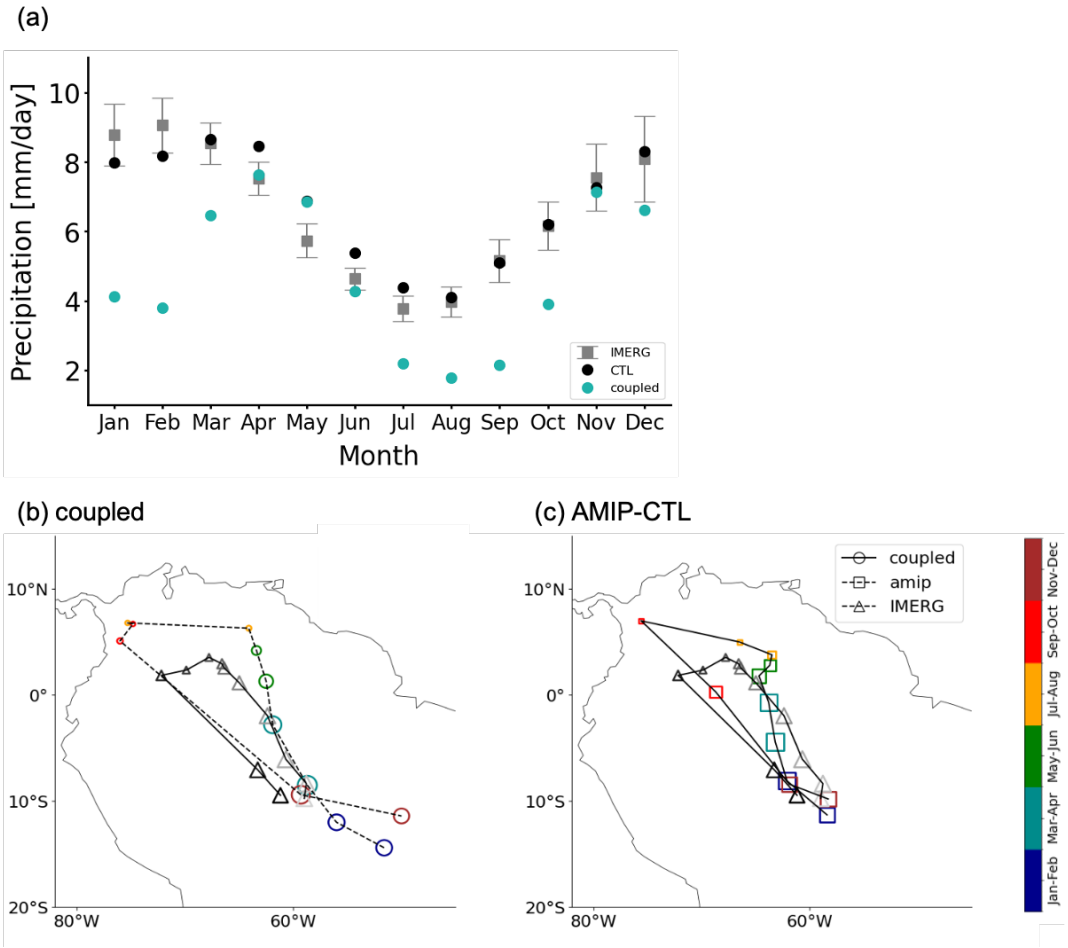

Figure C.1: (a) Monthly mean precipitation (mm day^{-1}) averaged over the Amazon region (outlined by the red contour in Figure C.3) from coupled (lightblue), AMIP-CTL (black) simulations, and 20-y (2020-2021) of averaged IMERG observations (light grey). IMERG is plotted with interannual variability (standard deviation). Seasonal migration of the monthly mean location of the centroid of the rainbelt over South America (82°W-30°W, 30°S-13°N) calculated by the SAL method (see Segura et al., 2022) for (b) the first 5 years of coupled and (c) AMIP-CTL simulations. Marker colors indicate the month, and for a better visualization, colors are grouped by 2 months.

Under increased CO_2 conditions, the coupled simulation shows a reduction in precipitation of 0.3 mm day^{-1} (-6.21% of its present-day amount), corresponding to a hydrological sensitivity of -5.73%/K with the increase in surface temperature over the Amazon of 1.08 K. Monthly precipitation generally decreases throughout the year, with expections in Feb, Aug, and Sep, even though these changes are not statistically significant (Fig. C.2). On the other hand, both AMIP simulations show an increase in annual mean precipitation by 0.27 mm day^{-1} (+4%) for 4CO2 and 0.14 mm day^{-1} (+2%) for P4K. Given the stronger warming over the Amazon in the P4K scenario, 4.71 K, hydrological sensitivity is low at 0.43%/K, compared to the higher sensitivity of 9.53%/K in the 4CO2 scenario with 0.42 K warming. In the monthly mean, the 4CO2 simulation consistently shows increased precipitation compared to the CTL throughout the year. In contrast, the P4K scenario exhibits

greater seasonality, with a significant increase during the wet season and a corresponding decrease during the dry season.

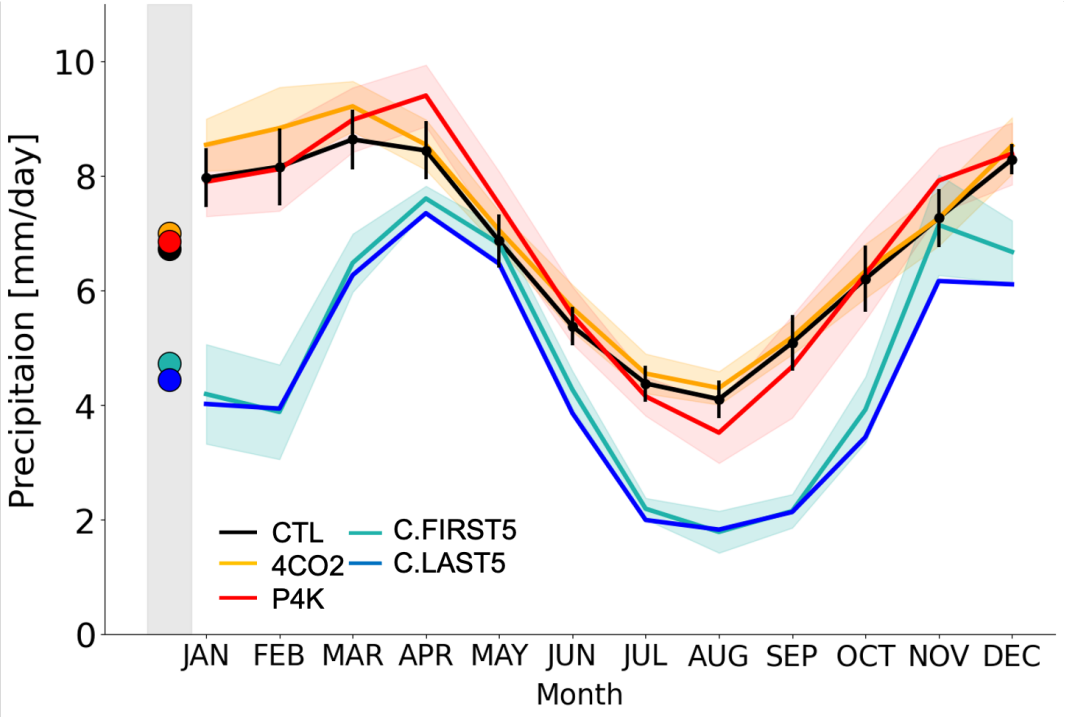

Figure C.2: Monthly mean precipitation (mm day^{-1}) averaged over the Amazon region. Coupled simulations are represented in light blue (C.FIRST5, the first 5-year average) and dark blue (C.LAST5, the end 5-year average). AMIP simulations are represented by black (CTL), orange (4CO2), and red (P4K) lines. To account for the internal variability, the standard deviation range from CTL is shown with black vertical lines. Shaded areas indicate the corresponding variability ranges for the first 5-year average (blue), 4CO2 (orange), and P4K (red).

To further check the spatial patterns of precipitation changes and their contributions from evapotranspiration and moisture convergence, we applied the moisture balance equation to disentangle the two components. Although the coupled simulation hasn't reached the equilibrium as it has a gradual CO_2 forcing, we assume the tendency of column water vapor is near zero. Hence, we calculate moisture convergence from the residual of evapotranspiration from precipitation. Spatially, the first thing that strikes out over the Amazon basin is that drying occurs in the coupled simulation versus moistening in the AMIP simulations. Coupled simulation has a reduction in precipitation over the entire Amazon, with the most pronounced decrease occurring in the east (Fig. C.3a). This spatial pattern aligns mainly with a reduction in evapotranspiration. Following the percentage changes (%) in each component of the atmospheric moisture budget, normalized by precipitation from the control simulations ($\frac{\Delta Pr}{Pr} \times 100 = \frac{\Delta CONVG}{Pr} \times 100 + \frac{\Delta EVP}{Pr} \times 100$), evapotranspiration accounting for 3.76% of the total 6.21% reduction in precipitation (Fig. C.3g). Moisture convergence also decreases by 2.45% which adds up with evapotranspiration changes (3.76%) to precipitation (6.21%). 4CO2, on the other hand, shows an increase in precipitation across the Amazon with less moistening on the east

(Fig. C.3b), which is consistent with the response in the coupled simulation (Fig. C.3a). This increase is primarily due to increased moisture convergence, accounting for 2.66% of the overall 4.04% precipitation increases (Fig. C.3e). The rest of the other changes happen through evapotranspiration, which contributes an additional 1.37% (Fig. C.3h). The P4K scenario presents a ring of drying (Fig. C.3c), which has a similar spatial pattern as Chadwick et al. (2019). While evapotranspiration uniformly increases across the Amazon, contributing positively by 3.64% to precipitation changes (Fig. C.3i), moisture convergence decreases by 1.64%, reflecting a spatial pattern similar to the precipitation changes (Fig. C.3f). One thing to be noted from 4CO2 and P4K is that both AMIP simulations show more rain despite the different precipitation changes over the ocean.

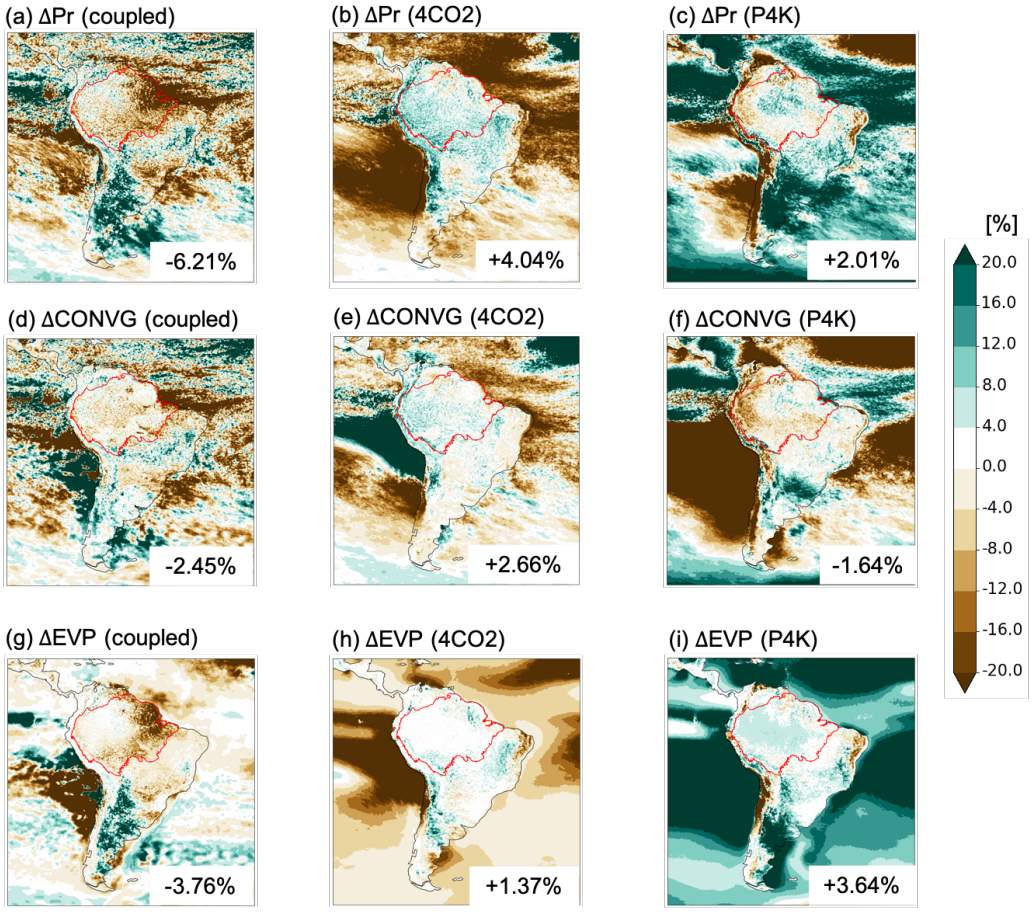

Figure C.3: Maps of percentage changes (%) in each component of the atmospheric moisture budget, normalized by precipitation from the control simulations ($\frac{\Delta Pr}{Pr} \times 100 = \frac{\Delta CONVG}{Pr} \times 100 + \frac{\Delta EVP}{Pr} \times 100$, Pr: precipitation, CONVG: moisture convergence, EVP: evapotranspiration). Values are expressed in percentages and averaged over the Amazon region, outlined in red contours. Numbers on the maps indicate Amazon mean changes.

What is the mechanism for changed precipitation?

To understand these changes, we first aim to understand evapotranspiration response through its controlling factors: net surface radiation, vapor pressure deficit (VPD), 10 m wind speed, and soil moisture. In the coupled simulation, where evapotranspiration decreases, we have more net surface radiation by 0.82 $W\,m^{-2}$, VPD by 2.02 K, and no change in 10 m wind (Fig. C.4). These changes in atmospheric controlling factors suggest that evapotranspiration should have increased, making soil moisture the primary limiting factor. In the AMIP simulations, which show higher evapotranspiration in both 4CO2 and P4K, 4CO2 shows +1.12 $W\,m^{-2}$ in net surface radiation, +0.14 K in VPD, and -0.01 $m\,s^{-1}$ in the surface wind, while P4K shows +11.4 $W\,m^{-2}$, +2.67 K in VPD, and -0.09 $m\,s^{-1}$ in the surface wind. Given that evapotranspiration increases in both experiments, these results from atmospheric values prevent the soil moisture from being a controlling factor in either case.

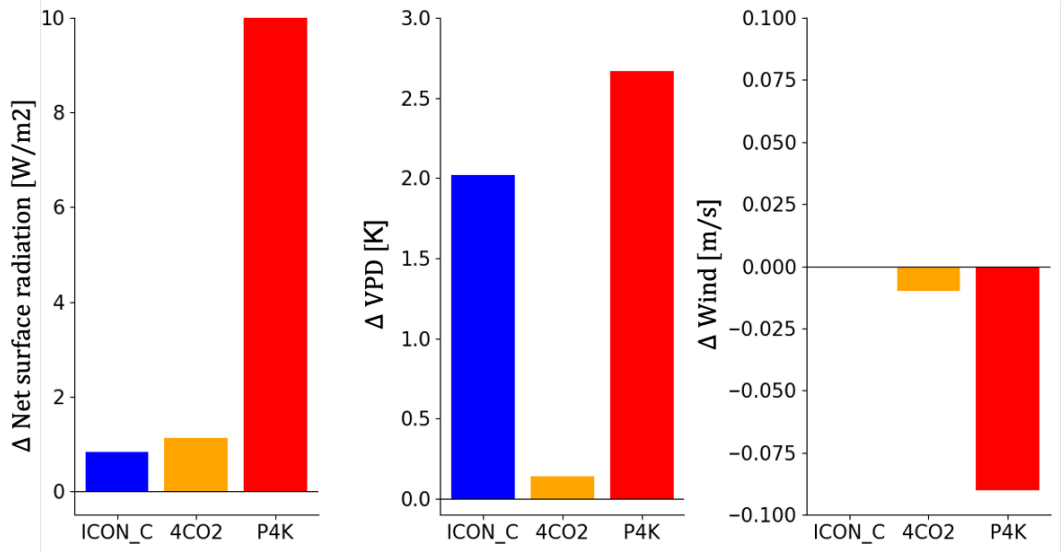

Figure C.4: Changes in atmospheric controlling factors on evapotranspiration compared to their control condition: net surface radiation ($W\ m^{-2}$), vapor pressure deficit (VPD; K), and 10m wind speed ($m\ s^{-1}$). Bars represent changes in the coupled simulation (ICON_C, blue), 4CO2 (orange), and P4K (red) simulations.

Based on this, we propose a hypothesis to explain the feedback loops starting from changes in moisture convergence within the moisture balance equation (Fig. C.5). Starting the feedback loop from evapotranspiration fails to capture the full dynamics of moisture changes, as moisture supplied by evapotranspiration cannot influence the inflow of atmospheric moisture via convergence. In contrast, moisture brought in by convergence affects both precipitation and soil moisture, which in turn regulate evapotranspiration. Therefore, feedback initiated by changes in convergence can propagate through the system, while those starting from evapotranspiration do not influence convergence, making evapotranspiration an incomplete starting point for explaining the full response. In the coupled simulation, reduced moisture transport by moisture convergence under warming initiates a

decrease in precipitation, which then lowers soil moisture. This reduction in soil moisture limits evapotranspiration, further suppressing precipitation. This forms a positive feedback loop: reduced moisture convergence leads to less precipitation, less soil moisture, less evapotranspiration, and less precipitation. In 4CO2, we can apply the same positive linkage as increased moisture convergence enhances precipitation, maintaining soil moisture and supporting higher evapotranspiration. Together, the coupled and 4CO2 show a positive feedback loop starting from moisture convergence. However, P4K breaks this pattern. Despite a decrease in moisture convergence – expected to reduce soil moisture and evapotranspiration – evapotranspiration still increases, and precipitation also increases. It raises the question of what mechanisms are missing and points to the need to examine soil moisture to confirm this hypothesis.

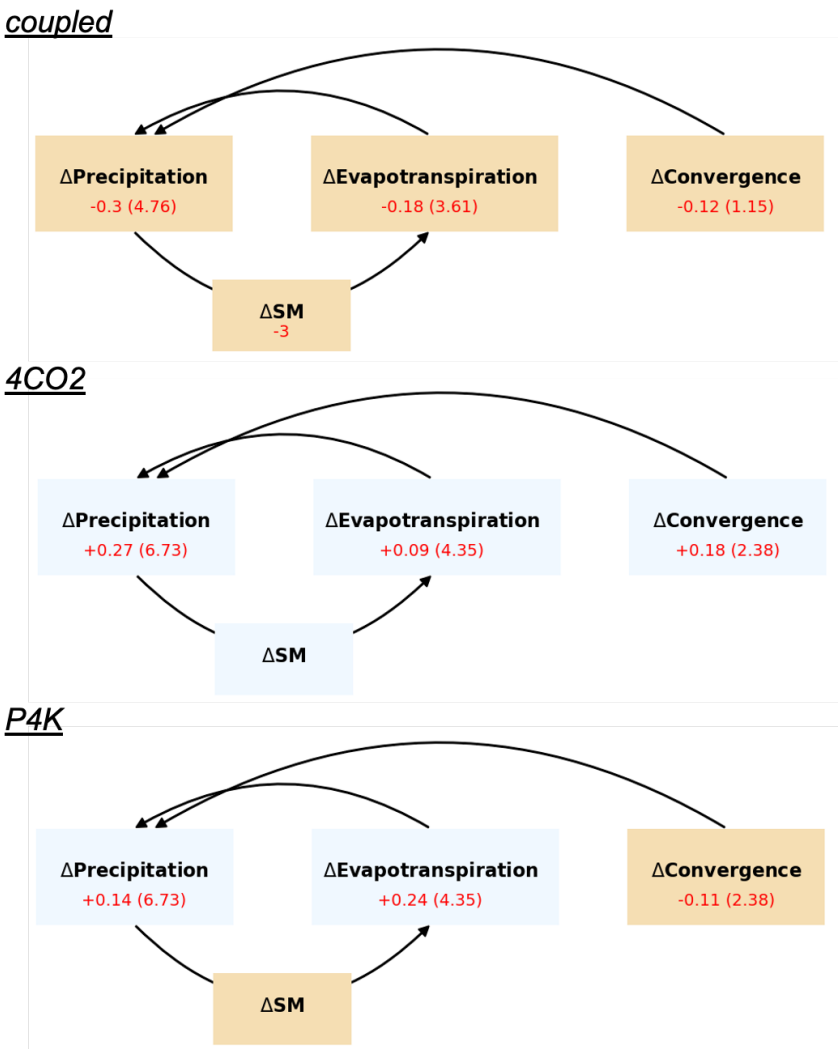

Figure C.5: Schematic of feedbacks in the moisture balance equation for each simulation. Brown boxes indicate a decrease relative to their control condition, while blue boxes indicate an increase. Amazon-averaged changes in values (mm day^{-1}) are written in red, with corresponding control values provided in parentheses. Soil moisture (m) represents a root-zone soil moisture averaged over the Amazon basin.

As expected, coupled simulation shows a 3 mm reduction in root zone soil moisture. Because the AMIP simulations lack direct soil moisture outputs (except for CTL), we use evaporative fraction (EF, $\frac{LatentHeat}{SensibleHeat+LatentHeat}$) as a proxy, based on the Budyko-like relationship between EF and root-zone soil moisture (Fig. C.6a). It shows a linear relationship between EF and soil moisture when EF is roughly between 0.3 to 0.8 in both AMIP and coupled simulations, while becoming less sensitive to soil moisture outside of the range. Coupled simulation falls within this transitional regime, with EF decreasing from 0.68 in the first five years of coupled simulation to 0.63 for the last five years. It shows that soil moisture in the coupled simulation strongly influences evapotranspiration and is influenced by moisture convergence, as we show (Fig. C.5). In contrast, both 4CO2 and P4K have nearly unchanged EF compared to CTL, increasing slightly from an annual mean of 0.81 in CTL to 0.82 in 4CO2 and decreasing to 0.79 in P4K (Fig. C.6b). These EF values above 0.8 imply that soil moisture is not in the range of limiting evapotranspiration, i.e., the soil moisture is abundant initially. The slight increase in 4CO2 reflects that soil moisture may increase slightly, supporting the positive feedback (Fig. C.5). On the other hand, a slight decrease in P4K indicates a small reduction in soil moisture, aligning with the effect of reduced moisture convergence. However, the reduction appears insufficient to cross the threshold where soil moisture would begin to limit evapotranspiration. Thus, despite decreased soil moisture in the P4K, evapotranspiration is maintained and even enhanced through increased atmospheric controlling factors such as net radiation, VPD, and wind. However, the loss of precipitation during the dry period (JAS) indicates that the same mechanism does not work throughout the year. Although the wet period shows a slight increase in moisture convergence, the decrease during the dry season outweighs its signal. Whereas, the increase in evapotranspiration is always bigger than the control simulation, except dry season, when it shows no change.

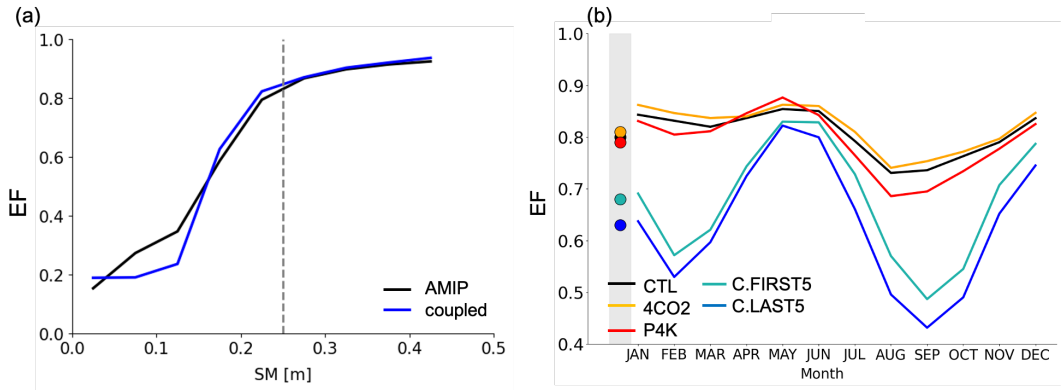

Figure C.6: (a) Relationship between evaporative fraction (EF) and root-zone soil moisture (m) for AMIP CTL (black line) and the first 5-year average of coupled simulation (blue line). The line represents the median EF within each bin with an interval of 0.05, based on daily values over the Amazon basin in the range of 0 to 0.5. (b) The monthly mean EF averaged over the Amazon is plotted with dots indicating the annual mean.

What is the mechanism behind changes in moisture convergence?

To complete the moisture budget analysis (Fig. C.5), we need to understand why moisture convergence over the Amazon responds differently in each simulation. For that, we use the energetic framework. We decompose the changes in moisture convergence into contributions from the net change in total column energy (Qnet) and the vertically integrated moist static energy, total gross moist stability (TGMS), following (See equation 15 from Jalihal et al. (2019).)

$$\Delta(P-E) = \underbrace{\frac{\frac{\Delta Q_{net}}{Q_{net}}}{1+\frac{\Delta TGMS}{TGMS}} \times (P-E)}_{\text{Contribution from Qnet}} + \underbrace{\frac{-\frac{\Delta TGMS}{TGMS}}{1+\frac{\Delta TGMS}{TGMS}} \times (P-E)}_{\text{Contribution from TGMS}}$$

As shown in Table C1, both the 4CO2 and P4K simulations show that the contribution from total column energy dominates over TGMS in explaining changes in moisture convergence. In the 4CO2 simulation, total column energy increases by 10.25 $W\,m^{-2}$, consistent with the enhancement of moisture convergence. This increase is primarily driven by reduced outgoing longwave radiation due to strong absorption of longwave radiation by CO_2, which reduces atmospheric cooling. In contrast, the P4K simulation shows a decrease in total column energy by 5.19 $W\,m^{-2}$, which aligns with a weakening of moisture convergence. SST warming increases outgoing longwave radiation as the land surface and troposphere warm, enhancing atmospheric cooling. Although less shortwave radiation is reflected, due to a reduction in low-level clouds (not shown here), this warming effect is outweighed by the stronger longwave cooling. On the other hand, in the coupled simulation, the net total column energy slightly increases. While outgoing longwave radiation increases due to tropospheric warming, it is offset by a reduction in outgoing shortwave radiation. This small increase in total column energy has little influence on moisture convergence, which appears to be more closely linked to the TGMS contribution, unlike AMIP simulations. Given that TGMS represents changes in vertical stability of the atmosphere, the atmosphere becomes more stable in the coupled simulation with increased CO_2, resulting in less moisture convergence.

SUMMARY AND CONCLUSION

In this study, we investigate how CO_2-induced warming influences Amazon precipitation by applying the moisture balance equation to both atmosphere-ocean coupled and atmospheric-only simulations. We use a global storm-resolving simulation at 10 km grid spacing, which explicitly represents convective processes and large-scale feedbacks. It removes systematic biases stemming from convective parameterization, which is pointed out as one of the factors contributing to wide uncertainties in their projection. Additionally, to isolate the atmospheric response from the ocean feedback, we use AMIP simulations with a prescribed ocean. Based

	Term1 (Qnet)	Term 2 (TGMS)	ΔConvg
4CO2	0.40	-0.22	0.18
P4K	-0.22	0.12	-0.11
Coupled	0.04	-0.16	-0.12

Table C1: The contribution of total column energy (Term 1) and total gross moist stability (TGMS, Term 2) to the changes in moisture convergence compared to their control situations. Values are averaged over the Amazon basin, and each contribution is calculated following the equation in section 3.3. All units are in mm day^{-1}. The main contribution of the two is colored in grey.

on ways to warm land and atmosphere corresponding to different timescales, we compare two experiments: fast radiative response with quadrupled CO_2 and prescribed SSTs (4CO2), and slow ocean-driven response with uniformly warmed SSTs by 4K. To understand their underlying mechanisms of rain change, we propose a feedback loop within the moisture balance equation in which changes in moisture convergence initiate a chain of interactions influencing evapotranspiration and precipitation. To close the loop, we apply an energetic perspective, attributing changes in moisture convergence to variations in total atmospheric energy or vertical stability, characterized by gross moist stability (GMS).

The main findings are:
- In the coupled simulation, precipitation decreases in response to increasing CO_2, whereas in both 4CO2 and P4K with prescribed SST, precipitation increases.
- We find two different feedback loops. The first one, where moisture convergence, evapotranspiration, and precipitation follow each other. In the coupled simulation, moisture convergence, precipitation, and evapotranspiration decrease. In contrast, in 4CO2, moisture convergence, precipitation, and evapotranspiration increase. The second one, where moisture convergence decreases, evapotranspiration increases, and precipitation increases, as in P4K.
- The level of soil moisture constrains the impact of moisture convergence on precipitation and differentiates the two feedback loops: when soil moisture is sufficient, evapotranspiration and precipitation can increase despite a reduction in moisture convergence.
- In AMIP simulations, changes in total column energy dominate the change of moisture convergence and explain the increase in moisture convergence in 4CO2 and the decrease in P4K. In contrast, in the coupled simulation, GMS, which represents vertical stability, explains the decrease in moisture convergence.

In both AMIP simulations, Amazon precipitation increases, but for different reasons. During the fast atmospheric adjustment to elevated CO_2, longwave absorption reduces atmospheric cooling, leading to an energetic surplus that strengthens moisture convergences. Regardless of its enhanced convergence, its abundant soil moisture enables the evapotranspiration to increase under a favorable atmospheric

environment, which in turn supports increased precipitation, a positive feedback. On the other hand, under pure SST warming, outgoing longwave increases radiative cooling due to surface and tropospheric warming, while shortwave reflection is decreased due to reduced low-level clouds. The net effect weakens moisture convergence. Nonetheless, abundant soil moisture buffers this reduction, and evapotranspiration can increase in response to warming and more than offset the reduction in moisture convergence, enhancing precipitation. In the coupled simulation, changes in the net total column energy are minimal and do not explain the variation in moisture convergence. Instead, the vertical stability, which is presented by TGMS, decreases moisture convergence. As soil moisture declines within a transitional regime, where its amount directly controls evapotranspiration, the system is sensitive to changes in moisture convergence. As a result, reduced moisture convergence leads to lower precipitation and a further decrease in evapotranspiration through reduced soil moisture. Through this study, we highlight the importance of moisture convergence to initiate the feedback loop in the moisture balance equation to decide the precipitation over the Amazon under increased CO_2 if soil moisture stays lower than a certain threshold.

Based on the results, we might expect a nonlinear precipitation response to SST warming, in contrast to the more continuous response to CO_2 radiative effects as we further enhance forcings. Under the gradually increasing radiative forcing without ocean interaction, precipitation may tend to rise due to a positive feedback between moisture convergence and evapotranspiration. However, with gradual SST warming, this feedback may eventually reverse. Reduced moisture convergence could lower soil moisture beyond a threshold, triggering a feedback that limits evapotranspiration and leads to a sudden drop in precipitation. Given that CO_2 radiative effects represent the fast response and SST warming reflects the slower response to elevated CO_2, it raises an open question. While the ocean-atmosphere coupled simulation begins with a drying trend, could there be a transitional regime where precipitation initially increases due to CO_2 radiative effects but later declines as SST warming intensifies and soil moisture becomes limiting? Alternatively, the coupled result may reflect a net outcome where radiatively driven moistening is overwhelmed by SST-driven drying due to soil moisture sensitivity. Although it is difficult to compare one-to-one due to the ocean interaction effect, to clarify this possible transition requires further investigation using coupled simulations with stronger CO_2 forcing.

BIBLIOGRAPHY

Abramian, Sophie, Caroline Muller, and Camille Risi (2023). "Extreme precipitation in tropical squall lines." In: *Journal of Advances in Modeling Earth Systems* 15.10, e2022MS003477.

Allan, Richard P and Brian J Soden (2008). "Atmospheric warming and the amplification of precipitation extremes." In: *Science* 321.5895, pp. 1481–1484.

Almeida, CT et al. (2017). "Spatiotemporal rainfall and temperature trends throughout the Brazilian Legal Amazon, 1973–2013." In: *International Journal of Climatology* 37.4, pp. 2013–2026.

Alves, Eliane G et al. (2016). "Seasonality of isoprenoid emissions from a primary rainforest in central Amazonia." In: *Atmospheric Chemistry and Physics* 16.6, pp. 3903–3925.

Alves, Lincoln Muniz et al. (2017). "Sensitivity of Amazon regional climate to deforestation." In: *American Journal of Climate Change* 6.1, pp. 75–98.

Avissar, Roni et al. (2002). "The large-scale biosphere-atmosphere experiment in Amazonia (LBA): Insights and future research needs." In: *Journal of Geophysical Research: Atmospheres* 107.D20, LBA–54.

Back, Larissa E and Christopher S Bretherton (2009). "On the relationship between SST gradients, boundary layer winds, and convergence over the tropical oceans." In: *Journal of Climate* 22.15, pp. 4182–4196.

Baldocchi, Dennis and Siyan Ma (2013). "How will land use affect air temperature in the surface boundary layer? Lessons learned from a comparative study on the energy balance of an oak savanna and annual grassland in California, USA." In: *Tellus B: Chemical and Physical Meteorology* 65.1, p. 19994.

Barnett, AG, Shilu Tong, and Archie CA Clements (2010). "What measure of temperature is the best predictor of mortality?" In: *Environmental research* 110.6, pp. 604–611.

Bayr, Tobias and Dietmar Dommenget (2013). "The tropospheric land–sea warming contrast as the driver of tropical sea level pressure changes." In: *Journal of Climate* 26.4, pp. 1387–1402.

Boisier, Juan P et al. (2015). "Projected strengthening of Amazonian dry season by constrained climate model simulations." In: *Nature Climate Change* 5.7, pp. 656–660.

Bolton, David (1980). "The computation of equivalent potential temperature." In: *Monthly weather review* 108.7, pp. 1046–1053.

Bonan, Gordon B (2008). "Forests and climate change: forcings, feedbacks, and the climate benefits of forests." In: *science* 320.5882, pp. 1444–1449.

Bony, Sandrine et al. (2013). "Robust direct effect of carbon dioxide on tropical circulation and regional precipitation." In: *Nature Geoscience* 6.6, pp. 447–451.

Bosilovich, Michael G (2002). "On the vertical distribution of local and remote sources of water for precipitation." In: *Meteorology and atmospheric physics* 80.1, pp. 31–41.

Boulton, Chris A, Timothy M Lenton, and Niklas Boers (2022). "Pronounced loss of Amazon rainforest resilience since the early 2000s." In: *Nature Climate Change* 12.3, pp. 271–278.

Bradshaw, Corey JA et al. (2021). "Underestimating the challenges of avoiding a ghastly future." In: *Frontiers in Conservation Science* 1, p. 615419.

Bröde, Peter et al. (2012). "Deriving the operational procedure for the Universal Thermal Climate Index (UTCI)." In: *International journal of biometeorology* 56, pp. 481–494.

Brown, Vincent M, Barry D Keim, and Alan W Black (2020). "Trend analysis of multiple extreme hourly precipitation time series in the southeastern United States." In: *Journal of Applied Meteorology and Climatology* 59.3, pp. 427–442.

Bullock, Eric L et al. (2020). "Satellite-based estimates reveal widespread forest degradation in the Amazon." In: *Global Change Biology* 26.5, pp. 2956–2969.

Burkart, Katrin et al. (2011). "The effect of atmospheric thermal conditions and urban thermal pollution on all-cause and cardiovascular mortality in Bangladesh." In: *Environmental Pollution* 159.8-9, pp. 2035–2043.

Butt, Edward W et al. (2023). "Amazon deforestation causes strong regional warming." In: *Proceedings of the National Academy of Sciences* 120.45, e2309123120.

Byrne, Michael P and Paul A O'Gorman (2013). "Link between land-ocean warming contrast and surface relative humidities in simulations with coupled climate models." In: *Geophysical Research Letters* 40.19, pp. 5223–5227.

Byrne, Michael P and Paul A O'Gorman (2015). "The response of precipitation minus evapotranspiration to climate warming: Why the "wet-get-wetter, dry-get-drier" scaling does not hold over land." In: *Journal of Climate* 28.20, pp. 8078–8092.

Chadwick, Robin, Ian Boutle, and Gill Martin (2013). "Spatial patterns of precipitation change in CMIP5: Why the rich do not get richer in the tropics." In: *Journal of climate* 26.11, pp. 3803–3822.

Chadwick, Robin et al. (2019). "Separating the influences of land warming, the direct CO2 effect, the plant physiological effect, and SST warming on regional precipitation changes." In: *Journal of Geophysical Research: Atmospheres* 124.2, pp. 624–640.

Chou, Chia and J David Neelin (2004). "Mechanisms of global warming impacts on regional tropical precipitation." In: *Journal of climate* 17.13, pp. 2688–2701.

Chou, Chia et al. (2009). "Evaluating the "rich-get-richer" mechanism in tropical precipitation change under global warming." In: *Journal of climate* 22.8, pp. 1982–2005.

Commar, Luiz Felipe Sant'Anna, Gabriel Medeiros Abrahão, and Marcos Heil Costa (2023). "A possible deforestation-induced synoptic-scale circulation that delays the rainy season onset in Amazonia." In: *Environmental Research Letters* 18.4, p. 044041.

Cook, Benjamin I et al. (2020). "Twenty-first century drought projections in the CMIP6 forcing scenarios." In: *Earth's Future* 8.6, e2019EF001461.

Correia, Francis Wagner Silva, Regina Célia dos Santos Alvalá, and Antônio Ocimar Manzi (2008). "Modeling the impacts of land cover change in Amazonia: a regional climate model (RCM) simulation study." In: *Theoretical and Applied Climatology* 93, pp. 225–244.

Costa, Marcos Heil and Jonathan A Foley (2000). "Combined effects of deforestation and doubled atmospheric CO 2 concentrations on the climate of Amazonia." In: *Journal of Climate* 13.1, pp. 18–34.

Crook, N Andrew and Mitchell W Moncrieff (1988). "The effect of large-scale convergence on the generation and maintenance of deep moist convection." In: *Journal of the atmospheric sciences* 45.23, pp. 3606–3624.

Da Silva, Renato Ramos, David Werth, and Roni Avissar (2008). "Regional impacts of future land-cover changes on the Amazon basin wet-season climate." In: *Journal of climate* 21.6, pp. 1153–1170.

Dai, Aiguo and Kevin E Trenberth (2004). "The diurnal cycle and its depiction in the Community Climate System Model." In: *Journal of Climate* 17.5, pp. 930–951.

Davies, Laura et al. (2013). "Relationships between the large-scale atmosphere and the small-scale convective state for Darwin, Australia." In: *Journal of Geophysical Research: Atmospheres* 118.20, pp. 11–534.

DeAngelis, Anthony et al. (2010). "Evidence of enhanced precipitation due to irrigation over the Great Plains of the United States." In: *Journal of Geophysical Research: Atmospheres* 115.D15.

Degola, TSD (2013). "Impacts and variability of the South Atlantic subtropical anticyclone on Brazil in the present climate and in future scenarios." PhD thesis. University of São Paulo São Paulo, Brazil.

Dickinson, Robert E and Patrick Kennedy (1992). "Impacts on regional climate of Amazon deforestation." In: *Geophysical Research Letters* 19.19, pp. 1947–1950.

Dickinson, Robert E et al. (1989). "A regional climate model for the western United States." In: *Climatic change* 15, pp. 383–422.

Dirmeyer, Paul A and John Shukla (1994). "Albedo as a modulator of climate response to tropical deforestation." In: *Journal of Geophysical Research: Atmospheres* 99.D10, pp. 20863–20877.

Dirmeyer, Paul A et al. (2013). "Trends in land–atmosphere interactions from CMIP5 simulations." In: *Journal of Hydrometeorology* 14.3, pp. 829–849.

Duveiller, Gregory, Josh Hooker, and Alessandro Cescatti (2018). "The mark of vegetation change on Earth's surface energy balance." In: *Nature communications* 9.1, p. 679.

Ek, MB, and AAM Holtslag (2004). "Influence of soil moisture on boundary layer cloud development." In: *Journal of hydrometeorology* 5.1, pp. 86–99.

Eltahir, Elfatih AB (1996). "Role of vegetation in sustaining large-scale atmospheric circulations in the tropics." In: *Journal of Geophysical Research: Atmospheres* 101.D2, pp. 4255–4268.

Emori, Seita and SJ Brown (2005). "Dynamic and thermodynamic changes in mean and extreme precipitation under changed climate." In: *Geophysical Research Letters* 32.17.

Endo, Hirokazu, Akio Kitoh, and Hiroaki Ueda (2018). "A unique feature of the Asian summer monsoon response to global warming: The role of different land–sea thermal contrast change between the lower and upper troposphere." In: *Sola* 14, pp. 57–63.

Espinoza, Jhan Carlo et al. (2019). "Contrasting North–South changes in Amazon wet-day and dry-day frequency and related atmospheric features (1981–2017)." In: *Climate Dynamics* 52.9, pp. 5413–5430.

Espinoza, Jhan-Carlo et al. (2021). "Recent changes in the atmospheric circulation patterns during the dry-to-wet transition season in south tropical South America (1979–2020): Impacts on precipitation and fire season." In: *Journal of Climate* 34.22, pp. 9025–9042.

Espinoza Villar, Jhan Carlo et al. (2009). "Spatio-temporal rainfall variability in the Amazon basin countries (Brazil, Peru, Bolivia, Colombia, and Ecuador)." In: *International Journal of Climatology: A Journal of the Royal Meteorological Society* 29.11, pp. 1574–1594.

Fasullo, J (2012). "A mechanism for land–ocean contrasts in global monsoon trends in a warming climate." In: *Climate Dynamics* 39.5, pp. 1137–1147.

Ferguson, Craig R, Eric F Wood, and Raghuveer K Vinukollu (2012). "A global intercomparison of modeled and observed land–atmosphere coupling." In: *Journal of Hydrometeorology* 13.3, pp. 749–784.

Feron, Sarah et al. (2024). "South America is becoming warmer, drier, and more flammable." In: *Communications Earth & Environment* 5.1, p. 501.

Findell, Kirsten L and Elfatih AB Eltahir (2003). "Atmospheric controls on soil moisture–boundary layer interactions. Part I: Framework development." In: *Journal of Hydrometeorology* 4.3, pp. 552–569.

Flores, Bernardo M et al. (2024). "Critical transitions in the Amazon forest system." In: *Nature* 626.7999, pp. 555–564.

Fowler, Hayley J et al. (2021). "Towards advancing scientific knowledge of climate change impacts on short-duration rainfall extremes." In: *Philosophical Transactions of the Royal Society A* 379.2195, p. 20190542.

Gallus Jr, William A and Moti Segal (2000). "Sensitivity of forecast rainfall in a Texas convective system to soil moisture and convective parameterization." In: *Weather and forecasting* 15.5, pp. 509–525.

Gandu, Adilson Wagner, Julia Clarinda Paiva Cohen, and JRS De Souza (2004). "Simulation of deforestation in eastern Amazonia using a high-resolution model." In: *Theoretical and Applied Climatology* 78, pp. 123–135.

Gao, Lu et al. (2018). "Contributions of natural climate changes and human activities to the trend of extreme precipitation." In: *Atmospheric Research* 205, pp. 60–69.

Garstang, M et al. (1998). "Convective cloud downdrafts as the cause of large blowdowns in the Amazon rainforest." In: *Meteorology and Atmospheric Physics* 67, pp. 199–212.

Gatti, Luciana V et al. (2021). "Amazonia as a carbon source linked to deforestation and climate change." In: *Nature* 595.7867, pp. 388–393.

Gatti, Luciana V et al. (2023). "Human impacts on carbon emissions and losses in ecosystem services: the need for restoration and innovative climate finance for the Amazon." In.

Ge, Jun et al. (2022). "Deforestation intensifies daily temperature variability in the northern extratropics." In: *Nature Communications* 13.1, p. 5955.

Gedney, Nicola and Paul J Valdes (2000). "The effect of Amazonian deforestation on the northern hemisphere circulation and climate." In: *Geophysical Research Letters* 27.19, pp. 3053–3056.

Gill, Ao E (1982). "Studies of moisture effects in simple atmospheric models: The stable case." In: *Geophysical & Astrophysical Fluid Dynamics* 19.1-2, pp. 119–152.

Gilliland, Joshua M and Barry D Keim (2018). "Position of the South Atlantic Anticyclone and its impact on surface conditions across Brazil." In: *Journal of Applied Meteorology and Climatology* 57.3, pp. 535–553.

Giorgetta, Marco A et al. (2018). "ICON-A, the atmosphere component of the ICON earth system model: I. Model description." In: *Journal of Advances in Modeling Earth Systems* 10.7, pp. 1613–1637.

Giorgi, Filippo and Gary T Bates (1989). "The climatological skill of a regional model over complex terrain." In: *Monthly Weather Review* 117.11, pp. 2325–2347.

Good, Peter et al. (2008). "An objective tropical Atlantic sea surface temperature gradient index for studies of south Amazon dry-season climate variability and change." In: *Philosophical Transactions of the Royal Society B: Biological Sciences* 363.1498, pp. 1761–1766.

Guerreiro, Selma B et al. (2024). "Unravelling the complex interplay between daily and sub-daily rainfall extremes in different climates." In: *Weather and Climate Extremes*, p. 100735.

Guillod, Benoit P et al. (2015). "Reconciling spatial and temporal soil moisture effects on afternoon rainfall." In: *Nature communications* 6.1, p. 6443.

Guo, Zhichang et al. (2006). "GLACE: the global land–atmosphere coupling experiment. Part II: analysis." In: *Journal of Hydrometeorology* 7.4, pp. 611–625.

Hahmann, Andrea N and Robert E Dickinson (1997). "RCCM2–BATS model over tropical South America: Applications to tropical deforestation." In: *Journal of Climate* 10.8, pp. 1944–1964.

Hastenrath, Stefan, Dierk Polzin, and Bernard Francou (2004). "Circulation variability reflected in ice core and lake records of the southern tropical Andes." In: *Climatic Change* 64.3, pp. 361–375.

Heisler-White, Jana L et al. (2009). "Contingent productivity responses to more extreme rainfall regimes across a grassland biome." In: *Global Change Biology* 15.12, pp. 2894–2904.

Held, Isaac M and Brian J Soden (2006). "Robust responses of the hydrological cycle to global warming." In: *Journal of climate* 19.21, pp. 5686–5699.

Henderson-Sellers, Ann and V Gornitz (1984). "Possible climatic impacts of land cover transformations, with particular emphasis on tropical deforestation." In: *Climatic Change* 6, pp. 231–257.

Hirota, Marina, Marcos Daisuke Oyama, and Carlos Nobre (2011). "Concurrent climate impacts of tropical South America land-cover change." In: *Atmospheric Science Letters* 12.3, pp. 261–267.

Hirschi, Martin et al. (2011). "Observational evidence for soil-moisture impact on hot extremes in southeastern Europe." In: *Nature Geoscience* 4.1, pp. 17–21.

Hohenegger, Cathy and Bjorn Stevens (2022). "Tropical continents rainier than expected from geometrical constraints." In: *AGU Advances* 3.4, e2021AV000636.

Hohenegger, Cathy et al. (2009). "The soil moisture–precipitation feedback in simulations with explicit and parameterized convection." In: *Journal of Climate* 22.19, pp. 5003–5020.

Hohenegger, Cathy et al. (2020). "Climate statistics in global simulations of the atmosphere, from 80 to 2.5 km grid spacing." In: *Journal of the Meteorological Society of Japan. Ser. II* 98.1, pp. 73–91.

Hohenegger, Cathy et al. (2023). "ICON-Sapphire: simulating the components of the Earth system and their interactions at kilometer and subkilometer scales." In: *Geoscientific Model Development* 16.2, pp. 779–811.

Huffman, GJ et al. (2019). "GPM IMERG final precipitation L3 half hourly 0.1 degree x 0.1 degree V06." In: *Goddard Earth Sciences Data and Information Services Center (GES DISC): Greenbelt, MD, USA*.

Jalihal, Chetankumar et al. (2019). "The response of tropical precipitation to Earth's precession: the role of energy fluxes and vertical stability." In: *Climate of the Past* 15.2, pp. 449–462.

Janzen, Daniel H (1967). "Why mountain passes are higher in the tropics." In: *The American Naturalist* 101.919, pp. 233–249.

Ji, Xuan et al. (2014). "Interhemispheric teleconnections from tropical heat sources in intermediate and simple models." In: *Journal of climate* 27.2, pp. 684–697.

Joetzjer, Emilie et al. (2013). "Present-day and future Amazonian precipitation in global climate models: CMIP5 versus CMIP3." In: *Climate dynamics* 41, pp. 2921–2936.

Johns, Robert H and Charles A Doswell III (1992). "Severe local storms forecasting." In: *Weather and Forecasting* 7.4, pp. 588–612.

Johnson, Christine K et al. (2020). "Global shifts in mammalian population trends reveal key predictors of virus spillover risk." In: *Proceedings of the Royal Society B* 287.1924, p. 20192736.

Jones, Todd R and David A Randall (2011). "Quantifying the limits of convective parameterizations." In: *Journal of Geophysical Research: Atmospheres* 116.D8.

Joshi, Manoj M et al. (2008). "Mechanisms for the land/sea warming contrast exhibited by simulations of climate change." In: *Climate dynamics* 30.5, pp. 455–465.

Kahana, Ron et al. (2024). "Future precipitation projections for Brazil and tropical South America from a Convection-permitting climate simulation." In: *Frontiers in Climate* 6, p. 1419704.

Karl, Thomas R, Richard W Knight, and Neil Plummer (1995). "Trends in high-frequency climate variability in the twentieth century." In: *Nature* 377.6546, pp. 217–220.

Kemp, Luke and Eric H Cline (2022). "Systemic risk and resilience: The bronze age collapse and recovery." In: *Perspectives on Public Policy in Societal-Environmental Crises: What the Future Needs from History*. Springer International Publishing Cham, pp. 207–223.

Kendon, Elizabeth J et al. (2017). "Do convection-permitting regional climate models improve projections of future precipitation change?" In: *Bulletin of the American Meteorological Society* 98.1, pp. 79–93.

Kent, Chris, Robin Chadwick, and David P Rowell (2015). "Understanding uncertainties in future projections of seasonal tropical precipitation." In: *Journal of Climate* 28.11, pp. 4390–4413.

King, Gregory P et al. (2022). "Correlating extremes in wind divergence with extremes in rain over the tropical Atlantic." In: *Remote Sensing* 14.5, p. 1147.

Kleidon, Axel and Martin Heimann (2000). "Assessing the role of deep rooted vegetation in the climate system with model simulations: mechanism, comparison to observations and implications for Amazonian deforestation." In: *Climate Dynamics* 16, pp. 183–199.

Knapp, Alan K et al. (2008). "Consequences of more extreme precipitation regimes for terrestrial ecosystems." In: *Bioscience* 58.9, pp. 811–821.

Korn, Peter et al. (2022). "ICON-O: The ocean component of the ICON earth system model—Global simulation characteristics and local telescoping capability." In: *Journal of Advances in Modeling Earth Systems* 14.10, e2021MS002952.

Koster, Randal D et al. (2004). "Regions of strong coupling between soil moisture and precipitation." In: *Science* 305.5687, pp. 1138–1140.

Koster, Randal D et al. (2006). "GLACE: the global land–atmosphere coupling experiment. Part I: overview." In: *Journal of Hydrometeorology* 7.4, pp. 590–610.

Kotz, Maximilian et al. (2021). "Day-to-day temperature variability reduces economic growth." In: *Nature Climate Change* 11.4, pp. 319–325.

Lambert, F Hugo, Mark J Webb, and Manoj M Joshi (2011). "The relationship between land–ocean surface temperature contrast and radiative forcing." In: *Journal of Climate* 24.13, pp. 3239–3256.

Langenbrunner, Baird et al. (2019). "Why does Amazon precipitation decrease when tropical forests respond to increasing CO2?" In: *Earth's future* 7.4, pp. 450–468.

Lapola, David M et al. (2023). "The drivers and impacts of Amazon forest degradation." In: *Science* 379.6630, eabp8622.

Lawrence, Deborah and Karen Vandecar (2015). "Effects of tropical deforestation on climate and agriculture." In: *Nature climate change* 5.1, pp. 27–36.

Lean, John and PR Rowntree (1993). "A GCM simulation of the impact of Amazonian deforestation on climate using an improved canopy representation." In: *Quarterly Journal of the Royal Meteorological Society* 119.511, pp. 509–530.

— (1997). "Understanding the sensitivity of a GCM simulation of Amazonian deforestation to the specification of vegetation and soil characteristics." In: *Journal of Climate* 10.6, pp. 1216–1235.

Lean, Judith and David A Warrilow (1989). "Simulation of the regional climatic impact of Amazon deforestation." In: *Nature* 342.6248, pp. 411–413.

Lee, Junhong and Cathy Hohenegger (2024). "Weaker land–atmosphere coupling in global storm-resolving simulation." In: *Proceedings of the National Academy of Sciences* 121.12, e2314265121.

Leite-Filho, Argemiro T, Marcos H Costa, and Rong Fu (2020). "The southern Amazon rainy season: the role of deforestation and its interactions with large-scale mechanisms." In: *International Journal of Climatology* 40.4, pp. 2328–2341.

Lejeune, Quentin et al. (2015). "Influence of Amazonian deforestation on the future evolution of regional surface fluxes, circulation, surface temperature and precipitation." In: *Climate Dynamics* 44, pp. 2769–2786.

Lemes, Murilo Ruv et al. (2023). "Impacts on South America moisture transport under Amazon deforestation and 2° C global warming." In: *Science of the Total Environment* 905, p. 167407.

Lenderink, Geert and Jisk Attema (2015). "A simple scaling approach to produce climate scenarios of local precipitation extremes for the Netherlands." In: *Environmental Research Letters* 10.8, p. 085001.

Lenderink, Geert and Erik Van Meijgaard (2008). "Increase in hourly precipitation extremes beyond expectations from temperature changes." In: *Nature Geoscience* 1.8, pp. 511–514.

Lenton, Timothy M et al. (2008). "Tipping elements in the Earth's climate system." In: *Proceedings of the national Academy of Sciences* 105.6, pp. 1786–1793.

Lettau, Heinz, Katharina Lettau, and Luiz Carlos B Molion (1979). "Amazonia's hydrologic cycle and the role of atmospheric recycling in assessing deforestation effects." In: *Monthly Weather Review* 107.3, pp. 227–238.

Levine, Paul A et al. (2016). "Evaluating the strength of the land–atmosphere moisture feedback in Earth system models using satellite observations." In: *Hydrology and Earth System Sciences* 20.12, pp. 4837–4856.

Li, Wenhong, Rong Fu, and Robert E Dickinson (2006). "Rainfall and its seasonality over the Amazon in the 21st century as assessed by the coupled models for the IPCC AR4." In: *Journal of Geophysical Research: Atmospheres* 111.D2.

Liu, Shaw Chen et al. (2009). "Temperature dependence of global precipitation extremes." In: *Geophysical Research Letters* 36.17.

Liu, Yimin, Guoxiong Wu, and Rongcai Ren (2004). "Relationship between the subtropical anticyclone and diabatic heating." In: *Journal of Climate* 17.4, pp. 682–698.

Llopart, Marta et al. (2018). "Land use change over the Amazon Forest and its impact on the local climate." In: *Water* 10.2, p. 149.

Lo, Min-Hui and James S Famiglietti (2013). "Irrigation in California's Central Valley strengthens the southwestern US water cycle." In: *Geophysical Research Letters* 40.2, pp. 301–306.

Loriaux, Jessica M, Geert Lenderink, and A Pier Siebesma (2017). "Large-scale controls on extreme precipitation." In: *Journal of Climate* 30.3, pp. 955–968.

Luo, Xing et al. (2022). "The biophysical impacts of deforestation on precipitation: results from the CMIP6 model intercomparison." In: *Journal of Climate* 35.11, pp. 3293–3311.

Malardel, Sylvie et al. (2016). "A new grid for the IFS." In: *ECMWF newsletter* 146.23-28, p. 321.

Malhi, Yadvinder et al. (2009). "Exploring the likelihood and mechanism of a climate-change-induced dieback of the Amazon rainforest." In: *Proceedings of the National Academy of Sciences* 106.49, pp. 20610–20615.

Marengo, José A (1992). "Interannual variability of surface climate in the Amazon basin." In: *International journal of climatology* 12.8, pp. 853–863.

— (2004). "Interdecadal variability and trends of rainfall across the Amazon basin." In: *Theoretical and applied climatology* 78, pp. 79–96.

Marengo, Jose A et al. (2018). "Changes in climate and land use over the Amazon region: current and future variability and trends." In: *Frontiers in Earth Science* 6, p. 228.

May, Ryan M et al. (2022). "MetPy: A meteorological Python library for data analysis and visualization." In: *Bulletin of the American Meteorological Society* 103.10, E2273–E2284.

McNeil, Cameron L, David A Burney, and Lida Pigott Burney (2010). "Evidence disputing deforestation as the cause for the collapse of the ancient Maya polity of Copan, Honduras." In: *Proceedings of the National Academy of Sciences* 107.3, pp. 1017–1022.

Medvigy, David, Robert L Walko, and Roni Avissar (2011). "Effects of deforestation on spatiotemporal distributions of precipitation in South America." In: *Journal of Climate* 24.8, pp. 2147–2163.

Medvigy, David et al. (2013). "Simulated changes in northwest US climate in response to Amazon deforestation." In: *Journal of Climate* 26.22, pp. 9115–9136.

Miralles, Diego G et al. (2019). "Land–atmospheric feedbacks during droughts and heatwaves: state of the science and current challenges." In: *Annals of the New York Academy of Sciences* 1436.1, pp. 19–35.

Miyasaka, Takafumi and Hisashi Nakamura (2010). "Structure and mechanisms of the Southern Hemisphere summertime subtropical anticyclones." In: *Journal of Climate* 23.8, pp. 2115–2130.

Molion, Luiz Carlos Baldicero (1975). *A climatonomic study of the energy and moisture fluxes of the Amazonas basin with considerations of deforestation effects*. The University of Wisconsin-Madison.

Moore, Nathan et al. (2007). "Uncertainty and the changing hydroclimatology of the Amazon." In: *Geophysical Research Letters* 34.14.

Morabito, Marco et al. (2014). "Environmental temperature and thermal indices: What is the most effective predictor of heat-related mortality in different geographical contexts?" In: *The Scientific World Journal* 2014.1, p. 961750.

Mu, Ye, Trent W Biggs, and Charles Jones (2023). "Importance in shifting circulation patterns for dry season moisture sources in the Brazilian Amazon." In: *Geophysical Research Letters* 50.9, e2023GL103167.

Muller, Caroline J and PA O'Gorman (2011). "An energetic perspective on the regional response of precipitation to climate change." In: *Nature Climate Change* 1.5, pp. 266–271.

Muller, Caroline J, Paul A O'Gorman, and Larissa E Back (2011). "Intensification of precipitation extremes with warming in a cloud-resolving model." In: *Journal of Climate* 24.11, pp. 2784–2800.

Mutton, Harry et al. (2024). "The impact of a uniform ocean warming on the West African monsoon." In: *Climate Dynamics* 62.1, pp. 103–122.

Neelin, J David and Isaac M Held (1987). "Modeling tropical convergence based on the moist static energy budget." In: *Monthly Weather Review* 115.1, pp. 3–12.

Newman, Erin B (1994). "Earth's vanishing medicine cabinet: rain forest destruction and its impact on the pharmaceutical industry." In: *American Journal of Law & Medicine* 20.4, pp. 479–501.

Nielsen, David Marcolino et al. (2019). "Dynamics-based regression models for the South Atlantic Convergence Zone." In: *Climate Dynamics* 52, pp. 5527–5553.

Nobre, Carlos A, Piers J Sellers, and Jagadish Shukla (1991). "Amazonian deforestation and regional climate change." In: *Journal of climate* 4.10, pp. 957–988.

Nobre, Paulo and John Shukla (1996). "Variations of sea surface temperature, wind stress, and rainfall over the tropical Atlantic and South America." In: *Journal of climate* 9.10, pp. 2464–2479.

Nobre, Paulo et al. (2009). "Amazon deforestation and climate change in a coupled model simulation." In: *Journal of Climate* 22.21, pp. 5686–5697.

Oglesby, Robert J et al. (2010). "Collapse of the Maya: Could deforestation have contributed?" In: *Journal of Geophysical Research: Atmospheres* 115.D12.

Oliveira, Beatriz Fátima Alves de et al. (2021). "Deforestation and climate change are projected to increase heat stress risk in the Brazilian Amazon." In: *Communications Earth & Environment* 2.1, p. 207.

O'Gorman, Paul A and Tapio Schneider (2009). "Scaling of precipitation extremes over a wide range of climates simulated with an idealized GCM." In: *Journal of Climate* 22.21, pp. 5676–5685.

Pan, Zaitao et al. (1996). "Influences of model parameterization schemes on the response of rainfall to soil moisture in the central United States." In: *Monthly Weather Review* 124.8, pp. 1786–1802.

Parsons, Luke A (2020). "Implications of CMIP6 projected drying trends for 21st century Amazonian drought risk." In: *Earth's Future* 8.10, e2020EF001608.

Perez, Timothy M, James T Stroud, and Kenneth J Feeley (2016). "Thermal trouble in the tropics." In: *Science* 351.6280, pp. 1392–1393.

Perugini, Lucia et al. (2017). "Biophysical effects on temperature and precipitation due to land cover change." In: *Environmental Research Letters* 12.5, p. 053002.

Phillips, Oliver L, Roel JW Brienen, and Rainfor Collaboration (2017). "Carbon uptake by mature Amazon forests has mitigated Amazon nations' carbon emissions." In: *Carbon Balance and Management* 12.1, p. 1.

Pires, Gabrielle Ferreira and Marcos Heil Costa (2013). "Deforestation causes different subregional effects on the Amazon bioclimatic equilibrium." In: *Geophysical Research Letters* 40.14, pp. 3618–3623.

Quine, Christopher P and Barry A Gardiner (2007). *Understanding how the interaction of wind and trees results in windthrow, stem breakage, and canopy gap formation*.

Reboita, Michelle Simões, Tatiana Rocha Amaro, and Marcelo Rodrigues de Souza (2018). "Winds: intensity and power density simulated by RegCM4 over South America in present and future climate." In: *Climate Dynamics* 51, pp. 187–205.

Reboita, Michelle Simões et al. (2019). "The South Atlantic subtropical anticyclone: present and future climate." In: *Frontiers in Earth Science* 7, p. 8.

Rehbein, Amanda and Tercio Ambrizzi (2023). "Mesoscale convective systems over the Amazon basin in a changing climate under global warming." In: *Climate Dynamics* 61.3, pp. 1815–1827.

Reick, Christian H et al. (2021). "JSBACH 3-The land component of the MPI Earth System Model: documentation of version 3.2." In.

Richter, Ingo, Carlos R Mechoso, and Andrew W Robertson (2008). "What determines the position and intensity of the South Atlantic anticyclone in austral winter?—An AGCM study." In: *Journal of climate* 21.2, pp. 214–229.

Richter, Ingo et al. (2012). "Tropical Atlantic biases and their relation to surface wind stress and terrestrial precipitation." In: *Climate dynamics* 38.5, pp. 985–1001.

Rodrigues, Regina R et al. (2019). "Common cause for severe droughts in South America and marine heatwaves in the South Atlantic." In: *Nature Geoscience* 12.8, pp. 620–626.

Rodwell, Mark J and Brian J Hoskins (2001). "Subtropical anticyclones and summer monsoons." In: *Journal of Climate* 14.15, pp. 3192–3211.

Ruv Lemes, Murilo et al. (2023). "Impacts of atmospheric CO2 increase and Amazon deforestation on the regional climate: A water budget modelling study." In: *International Journal of Climatology* 43.3, pp. 1497–1513.

Salati, Eneas et al. (1979). "Recycling of water in the Amazon basin: an isotopic study." In: *Water resources research* 15.5, pp. 1250–1258.

Sampaio, Gilvan et al. (2007). "Regional climate change over eastern Amazonia caused by pasture and soybean cropland expansion." In: *Geophysical Research Letters* 34.17.

Santos, Eliane Barbosa, Paulo Sérgio Lucio, and Cláudio Moisés Santos e Silva (2017). "Synoptic patterns of atmospheric circulation associated with intense precipitation events over the Brazilian Amazon." In: *Theoretical and applied climatology* 128, pp. 343–358.

Satoh, Masaki et al. (2019). "Global cloud-resolving models." In: *Current Climate Change Reports* 5, pp. 172–184.

Satyamurty, Prakki et al. (2010). "Rainfall trends in the Brazilian Amazon Basin in the past eight decades." In: *Theoretical and Applied Climatology* 99, pp. 139–148.

Schaefer, JT and CA Doswell III (1980). "The theory and practical application of antitriptic balance." In: *Monthly Weather Review* 108.6, pp. 746–756.

Schmidt, Hauke et al. (2024). "Effects of vertical grid spacing on the climate simulated in the ICON-Sapphire global storm-resolving model." In: *Geoscientific Model Development* 17.4, pp. 1563–1584.

Schultz, Natalie M, Peter J Lawrence, and Xuhui Lee (2017). "Global satellite data highlights the diurnal asymmetry of the surface temperature response to deforestation." In: *Journal of Geophysical Research: Biogeosciences* 122.4, pp. 903–917.

Schumacher, Russ S and Kristen L Rasmussen (2020). "The formation, character and changing nature of mesoscale convective systems." In: *Nature Reviews Earth & Environment* 1.6, pp. 300–314.

Schwingshackl, Clemens et al. (2021). "Heat stress indicators in CMIP6: estimating future trends and exceedances of impact-relevant thresholds." In: *Earth's Future* 9.3, e2020EF001885.

Seager, Richard, Naomi Naik, and Gabriel A Vecchi (2010). "Thermodynamic and dynamic mechanisms for large-scale changes in the hydrological cycle in response to global warming." In: *Journal of climate* 23.17, pp. 4651–4668.

Seager, Richard et al. (2003). "Air–sea interaction and the seasonal cycle of the subtropical anticyclones." In: *Journal of climate* 16.12, pp. 1948–1966.

Segal, Moti, Eric A Aligo, and William A Gallus Jr (2004). "A conceptual and scaling evaluation of the surface wetness effect on daytime moisture convergence along a surface cold front with differential cloud cover." In: *Journal of Hydrometeorology* 5.2, pp. 365–371.

Segura, Hans et al. (2022). "Learning by Doing: Seasonal and Diurnal Features of Tropical Precipitation in a Global-Coupled Storm-Resolving Model." In: *Geophysical Research Letters* 49.24, e2022GL101796.

Segura, Hans et al. (2025). "nextGEMS: entering the era of kilometer-scale Earth system modeling." In: *EGUsphere* 2025, pp. 1–39.

Seneviratne, Sonia I et al. (2006). "Land–atmosphere coupling and climate change in Europe." In: *Nature* 443.7108, pp. 205–209.

Shaw, Tiffany A and Aiko Voigt (2016). "Land dominates the regional response to CO2 direct radiative forcing." In: *Geophysical Research Letters* 43.21, pp. 11–383.

Smagorinsky, Joseph (1963). "General circulation experiments with the primitive equations: I. The basic experiment." In: *Monthly weather review* 91.3, pp. 99–164.

Smith, Melinda D (2011). "An ecological perspective on extreme climatic events: a synthetic definition and framework to guide future research." In: *Journal of Ecology* 99.3, pp. 656–663.

Spangler, Keith R, Shixin Liang, and Gregory A Wellenius (2022). "Wet-bulb globe temperature, universal thermal climate index, and other heat metrics for US Counties, 2000–2020." In: *Scientific data* 9.1, p. 326.

Spracklen, DV and LJGRL Garcia-Carreras (2015). "The impact of Amazonian deforestation on Amazon basin rainfall." In: *Geophysical Research Letters* 42.21, pp. 9546–9552.

Stein, U and PINHAS Alpert (1993). "Factor separation in numerical simulations." In: *Journal of Atmospheric Sciences* 50.14, pp. 2107–2115.

Stevens, Bjorn and Sandrine Bony (2013). "What are climate models missing?" In: *science* 340.6136, pp. 1053–1054.

Sud, YC, J Shukla, and Y1 Mintz (1988). "Influence of land surface roughness on atmospheric circulation and precipitation: A sensitivity study with a general circulation model." In: *Journal of Applied Meteorology (1988-2005)*, pp. 1036–1054.

Swann, Abigail LS et al. (2015). "Future deforestation in the Amazon and consequences for South American climate." In: *Agricultural and Forest Meteorology* 214, pp. 12–24.

Tao, Shengli et al. (2023). "Little evidence that Amazonian rainforests are approaching a tipping point." In: *Nature Climate Change* 13.12, pp. 1317–1320.

Taylor, Christopher M et al. (2012). "Afternoon rain more likely over drier soils." In: *Nature* 489.7416, pp. 423–426.

Taylor, Christopher M et al. (2013). "Modeling soil moisture-precipitation feedback in the Sahel: Importance of spatial scale versus convective parameterization." In: *Geophysical Research Letters* 40.23, pp. 6213–6218.

Taylor, Karl E, David Williamson, and Francis Zwiers (2000). *The sea surface temperature and sea-ice concentration boundary conditions for AMIP II simulations*. Program for Climate Model Diagnosis and Intercomparison, Lawrence Livermore ...

Thompson, Ross M et al. (2013). "Means and extremes: building variability into community-level climate change experiments." In: *Ecology Letters* 16.6, pp. 799–806.

Tiedtke, MICHAEL (1989). "A comprehensive mass flux scheme for cumulus parameterization in large-scale models." In: *Monthly weather review* 117.8, pp. 1779–1800.

Tierney, Jessica E, Caroline C Ummenhofer, and Peter B Demenocal (2015). "Past and future rainfall in the Horn of Africa." In: *Science advances* 1.9, e1500682.

Trenberth, Kevin E (1999). "Conceptual framework for changes of extremes of the hydrological cycle with climate change." In: *Climatic change* 42.1, pp. 327–339.

Trenberth, Kevin E et al. (2003). "The changing character of precipitation." In: *Bulletin of the American Meteorological Society* 84.9, pp. 1205–1218.

Ukkola, Anna M et al. (2020). "Robust future changes in meteorological drought in CMIP6 projections despite uncertainty in precipitation." In: *Geophysical Research Letters* 47.11, e2020GL087820.

Vianello, RL and LPG Maia (1986). "Preliminary study of the dynamic climatology of the State of Minas Gerais." In: *Proceedings of the 4th Brazilian Congress of Meteorology*.

Viscardi, Leandro Alex Moreira et al. (2024). "Environmental controls on isolated convection during the Amazonian wet season." In: *Atmospheric Chemistry and Physics* 24.15, pp. 8529–8548.

Voldoire, A and JF Royer (2004). "Tropical deforestation and climate variability." In: *Climate Dynamics* 22, pp. 857–874.

Wang, Jingfeng et al. (2009). "Impact of deforestation in the Amazon basin on cloud climatology." In: *Proceedings of the National Academy of Sciences* 106.10, pp. 3670–3674.

Wang, Ke et al. (2013). "Beijing storm of July 21, 2012: observations and reflections." In: *Natural hazards* 67, pp. 969–974.

Wedi, Nils P (2014). "Increasing horizontal resolution in numerical weather prediction and climate simulations: illusion or panacea?" In: *Philosophical Transactions of the Royal Society A: Mathematical, Physical and Engineering Sciences* 372.2018, p. 20130289.

Wernli, Heini et al. (2008). "SAL—A novel quality measure for the verification of quantitative precipitation forecasts." In: *Monthly Weather Review* 136.11, pp. 4470–4487.

Werth, David and Roni Avissar (2002). "The local and global effects of Amazon deforestation." In: *Journal of Geophysical Research: Atmospheres* 107.D20, LBA–55.

Winckler, Johannes et al. (2019). "Importance of surface roughness for the local biogeophysical effects of deforestation." In: *Journal of Geophysical Research: Atmospheres* 124.15, pp. 8605–8618.

Windmiller, JM et al. (2023). "Predicting convective downdrafts from updrafts and environmental conditions in a global storm resolving simulation." In: *Journal of Advances in Modeling Earth Systems* 15.3, e2022MS003048.

Wongchuig, Sly et al. (2023). "Changes in the surface and atmospheric water budget due to projected Amazon deforestation: Lessons from a fully coupled model simulation." In: *Journal of Hydrology* 625, p. 130082.

Wright, S Joseph, HELENE C MULLER-LANDAU, and JAN Schipper (2009). "The future of tropical species on a warmer planet." In: *Conservation biology* 23.6, pp. 1418–1426.

Ying, Jun et al. (2024). "Constraints on the projected tropical Pacific sea surface temperature warming pattern by the tropical North Atlantic cold SST bias in CMIP6 models." In: *Geophysical Research Letters* 51.21, e2024GL111233.

Yoon, Arim and Cathy Hohenegger (2024). “codes for "Muted Amazon rainfall response to deforestation in a global storm-resolving model".” In: Online; Edmond, V1.

— (2025). “Muted amazon rainfall response to deforestation in a global storm-resolving model.” In: *Geophysical Research Letters* 52.4, e2024GL110503.

Zemp, Delphine Clara et al. (2017). “Self-amplified Amazon forest loss due to vegetation-atmosphere feedbacks.” In: *Nature communications* 8.1, p. 14681.

Zhan, Zhiying et al. (2017). “Temperature change between neighboring days and mortality in United States: a nationwide study.” In: *Science of the Total Environment* 584, pp. 1152–1161.

EIDESSTATTLICHE VERSICHERUNG | DECLARATION ON OATH

Hiermit erkläre ich an Eides statt, dass ich die vorliegende Dissertationsschrift selbst verfasst und keine anderen als die angegebenen Quellen und Hilfsmittel benutzt habe. Sofern im Zuge der Erstellung der vorliegenden Dissertationsschrift generative Künstliche Intelligenz (gKI) basierte elektronische Hilfsmittel verwendet wurden, versichere ich, dass meine eigene Leistung im Vordergrund stand und dass eine vollständige Dokumentation aller verwendeten Hilfsmittel gemäß der Guten wissenschaftlichen Praxis vorliegt. Ich trage die Verantwortung für eventuell durch die gKI generierte fehlerhafte oder verzerrte Inhalte, fehlerhafte Referenzen, Verstöße gegen das Datenschutz- und Urheberrecht oder Plagiate.

Hamburg, February 3, 2026

Arim Yoon

EIDESSTATTLICHE VERSICHERUNG II | DECLARATION ON OATH II

Ich versichere, dass dieses gebundene Exemplar der Dissertation und das in elektronischer Form eingereichte Dissertationsexemplar (über den Docata-Upload) und das bei der Fakultät zur Archivierung eingereichte gedruckte gebundene Exemplar der Dissertationsschrift identisch sind. I, the undersigned, declare that this bound

copy of the dissertation and the dissertation submitted in electronic form (via the Docata upload) and the printed bound copy of the dissertation submitted to the faculty (responsible Academic Office or the Doctoral Office Physics) for archiving are identical. *Hamburg, February 3, 2026*

Arim Yoon

Hinweis / Reference

Die gesamten Veröffentlichungen in der Publikationsreihe des MPI-M
„Berichte zur Erdsystemforschung / Reports on Earth System Science“,
ISSN 1614-1199

sind über die Internetseiten des Max-Planck-Instituts für Meteorologie erhältlich:
https://mpimet.mpg.de/forschung/publikationen

All the publications in the series of the MPI -M
„Berichte zur Erdsystemforschung / Reports on Earth System Science“,
ISSN 1614-1199

are available on the website of the Max Planck Institute for Meteorology:
https://mpimet.mpg.de/en/research/publications